Universidade do Minho
Escola de Engenharia

Ana Georgina Gomes Alves

Enhancing Antileishmanial Therapy: Evaluating a Novel Screening Assay, Compounds, and a Delivery System

março de 2025

UMinho | 2025 Ana Georgina Gomes Alves **Enhancing Antileishmanial Therapy: Evaluating a Novel Screening Assay, Compounds, and a Delivery System**

This work was financed by the Foundation for Science and Technology (FCT) under the grant SFRH/BD/93766/2013 financed by POPH–QREN, subsidized by Fundo Social Europeu and Ministério da Ciência, Tecnologia e Ensino Superior and by FEDER - Fundo Europeu de Desenvolvimento Regional funds through the COMPETE 2020 - Operational Programme for Competitiveness and Internationalization (POCI), Portugal 2020, and by Portuguese funds through FCT in the framework of the project POCI-01-0145-FEDER-007274.

Cofinanciado por:

COMPETE 2020 · PORTUGAL 2020 · UNIÃO EUROPEIA Fundo Europeu de Desenvolvimento Regional · FCT Fundação para a Ciência e a Tecnologia

POPH QUALIFICAR É CRESCER. · QUADRO DE REFERÊNCIA ESTRATÉGICO NACIONAL PORTUGAL 2007.2013 · Governo da República Portuguesa · UNIÃO EUROPEIA Fundo Social Europeu

Universidade do Minho
Escola de Engenharia

Ana Georgina Gomes Alves

Enhancing Antileishmanial Therapy: Evaluating a Novel Screening Assay, Compounds, and a Delivery System

Tese de Doutoramento
Doutoramento em Bioengenharia

Trabalho efetuado sob a orientação da
Professora Doutora Ana Tomás
do
Professor Doutor Francisco Miguel Gama
e do
Professor Doutor Gert Storm

março de 2025

DIREITOS DE AUTOR E CONDIÇÕES DE UTILIZAÇÃO DO TRABALHO POR TERCEIROS

Este é um trabalho académico que pode ser utilizado por terceiros desde que respeitadas as regras e boas práticas internacionalmente aceites, no que concerne aos direitos de autor e direitos conexos.

Assim, o presente trabalho pode ser utilizado nos termos previstos na licença abaixo indicada.

Caso o utilizador necessite de permissão para poder fazer um uso do trabalho em condições não previstas no licenciamento indicado, deverá contactar o autor, através do RepositóriUM da Universidade do Minho.

Licença concedida aos utilizadores deste trabalho



Atribuição-NãoComercial-SemDerivações
CC BY-NC-ND

https://creativecommons.org/licenses/by-nc-nd/4.0/

Eleven years have passed... This journey has been one of learning, perseverance, and self-discovery, and I am deeply grateful to those who have supported me along the way. To my supervisor, Ana Tomás, a special thank you. Despite my long writing process, you were always available to help and guide me through it. Without your support, this would not have been possible. To my co-supervisors, Gert Storm and Miguel Gama, I am grateful for all the scientific input and guidance throughout this journey. To Wim Hennink, a heartfelt thank you for your willingness to read and provide input on my thesis right away. Your support was invaluable. To Helena Castro a special thank you for your scientific contribution. To Aida, my lab colleague who became a dear friend. I truly appreciate not only your scientific knowledge but also the warmth and friendship that made NL feel like home. To all my lab colleagues at UIPS, thank you for your support. To the wonderful friends I found in NL and will cherish for life – Alexandre, Johannes, Lucia, Rovertos, Salma, Stefanos, Yannis, Yanna – thank you for all the great moments. Your friendship made this journey even more special.

Tantos anos se passaram que, por momentos, cheguei a pensar que este dia nunca chegaria! Ao longo desta jornada foram-se juntando muitos, a outros tantos que já cá andavam. A minha família do coração cresceu e não há espaço suficiente para expressar a minha gratidão por ter tanta gente especial na minha vida. Sou, sem dúvida, uma sortuda! Às minhas companheiras de lab e de vida, Margarida, Sandra e Tânia que foram essenciais para a conclusão deste trabalho, tanto pelo vosso *input* científico, quanto pela amizade sincera. Aos restantes lab friends, Márcia, Mariana, Joana, Ricas, as meninas da Immunethep, obrigada por todas as maluqueiras, danças, jantares e consultas de psicologia gratuita. Vocês foram dos melhores achados desta jornada e tornaram tudo mais leve e divertido. Aos pilares mais fortes que tive durante todo este processo — Ana, Carina, Coelho, Dina, Márcia, Maria, Mariana, Nita, Sofia e Susete — não sei o que faria na minha vida sem vocês. Obrigada por TUDO! Alex, Ana Cristina, Aninhas, Bambia, Bi, Claudete, Cris, Dárcio, Di, Diogo, Filipa, Gabs, Isa, Ju, Noni, Paula, Pedro C., Pedro V., Pimas, Pime, Su, Raquel P., Raquel V., Rute C., Touni, vocês não imaginam a leveza que trazem para a minha vida. Obrigada! À família Bomboémia, que tantas vezes, e sem se aperceberem, foram o meu refúgio. Ao Eraldo, agradeço a tua paciência mesmo nos momentos em que não compreendias as minhas mudanças de humor. A tua paciência, o teu apoio e a tua confiança em mim foram muito importantes. E, last but not least, aos meus pais, ao meu irmão, à minha avó e à minha família, que sempre compreenderam as minhas ausências e nunca deixaram de ser o meu porto de abrigo. Esta jornada pode ser solitária e muito pesada, mas tive os melhores comigo, e por isso, obrigada de coração.

I hereby declare having conducted this academic work with integrity. I confirm that I have not used plagiarism or any form of undue use of information or falsification of results along the process leading to its elaboration.

I further declare that I have fully acknowledged the Code of Ethical Conduct of the University of Minho.

RESUMO | Aperfeiçoamento da Terapia anti-*Leishmania*: Novo protocolo de screening, novos compostos e um sistema de libertação controlada

As leishmanioses são classificadas pela Organização Mundial de Saúde como Doenças Tropicais Negligenciadas. Apesar do seu impacto na saúde pública e na economia, os investimentos da indústria farmacêutica permanecem limitados devido ao baixo retorno financeiro. Assim, o desenvolvimento nesta área tem sido maioritariamente liderado por instituições académicas e organizações sem fins lucrativos. Este projeto de doutoramento avaliou a atividade de compostos inovadores contra parasitas do género *Leishmania* bem como o uso de nanopartículas para a sua solubilização e libertação nos órgãos afetados. A nossa motivação surgiu do peso significativo das leishmanioses nas populações mais vulneráveis e das limitações terapêuticas atuais, caracterizadas por efeitos secundários graves, tratamentos de longa duração, eficácia limitada e custos elevados. No âmbito deste projeto, foi desenvolvido um novo protocolo de *high content screening* (HCS) que permite a identificação rápida de compostos com actividade anti-*Leishmania*. Este sistema possibilita a deteção de amastigotas intracelulares utilizando exclusivamente coloração com DAPI. A análise das imagens foi implementada em dois softwares: o IN Cell Analyzer e o CellProfiler, sendo que este último foi adaptado para ser utilizado por grupos de investigação sem acesso a microscópios de HCS. Através deste protocolo, identificou-se uma família de quinolina-(1*H*)-iminas com atividade *in vitro* contra *L. infantum*, *L. major* e *L. amazonensis*. Apesar do modo de ação não ter sido completamente elucidado, os ensaios sugerem uma interferência na respiração mitocondrial. No entanto, a baixa solubilidade destes compostos representa um desafio à sua administração. Para ultrapassar esta limitação, as quinolina-(1*H*)-iminas foram encapsuladas em micelas mPEG-*b*-p(HPMAm-Bz), formadas através de interações não covalentes, designadas por *π-π stacking*, descritas como capazes de aumentar a estabilidade das nanopartículas e a retenção das drogas. Este processo melhorou significativamente a solubilidade das quinolina-(1*H*)-iminas e estudos *in vitro* demonstraram que os compostos 1h e 1n, aquando encapsulados, mantêm uma atividade semelhante à da droga livre, mas com toxicidade significantemente menor. Num modelo de murganho, verificou-se que tanto as micelas poliméricas como os compostos encapsulados se acumularam nos órgãos tipicamente afetados pela leishmaniose visceral, nomeadamente fígado, baço e, em menor grau, medula óssea. Por outro lado, o fármaco livre, não foi detetado após 24 h ou apresentou concentrações significativamente mais baixas. Estes resultados sugerem que as micelas mPEG-*b*-p(HPMAm-Bz) têm potencial para a administração de quinolina-(1*H*)-iminas. No entanto, será necessária uma maior otimização da sua estabilidade e do regime de dosagem para maximizar o seu potencial terapêutico. **Keywords:** Antiparasitários; *High content screening*; *Leishmania;* Micelas poliméricas; Quinolina-(1*H*)-imina.

Leishmaniases, along with other 20 groups of communicable diseases, are classified by the World Health Organization as Neglected Tropical Diseases. Despite their significant economic and public health impact, they receive limited pharmaceutical investment due to low financial returns. As a result, developments in the field have been largely driven by academia and non-profit organizations. This PhD project focused on evaluating novel compounds against *Leishmania* parasites and assessing the potential of nanocarriers for their delivery. Our motivation stemmed from the significant burden of leishmaniases and the limitations of current treatments, which are associated with severe side effects, long treatment durations, limited efficacy, and high costs. A new image-based high content screening (HCS) assay was developed to enable faster and more reliable identification of compounds with anti-*Leishmania* effect. This protocol allows the detection of intracellular amastigotes using only DAPI staining, making it applicable to any *Leishmania* strain without the need for genetically modified parasites. Automated image analysis was implemented using two software platforms: i) IN Cell Analyzer, which facilitated additional studies on *Leishmania*-infected macrophages, such as analyzing the role of specific proteins in parasite infection and replication, and ii) CellProfiler, which was adapted for broader use by research groups without access to HCS microscopes. Using this protocol, a family of quinoline-(1*H*)-imines demonstrated activity *in vitro* against *L. infantum*, *L. major* and *L. amazonensis*. Although the mode of action was not fully disclosed, the results suggest interference with mitochondrial respiration. However, the poor aqueous solubility of quinoline-(1*H*)-imines poses a challenge for their *in vivo* administration. To overcome this, compounds were encapsulated in mPEG-*b*-p(HPMAm-Bz) micelles, formed through noncovalent π-π stacking interactions known to increase nanocarrier stability and drug retention. The use of polymeric micelles (PMs) substantially improved solubility. Efficacy and toxicity studies revealed that encapsulated 1h and 1n retained similar efficacy to free drugs while exhibiting significantly reduced toxicity toward primary macrophages. In a murine model, both PMs and drug administered in the micellar formulation, accumulated in organs typically affected by the visceral leishmaniasis, such as the liver, spleen and to a less extent the bone marrow, contrary to the free drug that after 24h was either undetected or present in a significantly lower amount. These findings suggest that mPEG-*b*-p(HPMAm-Bz) micelles hold promise for delivering quinoline-(1*H*)-imines. However, further optimization of their stability and dosing regimen is necessary to maximize therapeutic potential.

Keywords: Antiparasitic agents; High content screening; *Leishmania;* Polymeric micelles; Quinoline-(1*H*)-imines.

DIREITOS DE AUTOR E CONDIÇÕES DE UTILIZAÇÃO DO TRABALHO POR TERCEIROS II

ACKNOWLEDGMENTS/AGRADECIMENTOS III

STATEMENT OF INTEGRITY IV

RESUMO | APERFEIÇOAMENTO DA TERAPIA ANTI-*LEISHMANIA*: NOVO PROTOCOLO DE SCREENING, NOVOS COMPOSTOS E UM SISTEMA DE LIBERTAÇÃO CONTROLADA V

ABSTRACT | ENHANCING ANTILEISHMANIAL THERAPY: EVALUATING A NOVEL SCREENING ASSAY, COMPOUNDS, AND A DELIVERY SYSTEM VI

LIST OF CONTENTS VII

LIST OF ABBREVIATIONS AND SYMBOLS XI

LIST OF FIGURES XIV

LIST OF TABLES XVI

CHAPTER I. INTRODUCTION 1

1. GENERAL INTRODUCTION 2
2. THE LEISHMANIASES 4
   - 2.1. Transmission and Life cycle 4
   - 2.2. Clinical manifestations 7
3. CURRENT TREATMENTS 9
   - 3.1. Pentavalent antimonials 9
   - 3.2. Amphotericin B 10
   - 3.3. Miltefosine 11
   - 3.4. Paromomycin 12
   - 3.5. Pentamidine 13
   - 3.6. Combination chemotherapy 13
4. NEW CHEMICAL ENTITIES 14
   - 4.1. LXE408 14
   - 4.2. DNDI-0690 16
   - 4.3. DNDI-6148 16
   - 4.4. GSK3494245/DDD1305143 and DNDI-6899 16

4.5. DNDI-2319 16
4.6. DNDI-6174 17
4.7. Compounds not in clinical trials 17
5. NANOMEDICINE 18
5.1. LIPOSOMES 20
5.1.1. Encapsulation of approved anti-*Leishmania* drugs in liposomes 21
5.1.2. Encapsulation in liposomes of repurposed drugs with anti-*Leishmania* effect 22
5.1.3. Encapsulation of new anti-*Leishmania* drugs in liposomes 22
5.2. SOLID LIPID NPS 23
5.3. EMULSOMES AND METALLIC NPS 24
5.4. POLYMERIC NPS 25
6. AIMS 29
7. REFERENCES 30
CHAPTER II. DEVELOPMENT OF AN AUTOMATED IMAGE ANALYSIS PROTOCOL FOR QUANTIFICATION OF INTRACELLULAR FORMS OF *LEISHMANIA* SPP. 43
1. ABSTRACT 44
2. INTRODUCTION 44
3. MATERIALS AND METHODS 45
3.1. Parasites 45
3.2. Macrophages 46
3.3. Infections and drug assessment 46
3.4. Identification of parasites and macrophages in infection assays 46
3.5. Image acquisition 47
3.6. Image analysis using the IN Cell Investigator Developer Toolbox 47
3.7. Image analysis using CellProfiler 48
3.8. Ethical statement 48
3.9. Statistical analysis 51
4. RESULTS 51
4.1. Parasite and infected cell labelling 51
4.2. IN Cell Investigator Developer Toolbox and CellProfiler image analysis 51
4.3. Comparison of Cell Profiler with IN Cell Investigator Developer Toolbox 53

4.4. Pharmacological validation of IN Cell Investigator Developer Toolbox and Cell Profiler workflows 56
5. DISCUSSION 57
6. REFERENCES 59
7. SUPPORTING INFORMATION 62

CHAPTER III. BIOLOGICAL EVALUATION AND MECHANISTIC STUDIES OF QUINOLIN-(1*H*)-IMINES AS A NEW CHEMOTYPE AGAINST LEISHMANIASIS 63

1. ABSTRACT 64
2. INTRODUCTION 64
3. MATERIALS AND METHODS 65
3.1. Cells and parasites 65
3.2. Compound synthesis 66
3.3. Evaluation of compound activity against promastigotes of different *Leishmania* species and axenic amastigotes of *L. infantum* 66
3.4. Generation of BMDM 66
3.5. Determination of IC_{50}s against intramacrophagic *L. infantum*, *L. major*, and *L. amazonensis* 67
3.6. Cytotoxicity on BMDM 67
3.7. Determination of oxygen consumption in parasites 68
3.8. Evaluation of mitochondrial membrane potential 68
3.9. Analysis of ROS production 68
3.10. Ethical statement 69
4. RESULTS 69
4.1. Effect of chemical libraries on *L. infantum* proliferation: structure-activity relationships (SARs) 69
4.2. Effect of quinolin-4(1*H*)-imines on mitochondrial functions 73
4.3. Quinolin-4(1*H*)-imines inhibit oxygen consumption in *Leishmania* 73
4.4. Quinolin-4(1*H*)-imines alter the mitochondrial membrane potential 73
4.5. Quinolin-4(1*H*)-imines do not induce ROS production 74
5. DISCUSSION 75
6. REFERENCES 79

CHAPTER IV. Π-Π STACKING STABILIZED POLYMERIC MICELLES FOR HYDROPHOBIC DRUG DELIVERY IN THE TREATMENT OF LEISHMANIASIS 82

1. ABSTRACT 83
2. INTRODUCTION 83
3. MATERIALS AND METHODS 85
3.1. Synthesis of quinolin-4(1*H*)-imine derivatives 85
3.2. Preparation and characterization of quinolin-4(1*H*)-imines-loaded polymeric micelles 85
3.3. Generation of bone marrow-derived macrophages 86
3.4. *In vitro* activity 87
3.4.1. Parasite cultures 87
3.4.2. Determination of IC_{50}s against intramacrophagic *L. infantum* and *L. amazonensis* 87
3.4.3. Cytotoxicity of free and encapsulated quinolin-4(1*H*)-imine derivatives on BMDM 88
3.4.4. Localization of Cy3-labeled mPEG-*b*-p(HPMAm-Bz) micelles in infected BMDM 88
3.5. *In vivo* studies 88
3.5.1. Pharmacokinetics and biodistribution 89
3.5.2. *In vivo* therapeutic efficacy of 1n-loaded mPEG-*b*-p(HPMAm-Bz) micelles 90
3.6. Ethical statement 90
4. RESULTS AND DISCUSSION 91
4.1. Characterization of empty and loaded mPEG-*b*-p(HPMAm-Bz) micelles 91
4.2. *In vitro* cytotoxicity and leishmanicidal activity of quinolin-4(1*H*)-imines-loaded mPEG-*b*-p(HPMAm-Bz) micelles 92
4.3. Intracellular localization of mPEG-*b*-p(HPMAm-Bz) micelles in BMDM 95
4.4. Pharmacokinetics and biodistribution of Cy7-labelled mPEG-*b*-p(HPMAm-Bz) micelles and 1n 97
4.5. Potential therapeutic effect of 1n-loaded mPEG-*b*-p(HPMAm-Bz) micelles 101
5. CONCLUSION 102
6. REFERENCES 103

CHAPTER V. SUMMARY, DISCUSSION AND PROSPECTS 107

REFERENCES 115

$\Delta\Psi_m$	Mitochondrial membrane potential
8-HQN	8-hydroxyquinoline
8-HQN/M	8-HQN-loaded PMs
AA	Antimycin A
ACN	Acetonitrile
AmpB	Amphotericin B
BM	Bone marrow
BMDM	Bone marrow-derived macrophages
BNIP	Bisnapthalimidopropyl
BNIPdiaminooctane	BNIPDaoct
CC_{50}	50% cytotoxic concentration
CCCP	Carbonyl cyanide m-chlorophenyl hydrazine
cDMEM	Completed DMEM
CL	Cutaneous leishmaniasis
CMC	Critical micelle concentration
CpG-D35	Type D CpG oligonucleotides
CPSF3	Cleavage and polyadenylation specificity factor 3
CrEL	Cremophor EL
DALYs	Disability-adjusted life years
DAPI	4',6-diamidino-2-phenylindole
DGAV	Direção Geral de Alimentação e Veterinária
dLNs	Draining lymph nodes
DLS	Dynamic light scattering
DMEM	Dulbecco's Modified Eagle's Medium
DMSO	Dimethylsulfoxide
DNDi	Drugs for Neglected Diseases initiative
EE	Encapsulation efficiency
FOV	Field of view
G-FINDER	Global Funding of Innovation for Neglected Diseases
G6PD	Glucose-6-phosphate dehydrogenase
GFP	Green fluorescence protein
GIT	Gastrointestinal tract
GMP	Good manufacturing practice
HA	Hyaluronic acid
HAChol	Cholesterol-modified HA
HBSS	Hank's Balanced Salt Solution
HCA	High content analysis
HCS	High content screening
HPCD	2-hydroxypropyl-β-cyclodextrin
HPLC	High-performance liquid chromatography
HPMA	N-(2-hydroxypropyl)-methacrylamide
HPMA-Bz	Benzoyloxypropyl methacrylamide

HTS	High-throughput screening
IC50	Half maximal inhibitory concentrations
ID	injected dose
IFAT	Indirect fluorescent antibody test
iFBS	Heat inactivated fetal bovine serum
IM	Intramuscularly
IV	Intravenous
kDNA	Kinetoplast DNA
L-HA	HA covalently grafted onto the surface of the liposome
L-HAChol	Hydrophobic bond interaction between cholesterol-modified HA and phospholipid bilayer of the liposomes
LC	Loading capacity
LCCM	L929 cell conditioned medium
LSPN331	2,3-di-(4-methoxyphenyl)-quinoxaline
LT-HSC	Long-term hematopoietic stem cells
M-CSF	Macrophage-colony stimulating factor
MCL	Mucocutaneous leishmaniasis
MEM	Minimum Essential Medium Non-Essential
MF+PM	Miltefosine and paromomycin
MOI	Multiplicity of infection
mPEG-*b*-p(HPMA-Bz)	Metoxy poly(ethylene glycol)-*b*-poly(N-2-benzoyloxypropyl methacrylamide)
MPS	Mononuclear Phagocyte System
MTD	Maximum tolerated dose
NPs	Nanoparticles
NTDs	Neglected Tropical Diseases
p(HPMAm)	Hydrolyzed block
PBS	Phosphate-buffered saline
PCL	Poly-caprolactone
PDI	Polydispersity index
PEG	Polyethylene glycol
PGA	Poly-glycolic acid
PK	Pharmacokinetics
PKDL	Post-kala-azar dermal leishmaniasis
PLA	Poly-lactic acid
PLGA	Poly-lactide-co-glycolide
PMs	Polymeric micelles
PPO	Polypropylene oxide
PSG	Promastigote secretory gel
PTX	Paclitaxel
PVs	Parasitophorous vacuole
R&D	Research and development
ROS	Reactive oxygen species
SARs	Structure-activity relationships

Sb(III)	Pentavalent antimonials active and toxic trivalent form
Sb(V)	Pentavalent antimonials
Si	Selectivity index
SLNs	Solid-lipid nanoparticles
SNPs	Silver NPs
SQ	Sitamaquine
SSG+PM	Sodium stibogluconate and paromomycin
TFA	Trifluoroacetic acid
TFQ	Tafenoquine
THF	Tetrahydrofuran
TMRE	Tetramethylrhodamine ethyl ester
UPLC	Ultra-performance liquid chromatography
VL	Visceral leishmaniasis
WHO	World Health Organization
Zave	Z-average

CHAPTER I. General introduction

Fig 1 – Communicable diseases defined by WHO as Neglected Tropical Diseases.

Fig 2 – *Leishmania* life cycle.

Fig 3 – Status of endemicity of (A) cutaneous leishmaniasis and (B) visceral leishmaniasis worldwide in 2022.

Fig 4 – Chemical structure of currently used drugs against leishmaniases.

Fig 5 – Chemical structures of new drug molecules in development for the treatment of leishmaniases.

Fig 6 – Structural representation from some of the nanocarriers that have been explored for the encapsulation of antileishmanial drugs.

Fig 7 – Schematic representation of polymeric micelles.

CHAPTER II. Development of an automated image analysis protocol for quantification of intracellular forms of *Leishmania* spp.

Fig 1 – Detection of intramacrophagic parasites using IN Cell Investigator Developer Toolbox.

Fig 2 – Detection of intramacrophagic parasites using Cell Profiler.

Fig 3 – Intracellular *L. infantum* labeled with anti-parasite antibodies by IFAT and with DAPI.

Fig 4 – Heterogeneous morphology of BMDM.

Fig 5 – IN Cell Investigator Developer Toolbox infectivity parameters depends on the MOI.

Fig 6 – Comparison of IN Cell Investigator Developer Toolbox and CellProfiler image analysis protocols with manual counting.

Fig 7 – Correlation between IN Cell Investigator Developer Toolbox and CellProfiler image analysis protocols.

Fig 8 – Anti-*Leishmania* activity of amphotericin B assessed with IN Cell Investigator Developer Toolbox and CellProfiler.

S1 Fig – Detection of intramacrophagic *L. amazonensis* parasites using IN Cell Investigator Developer Toolbox and CellProfiler.

CHAPTER III. Biological Evaluation and Mechanistic Studies of Quinolin-(1*H*)-imines as a New Chemotype against Leishmaniasis

Fig 1 – Effects of selected quinolin-4(1*H*)-imines on oxygen consumption of *Leishmania* parasites.

Fig 2 – Effect of selected quinolin-4(1*H*)-imines on mitochondrial membrane potential ($\Delta\Psi m$) of *Leishmania* parasites.

Fig 3 – Analysis of ROS production in *Leishmania* parasites after the addition of selected quinolin-4(1*H*)-imines

CHAPTER IV. Π-Π stacking stabilized polymeric micelles for hydrophobic drug delivery in the treatment of leishmaniasis

Fig 1 – Chemical structures (A-D) and physicochemical properties (E) of quinolin-4(1*H*)-imines used in this study and loaded in mPEG-*b*-p(HPMAm-Bz) micelles.

Fig 2 – Characteristics of mPEG-*b*-p(HPMAm-Bz) micelles (10 mg/mL polymer) loaded with different amounts of quinolin-4(1*H*)-imines derivatives

Fig 3 – Representative images of BMDM infected with *L. infantum* (A-D) or *L. amazonensis* (E-G), incubated for 3h (A, B, E and F) and 6h (C, D, G and H) with Cy3-labeled mPEG-*b*-p(HPMAm-Bz) micelles

Fig 4 – Pharmacokinetics and biodistribution of Cy7-labeled mPEG-*b*-p(HPMAm-Bz) micelles and 1n (free and loaded in Cy7-labeled PMs).

Fig 5 – *In vivo* therapeutic activity of 1n-loaded PMs against *L. infantum*.

CHAPTER III. Biological Evaluation and Mechanistic Studies of Quinolin-(1*H*)-imines as a New Chemotype against Leishmaniasis

Table 1. Anti-*Leishmania* activities of chemical libraries against *L. infantum* promastigotes and axenic amastigotes

Table 2. Leishmanicidal activities for different forms of *L. infantum* and cytotoxicities of quinolin-4(1*H*)-imine derivatives

Table 3. Effects of selected quinolin-4(1*H*)-imines against promastigotes and intramacrophagic amastigotes of *L. major* and *L. amazonensis*

CHAPTER IV. Π-Π stacking stabilized polymeric micelles for hydrophobic drug delivery in the treatment of leishmaniasis

Table I – Leishmanicidal activities against *L. infantum* and *L. amazonensis* intramacrophagic amastigotes, and cytotoxicity of free and quinolin-4(1*H*)-imine loaded in mPEG-*b*-p(HPMAm-Bz) micelles.

Table II – Characteristics of Cy7-labelled mPEG-*b*-p(HPMAm-Bz) micelles empty or loaded with 1n.

1. General Introduction

World Health Organization (WHO) classifies 20 groups of communicable diseases, prevalent in 149 tropical and subtropical countries, as Neglected Tropical Diseases (NTDs) [1]. These include infectious and non-infectious diseases caused by different agents as depicted in Fig 1 [1]. It is estimated that more than one billion people worldwide can be affected by NTDs, usually those living in poor sanitary conditions, in close contact with vectors, domestic animals and livestock, and with no access to adequate education and health care [1].

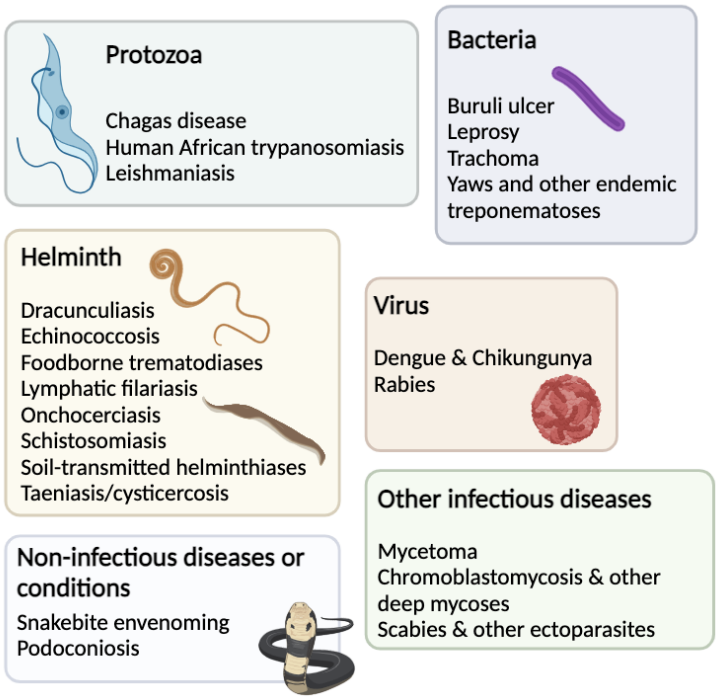

Fig 1 – Communicable diseases defined by WHO as Neglected Tropical Diseases. Created with Biorender. Adapted from WHO [1].

Although some NTDs show high mortality rates, their impact extends far beyond that. The morbidity associated reinforces the cycle of poverty of affected populations by impacting productivity of entire families and communities due to social stigma, discrimination, or to physical illnesses (disfigurement, malformations, malnutrition, blindness, cognitive impairment, etc) [2, 3]. In the 90s, a measure, designated as disability-adjusted life years (DALYs), was established to compare the burden of diseases that cause premature death with those that, although not immediately killing, lead to disabilities. The term DALYs refers to the numbers of years lost due to premature death plus the years living with disability in a population [3]. WHO reported that despite the efforts over the past decade to call

attention on NTDs, these maladies still account for at least 26 million DALYs, approximately half of the burden attributed to malaria or tuberculosis [4, 5].

The economic impact of NTDs is estimated to be billions of dollars a year [1]. In spite of this, treatments for these diseases are not profitable enough to foster the interest and investment from the pharmaceutical sector in the research and development of new drugs [6]. Trouiller P. et al (2002) showed that between 1975 and 1999, of the 1393 new drugs approved for the market only 9 (thus less than 1%) were developed for NTDs [7]. Between 2000 and 2014, of the 4006 new products that started phase I clinical trials only 66 (or 1.65%) were intended to prevent or treat NTDs [8]. Furthermore, between 2000 and 2013, 43 new approvals were referred to target NTDs; however, 67% of these were in fact developed for HIV/AIDS, malaria, and tuberculosis, and included only 3 new chemical entities [9]. While investment in drug development against these diseases has increased, their complexity, diversity, and long-standing neglect, demand considerably higher efforts.

In January 2012, inspired by the WHO roadmap on NTDs, over 80 organizations, including pharmaceutical companies, non-governmental organizations, academic and research partners, and governments from endemic countries, signed the London Declaration on Neglected Tropical Diseases, with the aim of eradicating, eliminating or controlling ten of these diseases by 2020 [10]. It was an ambitious mission, and to make it possible they relied on two approaches, mass drug administration and innovative and intensified disease management. The first approach, sponsored mainly by donation programs from pharmaceutical companies [11, 12], consisted on large scale treatments, with safe and effective drugs that could be used to control schistosomiasis, blinding trachoma, lymphatic filariasis, soil-transmitted helminths and river blindness (onchocerciasis). The second approach, aiming at better diagnosis, treatment, and improved rehabilitation measures of infected individuals, was used to control Chagas disease, visceral leishmaniasis, leprosy, sleeping sickness, and Guinea-worm disease [10]. The London Declaration on Neglected Tropical Diseases was not just about preventive chemotherapy, it rather acted also by investing on better living conditions, by giving the communities access to clean water and adequate sanitation, vector control strategies, better health care systems, and education [10].

There was a progress since the WHO publication of the first road map for NTDs, where the cooperation between countries leadership, industry, and partners, counteracted the evolution of some of these diseases, bringing some close to elimination and eradication. However, the 9 years established to

accomplish all proposals were not enough. So, learning from past experiences, WHO launched a new road map for NTDs to be executed by 2030 [13].

The next section focuses on the leishmaniases and the lack of reliable treatments against these diseases.

2. The leishmaniases

The leishmaniases are a group of vector-borne diseases caused by protozoan parasites of the *Leishmania* genus of the Trypanosomatidae family, endemic in 97 tropical and subtropical countries and territories, where around 1 billion people live at risk of contracting them [14-16]. WHO estimates that 700,000 to 1 million new cases of leishmaniases occur annually, being considered the second biggest parasite killer disease, after malaria [17, 18]. There are more than 50 species of *Leishmania* described, 20 of which are known to cause disease in humans, including the *L. donovani* complex (*L. donovani* and *L. infantum*, also known as *L. chagasi* in the New World), the *L. mexicana* complex (*L. mexicana*, *L. amazonensis*, and *L. venezuelensis), L. tropica*, *L. major*, *L. aethiopica*, and the subgenus *Viannia* (*L.* [*V.*] *braziliensis*, *L.* [*V.*] *guyanensis*, *L.* [*V.*] *panamensis*, and *L.* [*V.*] *peruviana*).

2.1. Transmission and Life cycle

Leishmania parasites are transmitted by the bite of infected female phlebotomine sandflies (genus *Phlebotomus* in the Old World and genus *Lutzomyia* in the New World) (Fig 2) [17]. There are other rare and poorly studied ways of transmission, related to organ transplantation, blood transfusion, congenital infection, or cross contamination through the use of syringes among drug-addicted people [19-21].

Leishmania are digenetic parasites that during their life cycle alternate between the promastigote form, motile parasites with an extended flagellum that proliferate extracellularly and reside in the insect vector, and the amastigote form, a non-motile stage that develops within the mononuclear phagocytes of their mammalian hosts, including humans (Fig 2) [22]. During a regular blood feeding, infected sandflies inoculate infective promastigotes into the skin. Simultaneously, a promastigote secretory gel (PSG) is also injected. This is a biological plug produced by parasites when they are still in the sandfly that alters the normal blood feeding behavior – as a consequence, longer and more attempts are required for the sandfly to feed, increasing the efficiency of infection [23-26]. Additionally, sandflies also regurgitate their saliva containing anti-inflammatory, antihemostatic, and immunomodulatory molecules

that facilitate the blood meal process and indirectly help *Leishmania* parasites to thrive [27, 28]. The combination of parasites, PSG, and saliva contribute to the recruitment of a high number of macrophages and neutrophils to the site of infection, which is favorable to promastigotes that will be promptly internalized and protected from the hostile extracellular environment of the mammalian host [29, 30]. Neutrophils play an important role in shaping the innate immune response by killing invading microorganisms. Studies have shown that neutrophils are among the first cells arriving to the site of infection, and their role on the development of leishmaniasis is dependent, among other factors, on the *Leishmania* species [31, 32]. There are *Leishmania* species capable of surviving and even replicating inside neutrophils, using them as safe shelters, while others are killed by these cells [32, 33]. Nevertheless, it is well established that *Leishmania* parasites use neutrophils transiently to finally invade macrophages. There are two potential mechanisms suggested for this silent relocation of promastigotes: 1) macrophages phagocytize parasites released from dying neutrophils, and/or 2) they phagocytize apoptotic neutrophils infected with *Leishmania*, a model known as 'Trojan Horse' [33] [34]. Either way, promastigotes are internalized by macrophages, where they survive and proliferate [35]. Upon internalization, promastigotes start to differentiate into amastigotes inside the newly formed phagosome, characterized by a moderate pH acidification. Subsequently, early phagosomes undergo a maturation process, characterized by the fusion with early and late endosomes and lysosomes, up to the formation of phagolysosome-like structures, known as parasitophorous vacuoles (PVs) [35]. Inside PVs, *Leishmania* spp. create a perfect niche to survive and replicate, acquiring host cell nutrients and evading host defense mechanisms [35]. The structure of *Leishmania* PVs differs morphologically depending on species. For instance, during *L. major*, *L. donovani*, and *L. infantum* infection, PVs are compact and contain a single amastigote, whereas infections with *L. amazonensis* or *L. mexicana* occur within large communal PVs harboring several amastigotes [36]. After several divisions, amastigotes are released, re-entering surrounding macrophages [15, 37]. While blood feeding from an infected mammalian host, sandflies ingest macrophages containing *Leishmania* amastigotes. Once in the sandfly abdominal midgut, amastigotes are released from macrophages and start to differentiate into procyclic promastigotes, that show low mobility capacity and a short flagellum. During the amastigote to metacyclic promastigote transition, promastigotes undergo a series of differentiation and replication steps. Metacyclic promastigotes, the *Leishmania* infectious form, are transmitted to the mammalian host during a blood meal, completing the cycle [38-41].

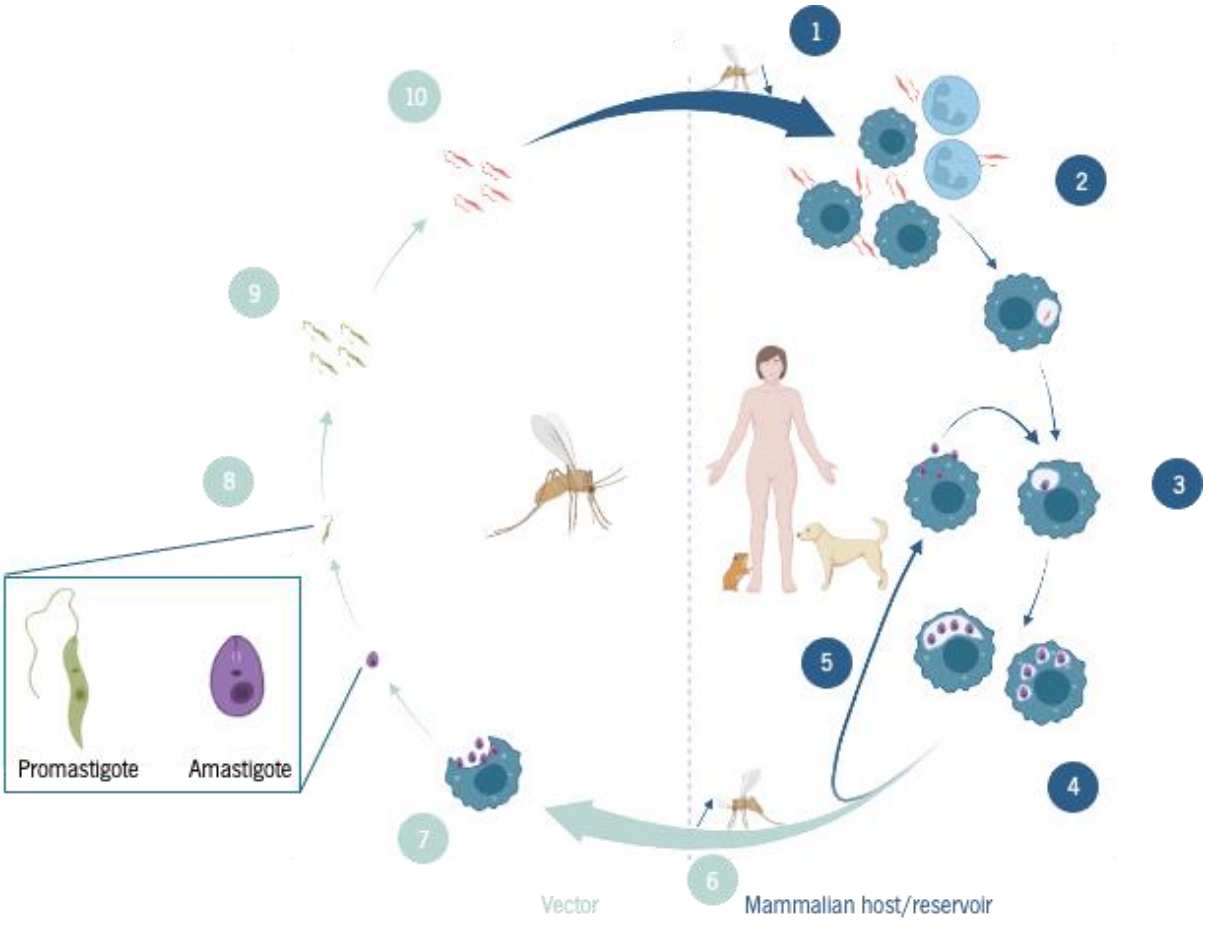

Fig 2 – *Leishmania* life cycle. *Leishmania* parasites have a digenetic life cycle that involve an insect vector and a mammalian host. The transmission starts with an infected female phlebotomine sandfly injecting promastigotes into the skin of a mammalian host, during a regular blood feeding (1). Promastigotes are then taken up by phagocytic cells, such as macrophages and neutrophils (2). Inside specific compartments of those cells, namely parasitophorous vacuoles (PVs), promastigotes differentiate into amastigotes (3). The structure of PVs varies among *Leishmania* species, with some species proliferating within compact PVs which harbor a single amastigote, while others develop within large communal PVs that accommodate several amastigotes (4). After some divisions, amastigotes are released and invade surrounding macrophages (5). During a blood meal, a new sandfly ingests *Leishmania*-infected macrophages that release the amastigotes in the insect gut (6,7). Amastigotes transform into procyclic promastigotes (8), which multiply in the midgut (9). Promastigotes differentiate into metacyclic promastigotes (10), the infective stage, which will be transmitted to a mammalian host, initiating a new cycle. Created with Biorender.

2.2. Clinical manifestations

The socioeconomic status of the most people affected by *Leishmania* parasites is a significant factor for the development of leishmaniases. Poor housing and the lack of proper sanitary conditions facilitate sandfly breeding and survival. Poverty is also associated with poor nutrition, a major contributor of progression to clinical disease. Lower levels of education and literacy together with inadequate healthcare services frequently lead to delays in diagnosis and proper treatment and, consequently, a worst prognosis [42, 43].

Leishmaniases are characterized by three main syndromes, whose manifestations depend on the parasite species and the host immune response. The most common form is cutaneous leishmaniasis (CL), with an estimated global incidence of 600,000 to 1 million new cases per year [17]. It is characterized by severe skin lesions at the site of inoculation, mostly self-healing, that often lead to disfiguration and stigmatizing scars, promoting morbidity, especially in women [17, 44]. According to WHO, 95% of new CL cases occur in the Middle East, central Asia, the Mediterranean basin, and the Americas (Fig 3) [17]. Mucocutaneous leishmaniasis (MCL) is characterized by parasite migration to mucosal tissues, such as nose, mouth, and throat, promoting their destruction. Around 90% of the cases occur in Bolivia, Brazil, Ethiopia, and Peru [17]. Finally, visceral leishmaniasis (VL), also known as kala-azar, is a life-threatening condition in over 95% of the cases. It is estimated that 50,000 – 90,000 new cases occur each year worldwide, affecting mainly children and young adults. *Leishmania* spp. causing VL disseminate to internal organs, such as spleen, liver, and bone marrow, leading to weight loss, fever, hepatosplenomegaly, and ultimately death. In 2022, about 85% of the new cases were reported in seven countries: Brazil, Ethiopia, India, Kenya, Somalia, South Sudan, and Sudan (Fig 3) [17].

Less common leishmaniasis manifestations include diffuse CL, disseminated CL, and post-kala-azar dermal leishmaniasis (PKDL). As the name indicates, they are all characterized by cutaneous lesions and, except for PKDL, are caused by dermotropic species. Diffuse CL is characterized by widely disseminated skin lesions showing no ulceration (except for some immunosuppressed individuals) that do not heal spontaneously and frequent relapses. Disseminated CL presents with 20 to hundreds of nodules or ulcerated lesions [44]. Lastly, PKDL, mostly caused by *L. donovani*, arises after the apparent cure of VL and manifests as macules that can later become nodular or papular. These lesions can act as parasite reservoirs and, curiously, they heal spontaneously in African but not in Indian patients [44].

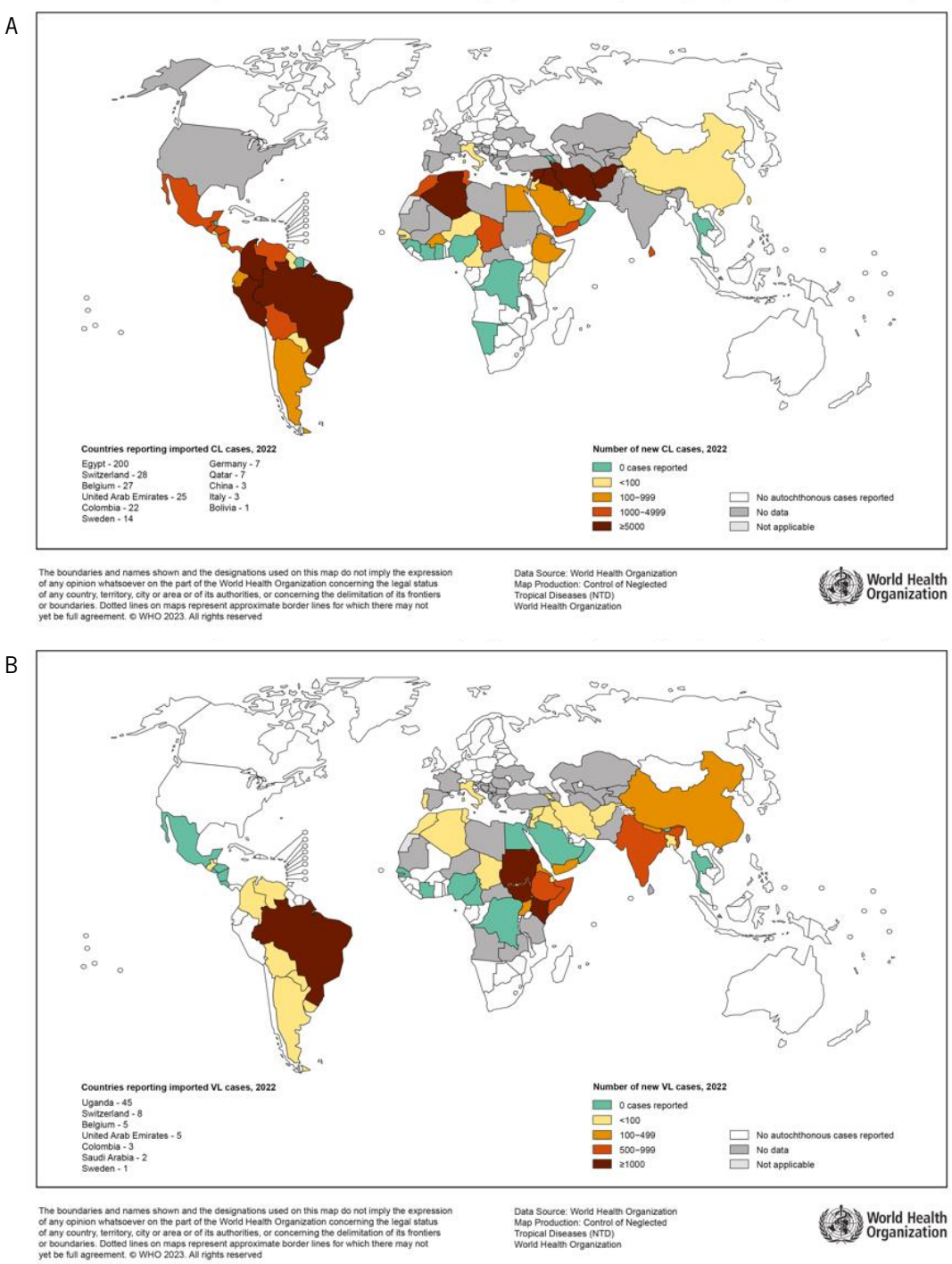

Fig 3 – Status of endemicity of (A) cutaneous leishmaniasis and (B) visceral leishmaniasis worldwide in 2022. The data presented was reported in November 2023. Image obtained from WHO [45].

3. Current treatments

In the absence of a human vaccine, leishmaniases control relies on chemotherapy. Treatment approaches should be carefully chosen because efficacy may vary, depending on the particular *Leishmania* spp., clinical manifestation, and host immune status [18]. The low number of available drugs, most in use for many years, is a major problem. Furthermore, these drugs are associated with severe side effects, long treatment durations, inadequate administration systems, variable efficacy, high cost, and emergence of resistance and therapeutic failures.

The following sections address the current treatments, with emphasis on the mechanism of action and the main side effects associated with each compound.

3.1. Pentavalent antimonials

Pentavalent antimony (Sb(V))-containing drugs are used against all forms of leishmaniasis since late 1930s. Despite concerns with toxicity and the development of resistance (as high as 60% in Bihar, India, and Nepal), these compounds remain the first choice in many endemic countries, largely due to their low price and high availability [15, 44, 46-49].

There are two Sb(V) compounds commercially available: meglumine antimoniate and sodium stibogluconate, each with approximately 8.5% and 10% of Sb(V), respectively (Fig 4) [44]. Sb(V) can be administered intramuscularly (IM) or by intralesional injection for treatment of CL/MCL and IM or by slow intravenous (IV) injection for treatment of VL. The mechanism of action is not fully known, but this compound is likely a prodrug that has to be reduced into its active and toxic trivalent form Sb(III) [50]. Trypanothione reductase, an enzyme essential to *Leishmania* by maintaining their major thiol, trypanothione, in its reduced state, and thus protecting parasites from oxidative damage, is targeted by the drug. Indeed, it was shown that Sb(III) binds trypanothione reductase with high affinity inhibiting its activity [51, 52]. Consequently, parasites are less capable to neutralize reactive oxygen species (ROS, including those produced by macrophages during infection), increasing oxidative stress and, eventually, dying [51].

The emergence of resistant strains and treatment failure are usually attributed to misuse of Sb(V), including inappropriate treatment regimens and interruption of treatments due to side effects. In India, the presence of arsenic, which shares many structural and chemical properties with antimony, in drinking water was also suggested to contribute to development of resistance [53].

The list of side effects associated with pentavalent antimonials is long, and the most common ones being nausea, abdominal pain, anorexia, vomiting, and lethargy. Although nephrotoxicity, cardiotoxicity, and death are rare, alterations in pancreatic and liver enzymes are common [44].

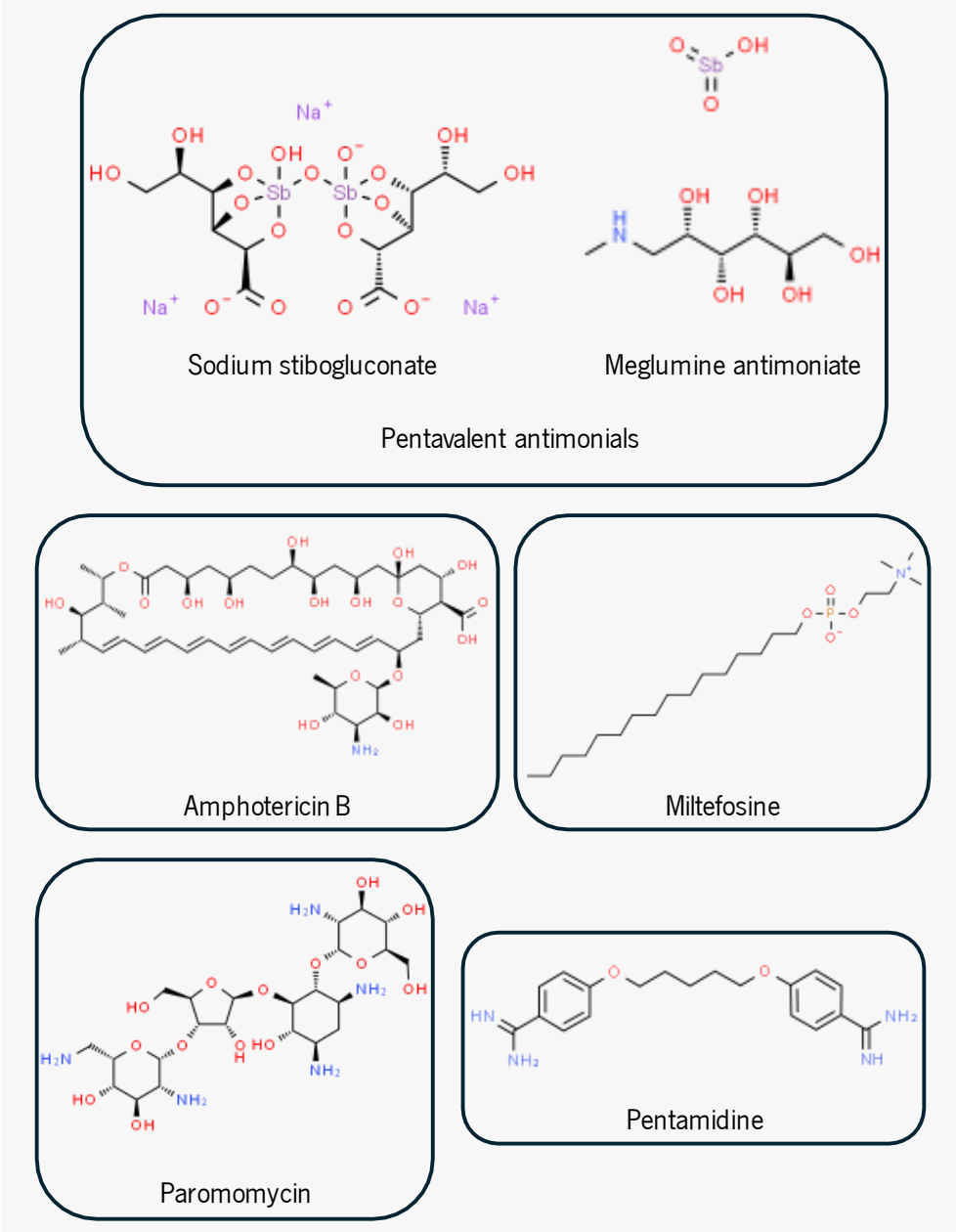

Fig 4 – Chemical structures of currently used drugs against leishmaniases. Images were designed using Chemicalize.

3.2. Amphotericin B

Amphotericin B (AmpB) is a polyene antibiotic with antifungal activity first isolated in the 1950s from *Streptomyces nodosus* and used since the 1960s in MCL and VL patients unresponsive to pentavalent

antimonials (Fig 4) [54-56]. AmpB shows selective toxicity towards *Leishmania* parasites, a fact justified by its preferential binding to ergosterol, the major parasite sterol, and not to cholesterol, present in mammals [57, 58]. This activity leads to the formation of pores, changes in cell permeability, and depolarization of the membrane, inducing metabolic shock and parasite death.

Administration of conventional AmpB (AmpB deoxycholate) requires a slow IV infusion for several hours, in hospital context, which increases the final cost of the treatment and decreases the patient compliance towards the treatment [44]. The drug unfortunately also shows serious side effects as severe fever, rigor and chills, thrombophlebitis, hypokalemia, cardiac toxicity, and commonly acute nephrotoxicity [44, 59, 60]. To improve AmpB pharmacokinetics and its biodistribution, several formulations were developed, namely, AmpB lipid complex (Abelcet®), AmpB colloidal dispersion (Amphocil®/Amphotec®), and liposomal AmpB (AmBisome®), all administered IV [61-63]. Although the efficacy of these formulations is similar to that of AmpB deoxycholate, their toxicity is much lower. This allows for the use of a higher dose of drug per patient, reducing treatment duration and hospitalization [44]. The advantages of using delivery systems to improve biodistribution and pharmacokinetics of drugs will be addressed in section 5 of this chapter. AmpB lipid complex and AmpB colloidal dispersion are not generally recommended for the treatment of leishmaniases due, mainly, to the lack of treatment trials [64]. However, these formulations are occasionally used as off-label therapeutic options for VL, with some clinical reports referring to complete remission [65-67].

In contrast to Abelcet® and Amphocil®/Amphotec®, AmBisome® has been object of many clinical trials that validated its safety and efficacy over AmpB deoxycholate as an antileishmanial drug [44]. Nevertheless, it still has some drawbacks, like its high cost and instability at high temperatures, both limiting its use in developing countries [68].

To make AmBisome® accessible to poor regions, a collaboration between WHO and Gilead Sciences was established in 2011, consisting in the donation of thousands of AmBisome® vials to control VL in strategically important endemic areas [69]. The use of AmBisome® is widely accepted in VL, PKDL, and MCL treatments, but its use in CL has not been properly addressed [44, 70-72].

3.3. Miltefosine

Miltefosine is a phosphatidylcholine analogue firstly developed for breast cancer and other solid tumors (Fig 4). Following on several studies showing its efficacy against *Leishmania in vitro* and in animal models, its clinical relevance for human leishmaniases was assessed [73-77]. In this way, miltefosine

emerged in the 21st century as the first and, up to now, single oral drug to treat CL, MCL, and VL [78-80]. This was a relevant progress as it allowed to overcome the need for hospital admission.

The leishmanicidal activity of miltefosine is attributed to several mechanisms, including inhibition of lipid metabolism, reduction of mitochondrial cytochrome *c* oxidase activity, which leads to the decrease in ATP levels and oxygen consumption, and the induction of an apoptosis-like cell death [81-83]. Miltefosine appears also capable of modulating the host immune system by inducing the activation of the Th1 cytokine response [84].

Contrary to efficiency rates observed in Indian patients with VL (>90%), a natural resistance to miltefosine was observed in Brazilian patients, which showed a cure rate lower than 70% [85]. Also, a study showed that after treatment of a dog with miltefosine and allopurinol, *L. infantum* parasites were less susceptible to miltefosine [86].

Most of the side effects associated with miltefosine (nausea, vomiting, diarrhea, and anorexia) are mild and solved with time; increased levels of hepatic transaminases and creatinine are usually of no major concern, reversible, and dose-dependent. Still, miltefosine is teratogenic, a fact that limits its use in age-bearing women [44, 87]. Some studies also reported severe and debilitating gastrointestinal symptoms. These drawbacks together with need for a long 28-day course of treatment can lead to treatment interruption and poor compliance towards the regimen [44, 88].

3.4. Paromomycin

Paromomycin is an aminoglycoside antibiotic first proposed in 1986 as a topical agent to treat CL (Fig 4) [89]. Later, in 2006, it was approved for VL in India, where it showed a cure rate of around 94% with a regimen of 15 mg/kg for 21 days [90]. However, in East Africa, efficacy dropped to less than 50%, and even longer treatments or a regimen of 20 mg/kg for 21 days could not surpass 90% and 85% efficacy, respectively [91, 92].

The activity of paromomycin against *Leishmania* parasites is not fully understood, but its effect in bacteria is mainly associated with protein synthesis interference by specifically binding to 16S ribosomal RNA.

Paromomycin has no serious side effects. Renal toxicity is rare and only some patients may register an increase in hepatic enzyme concentrations. Unfortunately, resistance develops easily when the drug is used in monotherapy [93].

3.5. Pentamidine

Pentamidine is an aromatic diamidine in use for the treatment of VL since the 50s as an alternative to antimonials when resistance to this drug is an issue (Fig 4).

The mechanism of action of pentamidine is not well established, but it has been reported that the drug enters parasites via arginine and polyamine transporters and binds to kinetoplast DNA [94, 95].

Pentamidine shows severe side effects, including diabetes mellitus, cardio and renal toxicity, and decrease in blood pressure when administered IV [95]. Given the reported toxicity and the low efficacy in certain regions, pentamidine has practically been abandoned in recent years. However, WHO still recommends its use as first-line treatment for DCL caused by *L. guyanensis*, *L. panamensis*, and *L. aethiopica* and also as a maintenance therapy to reduce relapse rates of VL in HIV patients [96].

3.6. Combination chemotherapy

Combination therapy aims at enhancing treatment efficacy by using multiple drugs with synergistic and/or additive effects. This therapeutic approach reduces the emergence of drug resistant parasites and allows for a decrease in the dosage, duration, toxicity, and costs of the treatment.

Combination of sodium stibogluconate and paromomycin (SSG+PM) administered twice a day for a 17-day period is currently used as first-line treatment for VL in Eastern Africa. Nevertheless, since daily injections are painful and require hospitalization, a Phase III clinical trial was completed in 2021 among patients in Ethiopia, Kenya, Sudan, and Uganda with the aim of replacing the SSG+PM treatment for a combination of miltefosine and paromomycin (MF+PM) [97]. The clinical outcome of the latter was similar to SSG+PM but has the advantage of being administered for a shorter period (14 days) and with only one and less painful injection per day. Besides, this new treatment showed a lower risk for development of PKDL.

Additional combination therapies have been tested worldwide in clinical leishmaniasis trials. The appropriate treatment option is always dependent on the *Leishmania* species, the geographical area, and the immune system of the patient. For instance, in the Indian subcontinent and South-East Asia, besides the MF+PM therapeutic option, a combination of liposomal AmpB with paromomycin or miltefosine is used to treat VL [15]. Also, due to the high incidence of PKDL in South Asia (5-15% of people treated for VL), a Phase II clinical trial was conducted to address the efficacy and safety of liposomal AmpB as a monotherapy or in combination with miltefosine with the aim of treating PKDL. The collected data indicated that, while both regimens demonstrated similar efficacy to the current first

line treatment, a shorter treatment duration reduces the risk of side effects, an improvement over standard treatments [97, 98].

Some Latin American countries record the highest burdens of CL worldwide. Hence, in Bolivia, Brazil, Panama, and Peru, a Phase III study is being conducted to address the likelihood of combining thermotherapy with miltefosine to treat uncomplicated CL. In the preceding Phase II, this therapeutic approach ranked better than thermotherapy alone [97].

While combination therapy using approved drugs constitutes a valid option to facilitate leishmaniases treatment, the development of new, safe, affordable, and easy to administer drugs should pursue [97, 99].

4. New chemical entities

Drugs for Neglected Diseases initiative (DNDi) is an international non-profit organization that works in drug research and development (R&D). The final goal of DNDi is to deliver new treatments for neglected diseases, including leishmaniases [97]. In addition to enhancing the safety, tolerability, and effectiveness of existing drugs, DNDi, in collaboration with more than 250 R&D partners, has been working since 2003 to deliver a portfolio of new antileishmanial compounds to improve patient care [97].

As part of these efforts, six novel chemical entities entered Phase I/II clinical trials (LXE408, DNDI-0690, DNDI-6148, GSK3494245/DDD1305143, DNDI-0699 and DNDI-2319), while a seventh (DNDI-6174) may soon start Phase I [100]. Among these alternatives, which are detailed below, DNDi expects to have at least two new oral treatments finishing Phase III by 2028.

4.1. LXE408

A collaboration of DNDi with Novartis initiated in 2020 led to LXE408, a possible new oral treatment for VL. This compound resulted from the optimization of GNF6702, a selective inhibitor of the kinetoplastid proteasome [101]. LXE408 is the most advanced candidate in clinical trials, currently undergoing Phase II trials in India and Ethiopia since late 2023 and 2024, respectively [102].

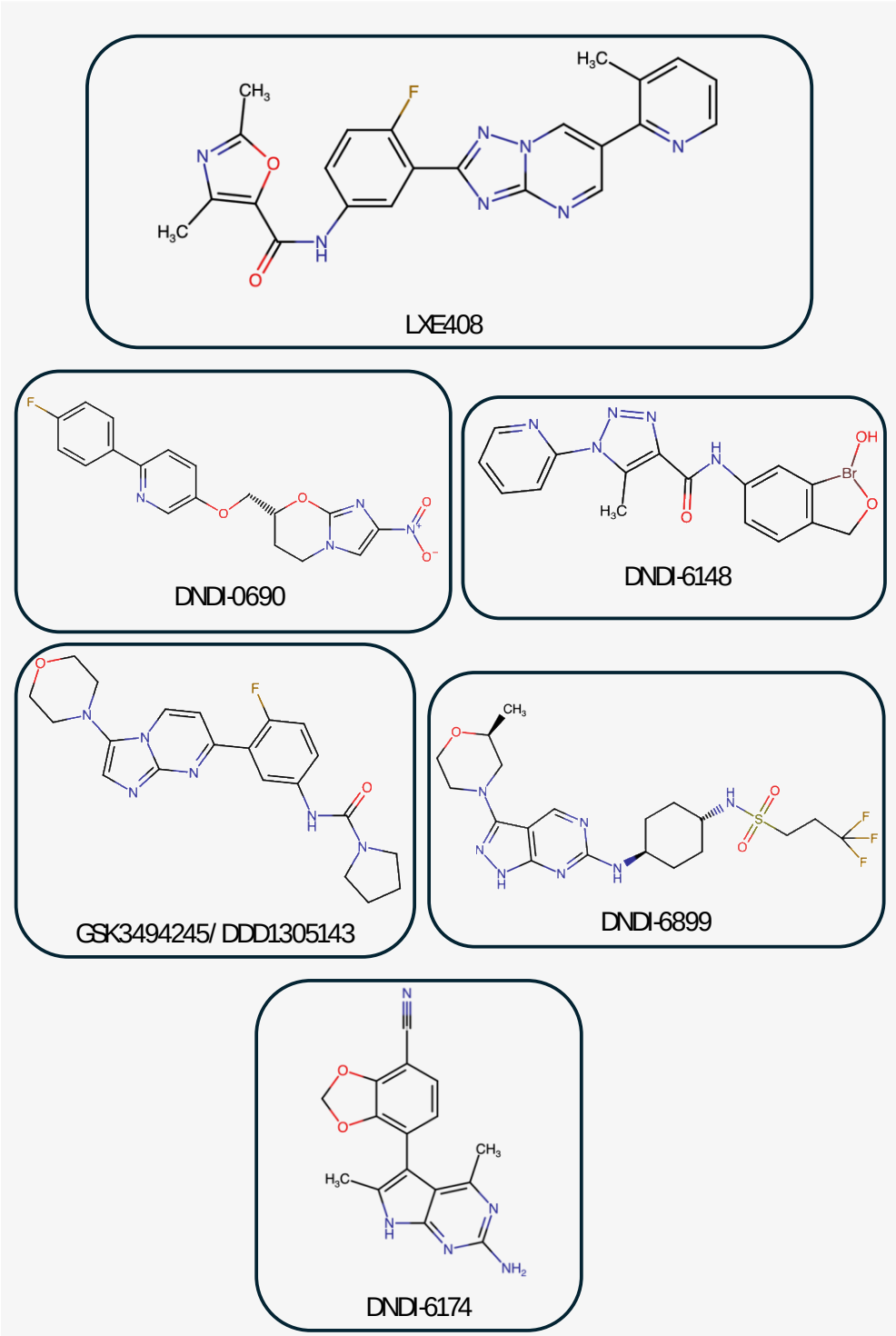

Fig 5 – Chemical structures of new drug candidates in development for the treatment of leishmaniases. Images were designed using Chemicalize according to literature: LXE408 [101]; DNDI-0690 [103]; DNDI-6148 [104]; GSK3494245/DDD1305143 [105]; DNDI-6899 [106]; DNDI-6174 [107].

4.2. DNDI-0690

DNDI-0690 was identified upon an agreement established between DNDi and TB Alliance, which allowed access to a selected library of nitroimidazoles, primarily investigated for their efficacy against tuberculosis. DNDI-0690 is a clinical drug candidate for VL and possibly for CL [103, 108]. The mechanism of action is yet to be determined. During the Phase I multiple-ascending dose study, after a 10-day exposure to the treatment, some participants exhibited biological abnormalities, the mechanism of which could not be elucidated. Consequently, the clinical development of DNDI-0690 has been suspended [100].

4.3. DNDI-6148

DNDI-6148, an analogue of acoziborole (a clinical candidate for sleeping sickness), was identified as a potential option for the treatment of VL [104]. DNDI-6148 targets the cleavage and polyadenylation specificity factor 3 (CPSF3) endonuclease, which constitutes a previously unexplored drug target [104]. Following a Phase I clinical trial for a single oral dose, preparations began for a multiple-ascending dose study. Unfortunately, the development of DNDI-6148 ended up being deprioritized due to reproductive toxicity observed in pre-clinical studies, which could require contraceptive use for women of childbearing potential [100].

4.4. GSK3494245/DDD1305143 and DNDI-6899

DNDi together with GSK and the Drug Discovery Unit of the University of Dundee developed two compounds. One, GSK3494245/DDD1305143, resulted from optimization of a series of molecules previously screened against *Trypanosoma cruzi* and acts as a proteasome inhibitor [105]. It is currently undergoing a Phase I clinical study, and the single-ascending dose is completed. The other, DNDI-6899 (GSK3186899/DDD853651), is a pyrazolopyrimidine analog which inhibits cdc-2-related kinase 12 [106, 109]. There are few chemically well-validated drug targets in *Leishmania*, making this drug a priority for development [109]. Preparations are underway for the initiation of a clinical Phase I multiple-ascending dose study set to begin in 2024 [100].

4.5. DNDI-2319

DNDI-2319, a type D CpG oligonucleotide (CpG-D35), is being developed as a combination therapy with pentavalent antimony since it functions as an immunomodulator to stimulate the innate immune system. It is being developed for the treatment of complicated CL and PKDL. Preclinical studies in

nonhuman primates showed no toxicity, even at doses ten times higher than the therapeutic dose [110]. In June 2023, a Phase I multiple-ascending dose study was approved in Colombia. Unfortunately, by the end of December, the study encountered unexpected issues related to the low number of participants meeting the enrollment criteria. As a result, adjustments to the protocol are currently underway, with the aim of completion by the end of 2024 [100].

4.6. DNDI-6174

DNDI-6174 emerged as a pre-clinical candidate for VL upon lead optimization of the L205 series. It is a pyrrolopyrimidine derivative, and its activity is related to inhibition of the *Leishmania* cytochrome bc_1 complex (complex III) of the mitochondrial electron transport chain [107]. This compound showed good efficacy in preclinical studies using both mice and hamster models for VL. Its enrollment into Phase I will depend on the data generated from these studies [107]. DNDi and partners also conducted stability analyses from a pharmaceutical development perspective, including a six-month stability assessment of the good manufacturing practice (GMP) material, as well as evaluations of storage and packaging conditions, achieving successful results. According to project updates by DNDi, an *in vivo* study showed the potential of DNDI-6174 against CL [100].

4.7. Compounds not in clinical trials

In addition to the clinical candidates referred to above, there are other promising drug candidates although still in an embryonic stage of development. Next, we will review quinolines and structurally related heterocyclic compounds, some of which are proven antimalarials, as potential sources of new treatments against *Leishmania* parasites. Heterocycles are defined as organic compounds with a ring structure composed of at least one heteroatom, usually nitrogen, oxygen, or sulfur. For instance, pentavalent antimonials and paromomycin are heterocyclic compounds [111]. The derivatives of quinoline, a heterocyclic nitrogen compound, are known for their activity against malaria parasites. This is the case of quinine, the first naturally isolated compound used as an antimalarial drug, and of its 4'- or 8'-aminoquinolines derivatives, chloroquine and mefloquine and primaquine, tafenoquine, and sitamaquine, respectively.

The 4-aminoquinolines chloroquine and mefloquine were both active *in vivo* against *L. amazonensis*, reducing the lesion size of a CBA infected-mice. However, only chloroquine reduced the parasite burden in the draining lymph nodes [112]. Among the 8-aminoquinolines, primaquine-loaded nanoparticles were more efficient than free drug in reducing the parasite burden in the liver of BALB/c mice infected

with *L. donovani* with no signs of severe toxicity [113]. Tafenoquine, recently approved by FDA for the treatment of *Plasmodium vivax*, has been extensively studied for its potential against VL by *L. donovani*. It is known to cause parasite mitochondrial disfunction by inhibiting cytochrome bc_1 complex (complex III) and subsequent depolarization of mitochondrial membrane potential [114]. This 8-aminoquinoline compound induces an apoptosis-like death in promastigotes by promoting generation of ROS and deregulation of Ca^{2+} levels, followed by DNA fragmentation [114]. Sitamaquine, another 8-aminoquinoline, reached Phase II clinical trials as an oral drug for treatment of VL. Similar to tafenoquine, sitamaquine induces apoptosis-like death of *L. donovani* but it targets mitochondrial succinate dehydrogenase (complex II) [115]. The fact that this drug can be administered orally is a major advantage. Nevertheless, adverse side effects observed in humans (e.g. methemoglobinemia and nephrotoxicity) limited further pharmaceutical development of sitamaquine as an antileishmanial drug [116].

Another quinoline derivative, 8-hydroxyquinoline (8-HQN), was found to have better *in vitro* efficacy than amphotericin B against several cutaneous or visceral *Leishmania* species, namely *L. amazonensis*, *L. braziliensis*, and *L. infantum* [117]. Although the drug causes significant depolarization of the membrane potential in promastigotes, the underlying mechanism responsible for this phenomenon is not yet known. No alteration in ROS production or plasma membrane permeability were observed. The 8-HQN are known for their metal chelation properties, namely of iron, which could diminish the ability of parasites to infect mammalian cells [118, 119]. The *in vivo* efficacy of 8-HQN was evaluated in *L. amazonensis*-infected BALB/c mice [117]. The quinoline derivative prompted a significant reduction of lesion size and of parasite load in the liver, spleen, and draining lymph nodes (dLNs), when compared to untreated animals. The parasite number in lesions and dLNs was even significantly lower than that of the amphotericin B-treated group [117]. Future therapeutic optimizations can include the use of delivery systems in order to improve *in vivo* efficacy and safety of these drugs (see 5. Nanomedicine).

The following sections will address delivery systems that have been investigated for the treatment of the leishmaniases.

5. Nanomedicine

The term nanomedicine refers to the application of nanomaterials in biomedical research and clinical practice [120]. The use of nanocarriers as a means to improve treatment has been extensively studied in several diseases [121]. By choosing and controlling the chemical and physical properties of nanoparticles (NPs), it is possible to encapsulate a large amount of drug molecules, considerably

increasing the solubility of poor water-soluble compounds [122, 123]. The protection granted by nanoparticles may also increase the stability of the loaded drug, their blood circulation time, and their delivery into infected cells/tissues [122, 123]. This strategy enhances biodistribution and promotes stronger therapeutic performance by controlling drug release kinetics while minimizing side effects [124]. There are two typical categories of NPs that can be used for therapeutic and diagnostic purposes: organic NPs produced from natural or synthetic organic molecules (e.g. polymeric micelles, protein-based NPs, liposomes, and dendrimes) and inorganic NPs (e.g. gold NPs, silica NPs, iron oxide, and quantum dots) [125]. The use of NPs for drug delivery in humans was first authorized by FDA (1995) and EMA (1996) with Doxil®, a PEGylated liposomal formulation of doxorubicin used as an anticancer chemotherapy.

Most of the drugs available for NTDs suffer from poor pharmacokinetics and limited specificity for infected tissues, causing major side effects and increasing resistance and treatment failure [126-129]. Similarly to other diseases, NPs can bring advantages to NTD therapies, with several types showing promising results in this context, including liposomes, solid-lipid nanoparticles (SLNs), polymeric NPs, inorganic NPs, and nanoemulsions, among others [123]. The development of such nanoparticle systems suffers from the same problem as general drug development against NTDs, i.e. an almost non-existent investment, mainly due to their lower financial return for pharmaceutical industries. According to the Global Funding of Innovation for Neglected Diseases (G-FINDER) project, despite the overall increase in funding for neglected diseases over the past decades, most of the investments were allocated to HIV, malaria, and tuberculosis [130, 131].

The fact that *Leishmania* amastigotes survive and proliferate inside parasitophorous vacuoles of macrophages, mainly of the liver, spleen, and bone marrow, places leishmaniases among the NTDs in which NPs can be particularly useful. First, drugs must overcome several structural barriers for successful accumulation at the target site, and second, macrophages belong to the Mononuclear Phagocyte System (MPS) that promotes the sequestration of the nano formulations immediately upon injection. This is due to adsorption of plasma proteins onto NP surface, promoting their internalization by phagocytes, mainly in the liver and spleen [132-134]. In most diseases, uptake of opsonized NPs by the MPS is problematic as it leads to high NP clearance rates and poor delivery to the target cells/tissues [134]. In such cases, strategies like the modification of the NP surface, such as coating them with polyethylene glycol (PEG), reduces their recognition and uptake by MPS, increasing their circulation time [135]. However, in the case of leishmaniases, where parasites infect macrophages, rapid internalization by phagocytic cells is not a problem. Nevertheless, the therapeutic concentration of

drugs in less reachable targets like the skin and bone marrow can also benefit from coating NPs with PEG. On a study using naturally infected dogs with *L. infantum*, PEGylated meglumine antimonate-containing liposomes exhibited higher stability, increased circulation lifetime, and better accumulation in liver, spleen, and bone marrow, when compared with conventional liposomes [136]. Also, although conventional and PEGylated liposomes did not show significantly different levels of meglumine antimonate in the skin, the latter appear to have better targeting efficiency.

Up to now, AmBisome®, a liposomal form of AmpB, is the only approved NP for treatment of leishmaniases. Even though there are several other drugs showing promising results *in vitro*, these need to be confirmed *in vivo* [137]. Since AmBisome® is currently the most potent treatment against *Leishmania* parasites, efforts towards the development of new nanocarriers for these diseases used mostly AmpB [138-140]. However, the non-translation of these studies into effective anti-*Leishmania* therapies prompted the study of alternative drugs, changes in treatment regimens, or the development of better drug delivery systems [141].

Nanocarrier properties can be adjusted to encapsulate approved and new or repurposed anti-*Leishmania* drugs, i.e. approved compounds that can be used in the treatment of a new medical condition (e.g. miltefosine). In the next sections some NPs for their capacity to encapsulate currently authorized or new antileishmanial drugs are discussed (Fig 6).

5.1. Liposomes

The most common nanocarriers studied for leishmaniases are liposomes as they are biocompatible, biodegradable, can be functionalized for internalization by infected macrophages, and can carry both hydrophilic and hydrophobic drugs [142]. As previously mentioned, the fact that macrophages are responsible for the clearance of liposomes *in vivo* favors the delivery of the drugs to the cells most affected by *Leishmania* [143]. Liposomes, first described in the 1960s by Alec Douglas Bangham, are defined as small artificial spherical vesicles ranging from 30 nm to several micrometers and composed by one or more phospholipid bilayers. The particular arrangement of the phospholipid polar heads creates an aqueous core that can accommodate hydrophilic drugs while lipophilic molecules can be solubilized in the bilayer. The properties of liposomes, e.g. circulation time, amount of drug that can be loaded, and NP stability, differ depending on their lipid composition, size, surface charge, and method of preparation. Liposome surfaces can also be decorated with ligand that recognize receptors that are overexpressed on target specific cells [144-146].

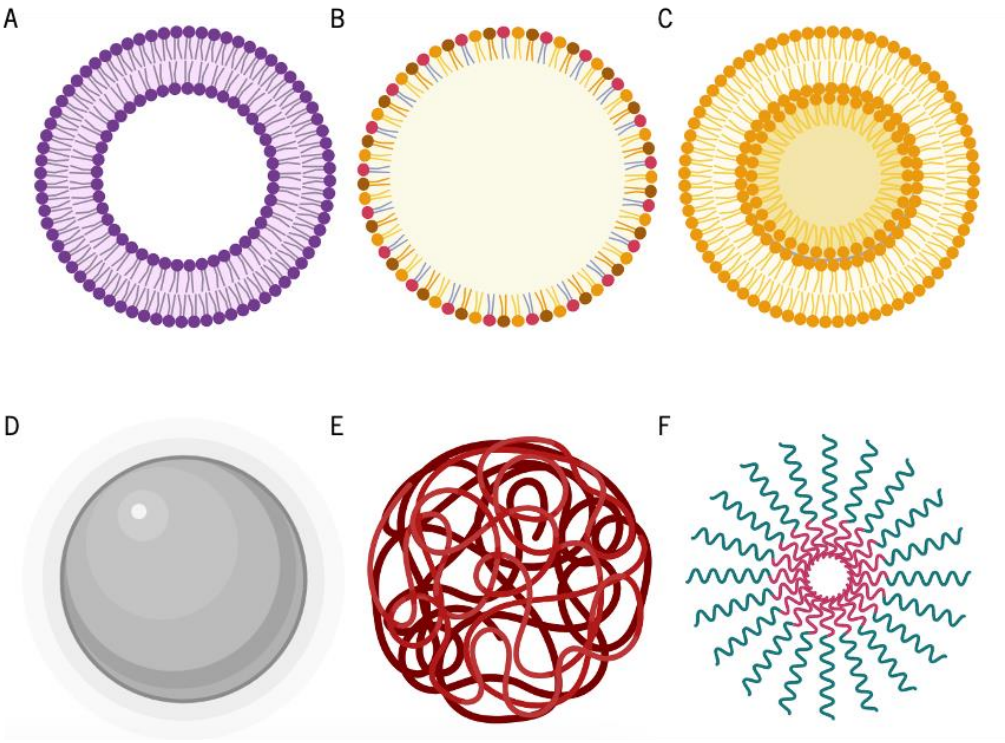

Fig 6 – Structural representation from some of the nanocarriers that have been explored for the encapsulation of antileishmanial drugs. A – Liposome; B – Solid lipid nanoparticle; C – Emulsome; D – Silver nanoparticle; E – Polymeric nanoparticle; F – Polymeric micelle. Created with Biorender.

5.1.1. Encapsulation of approved anti-*Leishmania* drugs in liposomes

Miltefosine is one of the approved drugs successfully encapsulated in PEGylated liposomes, which showed enhanced efficacy against CL caused by *L. major* [147]. The therapeutic effects of free miltefosine and miltefosine encapsulated in conventional or PEGylated liposomes were evaluated in *L. major*-infected mice. Both liposomal formulations significantly reduced lesion size and parasite burden in the spleen compared to free drug. Notably, PEGylated liposomes revealed superior efficiency, attributed to the use PEG, which stabilizes liposomes, prevents aggregation and promote long circulation, ultimately leading to better therapeutic outcomes. Additionally, histopathological analysis of the kidneys demonstrated that both liposomal formulations were safer than the free drug, further corroborating the potential of the nanocarriers to minimize drug toxicity while maintaining or improving therapeutic efficacy [147].

5.1.2. Encapsulation in liposomes of repurposed drugs with anti-*Leishmania* effect

Currently available drugs for leishmaniases were introduced through a repurposing approach, which offers significant advantages for NTDs due to their reduced developmental time and costs. Notably, some antidepressants, such as imipramine and sertraline, have demonstrated activity against *Leishmania* parasites in both *in vitro* and *in vivo* studies with liposomes improving their leishmanicidal efficacy [141, 148-150]. After entrapment, both compounds showed higher parasite clearance and reduced toxicity. Sertraline encapsulated into phosphatidylserine liposomes was administered subcutaneously to BALB/c mice infected with *L. infantum* and reduced liver parasite load by 89% at 1 mg/kg when compared to the controls [148]. Imipramine was shown to be highly effective against antimony-unresponsive *L. donovani* isolates, but complete clearance of parasites was only achieved with a dose of 140 mg/kg for 28 days, given orally [150]. Its encapsulation in squalene-phosphatidylcholine liposomes increased its efficacy at lower concentrations and a significantly shorter regimen of a 10-day treatment when compared to the free drug [141]. This new strategy reduces the toxicity previously reported for imipramine monotherapy.

5.1.3. Encapsulation of new anti-*Leishmania* drugs in liposomes

Several anti-*Leishmania* drugs under development have also been entrapped in liposomes, some with encouraging results. One example is a quinoxaline derivative, 2,3-di-(4-methoxyphenyl)-quinoxaline (LSPN331), that showed promising activity against promastigotes and intracellular amastigotes of *L. amazonensis*, with selectivity indexes higher than those registered for miltefosine or amphotericin B. The lesion thickness in *L. amazonensis*-infected BALB/c mice was also significantly decreased following intralesional treatment with LSPN331 when compared to control mice [151]. Nevertheless, this level of efficacy did not surpass the activity of oral miltefosine, which revealed a higher efficiency in reducing skin lesions. To improve its anti-*Leishmania* activity, LSPN331 was encapsulated into hyaluronic acid (HA)-coated liposomes [152]. Considering that surface modifications of liposomes may alter their physicochemical properties and consequently their behavior in the body, two different types of HA-coated liposomes were developed. In one, HA was covalently grafted onto the surface of the liposome (L-HA), and in the other, cholesterol-modified HA (HAChol) interacted with the phospholipid bilayer of the liposomes via a hydrophobic bond (L-HAChol) [152]. Biodistribution studies in healthy and *L. amazonensis*-infected mice revealed the presence of both liposomes mainly in liver and spleen after IV administration. Interestingly, L-HA and L-HAChol were also detected in the paw of infected mice. An *in*

vitro skin permeation test revealed the potential of L-HAChol as a topical agent for delivering LSPN331, by reaching deeper layers of the skin [152].

5.2.Solid lipid NPs

Solid Lipid NPs (SLNs) were introduced in the 90s and can be defined as solid lipid colloidal particles, typically spherical, with diameters ranging from 50 to 1000 nm. Contrary to liposomes, SLNs are composed of a solid hydrophobic core matrix coated with a phospholipid monolayer [153, 154].

The group of Mudavath characterized three modified SLNs for the oral delivery of AmpB as a new therapeutic approach against leishmaniasis [99, 155, 156]. First, SLNs were coated with vitamin B12-stearic acid and loaded with AmpB [155]. The use of stearic acid is known to improve oral bioavailability and safety, while vitamin B12 enhances absorption of biomolecules. The ability of these NPs to adhere to mucin and remain stable in gastric and intestinal fluids is essential for their transfer into the bloodstream, which in turn enhances the bioavailability of AmpB. An *in vitro* cytotoxicity assay demonstrated the biocompatibility of these AmpB-loaded SLNs, with a 50% cytotoxic concentration (CC_{50}) fivefold higher when compared with free AmpB. The antileishmanial activity, tested on *L. donovani*-infected J774A.1 macrophages, was significantly higher using the NPs [155]. Second, SLNs were modified with 2-hydroxypropyl-β-cyclodextrin (HPCD), cyclic oligosaccharides known for their capability to incorporate water insoluble molecules by a non-covalent interaction inside their hydrophobic core [99]. A combinational cargo system of AmpB and paromomycin was then incorporated into these modified SLNs to be administered orally for the treatment of visceral leishmaniasis. Both *in vitro* and *in vivo* studies using the murine experimental VL model showed that HPCD increased the stability of SLNs and significantly reduced the release of AmpB and paromomycin in gastrointestinal tract. HPCD-modified SLNs did not affect liver and kidney functions, contrary to conventional AmpB that increased the renal and hepatic toxicity markers in serum. Also, the SLNs formulation was significantly more efficient in reducing liver parasite burden in *L. donovani*-infected BALB/c mice when compared to miltefosine. Altogether, both studies showed a better anti-leishmanial effect of HPCD-modified dual drug-loaded SLNs in comparison to miltefosine, the only oral drug available for leishmaniasis treatment [99].

In a third publication, HPCD-modified SLNs were used to encapsulate both AmpB and melatonin [156]. This formulation presented a better anti-leishmanial activity in *L. donovani*-infected BALB/c when compared to HPCD-modified SLNs encapsulated with AmpB and paromomycin. Kidney and liver toxic markers did not show significant increases when compared to control. Surface modification of these

SLNs together with the dual cargo system adopted enhanced the efficacy of the drugs used, making them potential treatments against VL.

5.3. Emulsomes and Metallic NPs

The complexity of leishmaniases, with different clinical manifestations, and many causative species, drove the scientific community to develop and improve a panoply of other NPs, already showing interesting results. Some examples of those NPs are discussed in this section for a better appraisal of the development in the field.

Emulsomes are biocompatible lipid-based nanocarriers systems with a particle size distribution of 10-250 nm, composed by phospholipid multi-layers. Contrarily to liposomes, their internal core comprises a solid fat or triglyceride, which gives these NPs a higher loading capacity for lipophilic drugs. Emulsomes played a pivotal role in enhancing the efficacy of the bisnapthalimidopropyl (BNIP) derivative BNIPdiaminooctane (BNIPDaoct), a sirtuin inhibitor. Although BNIPDaoct initially demonstrated faster reduction of spleen and liver parasite loads in *L. infantum*-infected BALB/c mice compared to AmpB, its effect was eventually surpassed by AmpB after fifteen administrations [157]. To address BNIPDaoct limitations, including cytotoxicity, low bioavailability, and poor aqueous solubility, it was incorporated into emulsomes. BNIPDaoct-loaded emulsomes significantly inhibited *L. infantum* promastigote growth, improved the drug's efficacy and selectivity against intramacrophagic parasites, and reduced cytotoxicity by 11-fold compared to the free drug [158].

Metallic NPs might provide a new approach for leishmaniases treatment, because they can be used both as drug delivery systems and directly as therapeutic agents (reviewed in [159]). Silver NPs (SNPs) synthesized using *Commiphora myrrha* (myrrh) effectively inhibited the growth of *L. major* promastigotes, and topical application of these SNPs led to the healing of lesions in BALB/c mice after 21 days of treatment [160].

The literature reports many other studies documenting the efficacy of metallic NPs in leishmaniases, but most of them were only tested against promastigotes and axenic and intracellular amastigotes in *in vitro* settings. Despite more progress being needed in this field, *in vitro*, metallic NPs proved to be more effective than the traditional medicines and more effective against drug-resistant *Leishmania* parasites [159].

5.4. Polymeric NPs

Polymers are macromolecules formed by the polymerization of smaller units, monomers, or covalent linkage or physical association of oligomers. For the preparation of polymeric NPs both natural (e.g. dextran, albumin, gelatin, hyaluronic acid etc) and synthetic polymers (e.g. aliphatic polyesters based PLLA/PGLA) are used [121]. The proven biocompatibility of many polymeric systems constitutes a great advantage for its use in clinics, and several formulations based on polymers, such as poly(-lactic acid) (PLA), poly(-glycolic acid) (PGA), poly(ε-caprolactone) (PCL), and poly(-lactide-co-glycolide) (PLGA), are approved by FDA [161]. The latter, one of the most studied polymers for drug delivery purposes, undergoes hydrolysis in the body resulting in the formation of lactic and glycolic acid, with minimal systemic toxicity [162]. A number of studies established the high efficiency of PLGA as a drug delivery system for several anti-*Leishmania* compounds. Miltefosine entrapped in PLGA-PEG NPs was found more effective against *L. donovani* promastigotes *in vitro* than the free compound or AmpB. Also, a 7-day treatment with encapsulated miltefosine resulted in a statistically significant reduction in parasite burden in hamster spleens, when compared to standard miltefosine and AmpB [163]. The previously mentioned BNIPDaoct (see section 5.3.), the most active BNIP compound *in vivo*, was successfully encapsulated into PLGA NPs, which reduced its cytotoxicity and increased its aqueous solubility. When administered intraperitoneally, PLGA NPs improved BNIPDaoct bioavailability and efficacy, translating into a significant reduction of parasite burden in the spleen of *L. infantum*-infected BALB/c mice, compared to free drug. Importantly this nanoformulation retained its activity after oral administration [164].

An advantage of PLGA NPs is the possibility of easily modifying their surface for selective targeting. Mannose-modified PLGA NPs synthesized to target *Leishmania*-infected macrophages (known to overexpress mannose receptors) were loaded with AmpB. In *L. donovani*-infected BALB/c mice, the mannose-modified AmpB-loaded PLGA NPs were more effective than both non-modified AmpB-loaded PLGA NPs and free AmpB [165]. Targeting macrophages as studied in this paper proved advantageous and encourages further research.

In the past three decades, polymeric micelles (PMs) have emerged as promising drug delivery systems due to their ease of preparation, small size, and ability to solubilize poorly water-soluble compounds. These nanocarriers are spontaneously formed in an aqueous solution by the self-assembly of amphiphilic block copolymers. Below the critical micelle concentration (CMC), free polymer chains are

present in aqueous solution, while above the CMC they form core-shell micellar structures, with an internal hydrophobic core and an external hydrophilic shell (Fig 7). The separation of the core segment from the surrounding aqueous solution is driven by intermolecular forces, such as hydrophobic or electrostatic interactions and metal complexation, and the formed core can accommodate poorly water-soluble molecules, but also proteins, nucleic acids, and diagnostic agents [166-171]. The hydrophilic shell, usually composed of PEG, allows interaction with surrounding water molecules and gives the micelles their thermodynamic stability, thereby preventing their aggregation and precipitation. This hydrophilic PEG shell in combination with small size of PMs results in good circulation kinetics, provided that the micelles are stable in contact with blood constituents. Polymeric micelle features, such as stability, size, drug loading, and drug release, can be tailored by the chemical structure, molecular weight, and mass ratio of the inner core-forming polymer blocks, as well as by their concentration [168, 172-174]. Also, the possibility of decorating the hydrophilic shell with specific ligands, enables PMs to actively target specific cells and tissues, increasing drug concentration at the target site [175].

Therapeutic compounds present specific physicochemical properties, which prompts the need for the adequate block copolymer design. Although hydrophobic interactions are the main driving force for drug encapsulation into the polymeric micelle inner core, other molecular interactions, such as hydrogen bonding or π-π stacking interactions, help micelle formation and stabilization of its structure [176].

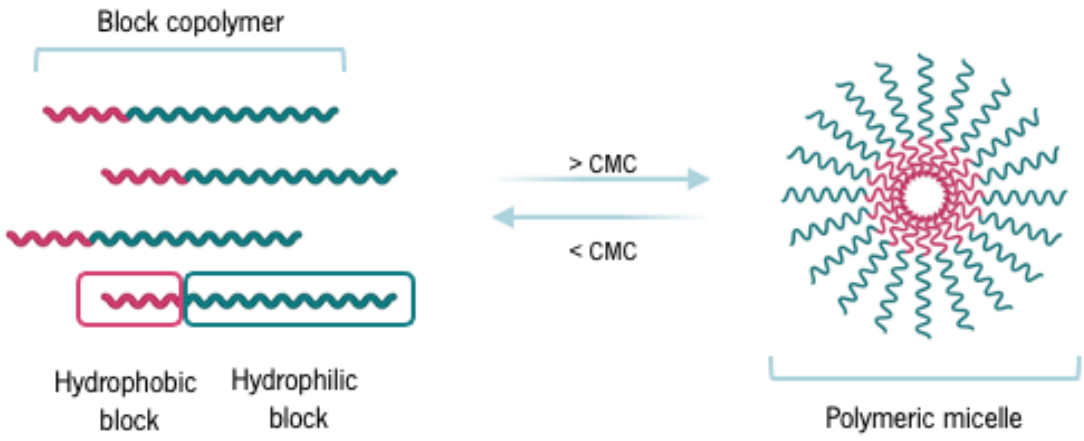

Fig 7 – Schematic representation of polymeric micelles. Created with Biorender.

Highlighting the potential of NPs as delivery systems for leishmaniases therapy, a Poloxamer 407-based NP was used to encapsulate 8-HQN and optimize its therapeutic efficacy against CL and VL [177, 178]. This drug – addressed for its leishmanial activity in section 4.7 – and their derivatives are known to

possess anticancer, anti-neurodegenerative, and antimicrobial activities, and some, as clioquinol, are authorized for human use [118, 179]. Poloxamer 407 is a thermo-reversible amphiphilic triblock copolymer composed of a central hydrophobic block of polypropylene oxide (PPO) flanked by two hydrophilic blocks of PEG. As a result, it has been used as a polymeric micelle to solubilize hydrophobic molecules. In a first study, 8-HQN-loaded PM (8-HQN/M) displayed an efficacy greater than AmpB against *L. amazonensis* promastigotes, however, not against intracellular amastigotes [177]. Interestingly, despite the apparent lower efficacy *in vitro*, infected mice treated with 8-HQN/M had a statistically significant reduction in the average lesion size when compared to saline, free 8-HQN, or the placebo micelle groups. Also, the parasite burden in all tissues and organs analyzed (lesion, spleen, liver, and draining lymph nodes) was significantly reduced in the free 8-HQN and 8-HQN/M groups, the latter displaying better results. These data highlight the potential of this Poloxamer 407 based nanocarrier for the treatment of CL [177].

A second study showed higher *in vitro* efficacy of 8-HQN/M against *L. infantum* promastigotes and amastigotes compared to AmpB, due to lower toxicity towards macrophages [178]. This treatment significantly reduced parasite burden in the different organs (spleen, liver, draining lymph node, and bone marrow) of *L. infantum*-infected BALB/c mice, compared to free AmpB, free 8-HQN, and the control groups. Furthermore, while AmpB alters liver and kidney enzymes, animals treated with 8-HQN/M did not display changes in these enzymes. Therefore, 8-HQN/M emerged as a possible alternative for the treatment of VL [178].

Despite the high drug loading, small size, and drug accumulation at target sites, PMs also have some drawbacks, the main being their sometimes low stability in physiological environments, including dissolution in the blood when administered IV, and their tendency for low drug retention. Once the concentration is below CMC, PMs can dissociate, simultaneously releasing encapsulated drugs into the bloodstream, which could adversely affect drug biodistribution and, consequently, the therapeutic outcome and toxicity [172]. Uncontrolled drug release from the hydrophobic inner core of PMs can also occur due to interactions with blood components, which may cause PMs disruption and/or aggregation. Additionally, the encapsulated drugs can bind to plasma proteins such as albumin, further contributing to this premature release [180]. Several physicochemical strategies have been applied to improve stability of PMs and increase drug retention. This includes exploitation of strong physical interactions, chemical crosslinking within the shell or the core domains, and chemical conjugation of drug molecules to PMs [172, 181].

The use of chemical crosslinking for PMs stabilization, despite increasing circulation kinetics, does not necessarily have a positive impact on the retention of the drug. Drug retention can be attempted by chemically conjugating the drug to PMs, but the techniques are challenging and can affect the overall therapeutic effect [182]. The use of noncovalent interactions therefore presents several advantages over chemical crosslinking or covalent drug conjugation. As referred before, chemical conjugation requires extra steps during synthesis, which leads to longer, more complicated and thus less costs effective processes. Differently, noncovalent interactions do not require the chemical or structural modification of drug molecules, eliminating concerns on unexpected alteration of the safety profile or the pharmacological effect of the drug molecule [183]. A physical method, namely π-π stacking interaction, has been considered a good alternative in the development of nanocarriers [183]. These π-π stacking interactions promote the self-assembly of micelles, allow the drug molecules to be loaded and retained in the micelle core region, and maintain the nanocarrier stability. These interactions are due to the presence of aromatic groups containing π bonds in the core forming hydrophobic blocks. Moreover, the presence of aromatic rings in drug molecules facilitates their loading into delivery systems capable of π-π stacking interactions [183]. An example of this system are the micelles composed of block copolymers of methoxy poly(ethylene glycol)-b-poly(N-2-benzoyloxypropyl methacrylamide) (mPEG-*b*-p(HPMA-Bz)), which were obtained by free radical polymerization via a macroinitiator route, with mPEG2-ABCPA as macroinitiator and HPMAm-Bz as monomer [184-186]. This monomer has attractive features, such as its easy synthesis performed by reaction of the hydroxyl group of HPMAm with benzoyl chloride. Also, the hydrolyzed block (p(HPMAm)) has been considered clinically safe and easily excreted by the kidney when presenting a molecular weight lower than 50kDa [187, 188]. mPEG-*b*-p(HPMA-Bz) micelles were optimized for the encapsulation of paclitaxel (PTX), a chemotherapy medication used to treat several types of cancer. A higher amount of aromatic substitution of the HPMAm repeating units in the block copolymer of mPEG-*b*-pHPMAm led to more stable micelles and a higher PTX loading capacity and retention, improving this drug's pharmacokinetics and biodistribution. A high accumulation of PTX in the tumor and complete regression of the breast carcinoma xenografts in mice was observed, without any significant side effects, when using PTX-loaded mPEG-*b*-p(HPMA-Bz) micelles [184].

6. Aims

The aim of this PhD project was to identify new candidate molecules and take advantage of advances in nanomedicine to select the most appropriate nanocarrier for effective treatment against *Leishmania* infection. To achieve this goal, the following specific objectives were defined: i) to implement a new method for the quantification of intramacrophagic parasites *in vitro*; ii) to identify novel drug molecules with antileishmanial activity through drug screening assays; and iii) to encapsulate the identified compounds in order to assess both the suitability of a new nanocarrier system for the treatment of these diseases and the potential enhancement on the therapeutic potential of the new drugs.

The discovery of new molecules against a specific disease is laborious and highly demanding due to high costs, limitations on the available experimental models, and, sometimes, to an incomplete understanding of underlying disease mechanisms. To simplify the process, we developed a new high-content screening (HCS) assay and an image analysis script, which allow testing dozens of compounds simultaneously. In **Chapter II**, we demonstrated their suitability for drug development in two different species, *L. infantum* and *L. amazonensis*. The setup of a pipeline in a freely available image analysis software can help other laboratories, without easy access to HCS microscopes, to perform *Leishmania* drug studies or other *in vitro* analysis using intramacrophagic parasites.

In **Chapter III**, we tested different quinolin-4(1*H*)-imines derivatives, previously determined as potent antiplasmodial drugs. Their efficiency to inhibit parasite growth was demonstrated *in vitro* against different *Leishmania* species, known to develop clinically distinct syndromes, namely *L. infantum*, *L. major*, and *L. amazonensis*. Further analyses were performed to identify the mechanism of action of some quinolin-4(1*H*)-imines, which showed their ability to interfere, at least partially, with the parasites mitochondrial function.

In **Chapter IV**, we explored the potential of mPEG-*b*-p(HPMA-Bz) micelles as proper nanocarriers for the most efficient compounds identified in the previous chapter. Polymeric micelles substantially improved the solubility of quinolin-4(1*H*)-imines, exhibiting a high drug retention capacity and leading to a significant decrease in drug toxicity, both *in vitro* and *in vivo*. The pharmacokinetics and biodistribution of quinolin-4(1*H*)-imines were improved when loaded into PMs.

Finally, in **Chapter V**, we overviewed the main results of this thesis and presented a final discussion.

7. References

1. World Health, O. *Neglected tropical diseases*. Accessed on April 2023]; Available from: https://www.who.int/neglected_diseases/diseases/en/.

2. Kirigia, J.M. and G.N. Mburugu, *The monetary value of human lives lost due to neglected tropical diseases in Africa.* Infect Dis Poverty, 2017. **6**(1): p. 165.

3. Mitra, A.K. and A.R. Mawson, *Neglected Tropical Diseases: Epidemiology and Global Burden.* Trop Med Infect Dis, 2017. **2**(3).

4. Organization, W.H., *Integrating Neglected Tropical Diseases in Global Health and Development: Fourth Who Report on Neglected Tropical Diseases*. 2018: World Health Organization.

5. World Health, O. *WHO global burden of disease estimates for 2000–2015*. Accessed on January 2020]; Available from: http://www.who.int/healthinfo/global_burden_disease/estimates/en/index2.html.

6. Weng, H.B., H.X. Chen, and M.W. Wang, *Innovation in neglected tropical disease drug discovery and development.* Infect Dis Poverty, 2018. **7**(1): p. 67.

7. Trouiller, P., et al., *Drug development for neglected diseases: a deficient market and a public-health policy failure.* Lancet, 2002. **359**(9324): p. 2188-94.

8. Jain, N., et al., *Association of the Priority Review Voucher With Neglected Tropical Disease Drug and Vaccine Development.* JAMA, 2017. **318**(4): p. 388-389.

9. Cohen, J.P., G. Sturgeon, and A. Cohen, *Measuring progress in neglected disease drug development.* Clin Ther, 2014. **36**(7): p. 1037-42.

10. *London Declaration on Neglected Tropical Diseases*. Accessed on April 2023]; Available from: https://unitingtocombatntds.org/resource-hub/who-resources/london-declaration-neglected-tropical-diseases/.

11. Cohen, J.P., et al., *Progress Report on Neglected Tropical Disease Drug Donation Programs.* Clin Ther, 2016. **38**(5): p. 1193-204.

12. Liese, B.H., N. Houghton, and L. Teplitskaya, *Development assistance for neglected tropical diseases: progress since 2009.* Int Health, 2014. **6**(3): p. 162-71.

13. Organization, W.H. *Ending the neglect to attain the Sustainable Development Goals: A road map for neglected tropical diseases 2021–2030*. [cited Accessed on April 2023; Available from: https://www.who.int/publications/i/item/9789240010352.

14. World Health, O. *Global Health Observatory (GHO) data*. Leishmaniasis: Situation and trends Accessed on April 2023]; Available from: https://apps.who.int/gho/data/node.main.NTDLEISH?lang=en.

15. Bruschi, F. and L. Gradoni, *The Leishmaniases: Old Neglected Tropical Diseases*. Leishmania Taxonomy. 2018: Springer International Publishing.

16. Akhoundi, M., et al., *A Historical Overview of the Classification, Evolution, and Dispersion of Leishmania Parasites and Sandflies.* PLoS Negl Trop Dis, 2016. **10**(3): p. e0004349.

17. World Health, O. *Fact sheets: Leishmaniasis*. 2019 on April 2023]; Available from: https://www.who.int/news-room/fact-sheets/detail/leishmaniasis.

18. eBioMedicine, *Leishmania: an urgent need for new treatments.* EBioMedicine, 2023. **87**: p. 104440.

19. Clemente, W.T., P.H.O. Mourao, and J.M. Aguado, *Current approaches to visceral leishmaniasis treatment in solid organ transplant recipients.* Expert Rev Anti Infect Ther, 2018. **16**(5): p. 391-397.

20. Argy, N., et al., *Congenital Leishmaniasis in a Newborn Infant Whose Mother was Coinfected With Leishmaniasis and HIV.* Journal of the Pediatric Infectious Diseases Society, 2019.

21. Mansueto, P., et al., *Transfusion transmitted leishmaniasis. What to do with blood donors from endemic areas?* Travel Med Infect Dis, 2014. **12**(6 Pt A): p. 617-27.

22. Burchmore, R.J. and M.P. Barrett, *Life in vacuoles–nutrient acquisition by Leishmania amastigotes.* Int J Parasitol, 2001. **31**(12): p. 1311-20.

23. Rogers, M.E., et al., *Transmission of cutaneous leishmaniasis by sand flies is enhanced by regurgitation of fPPG.* Nature, 2004. **430**(6998): p. 463-7.

24. Stierhof, Y.D., et al., *Filamentous proteophosphoglycan secreted by Leishmania promastigotes forms gel-like three-dimensional networks that obstruct the digestive tract of infected sandfly vectors.* Eur J Cell Biol, 1999. **78**(10): p. 675-89.

25. Beach, R., G. Kiilu, and J. Leeuwenburg, *Modification of sand fly biting behavior by Leishmania leads to increased parasite transmission.* Am J Trop Med Hyg, 1985. **34**(2): p. 278-82.

26. Rogers, M.E., *The role of leishmania proteophosphoglycans in sand fly transmission and infection of the Mammalian host.* Front Microbiol, 2012. **3**: p. 223.

27. Abdeladhim, M., S. Kamhawi, and J.G. Valenzuela, *What's behind a sand fly bite? The profound effect of sand fly saliva on host hemostasis, inflammation and immunity.* Infect Genet Evol, 2014. **28**: p. 691-703.

28. Lestinova, T., et al., *Insights into the sand fly saliva: Blood-feeding and immune interactions between sand flies, hosts, and Leishmania.* PLoS Negl Trop Dis, 2017. **11**(7): p. e0005600.

29. Rogers, M., et al., *Proteophosophoglycans regurgitated by Leishmania-infected sand flies target the L-arginine metabolism of host macrophages to promote parasite survival.* PLoS Pathog, 2009. **5**(8): p. e1000555.

30. Bruschi, F. and L. Gradoni, *The Leishmaniases: Old Neglected Tropical Diseases*. 2018: Springer International Publishing.

31. Passelli, K., O. Billion, and F. Tacchini-Cottier, *The Impact of Neutrophil Recruitment to the Skin on the Pathology Induced by Leishmania Infection.* Front Immunol, 2021. **12**: p. 649348.

32. Hurrell, B.P., I.B. Regli, and F. Tacchini-Cottier, *Different Leishmania Species Drive Distinct Neutrophil Functions.* Trends Parasitol, 2016. **32**(5): p. 392-401.

33. Regli, I.B., et al., *Survival Mechanisms Used by Some Leishmania Species to Escape Neutrophil Killing.* Front Immunol, 2017. **8**: p. 1558.

34. Chaves, M.M., et al., *The role of dermis resident macrophages and their interaction with neutrophils in the early establishment of Leishmania major infection transmitted by sand fly bite.* PLoS Pathog, 2020. **16**(11): p. e1008674.

35. Lievin-Le Moal, V. and P.M. Loiseau, *Leishmania hijacking of the macrophage intracellular compartments.* FEBS J, 2016. **283**(4): p. 598-607.

36. Real, F. and R.A. Mortara, *The diverse and dynamic nature of Leishmania parasitophorous vacuoles studied by multidimensional imaging.* PLoS Negl Trop Dis, 2012. **6**(2): p. e1518.

37. Real, F., et al., *Cell-to-cell transfer of Leishmania amazonensis amastigotes is mediated by immunomodulatory LAMP-rich parasitophorous extrusions.* Cell Microbiol, 2014. **16**(10): p. 1549-64.

38. Sunter, J. and K. Gull, *Shape, form, function and Leishmania pathogenicity: from textbook descriptions to biological understanding.* Open Biol, 2017. **7**(9).

39. Dostalova, A. and P. Volf, *Leishmania development in sand flies: parasite-vector interactions overview.* Parasit Vectors, 2012. **5**: p. 276.

40. Pimenta, P.F., et al., *Stage-specific adhesion of Leishmania promastigotes to the sandfly midgut.* Science, 1992. **256**(5065): p. 1812-5.

41. Sacks, D.L., et al., *The role of the lipophosphoglycan of Leishmania in vector competence.* Parasitology, 1994. **108 Suppl**: p. S55-62.

42. Alvar, J., S. Yactayo, and C. Bern, *Leishmaniasis and poverty.* Trends Parasitol, 2006. **22**(12): p. 552-7.

43. Okwor, I. and J. Uzonna, *Social and Economic Burden of Human Leishmaniasis.* Am J Trop Med Hyg, 2016. **94**(3): p. 489-93.

44. World Health, O., *Control of the leishmaniases.* World Health Organ Tech Rep Ser, 2010(949): p. xii-xiii, 1-186, back cover.

45. World Health, O. *GLOBAL HEALTH OBSERVATORY - Explore a world of health data*. Map Gallery Search Results - Leishmaniasis Accessed on May 2024]; Available from: https://www.who.int/data/gho/map-gallery-search-results?&maptopics=910b5dfc-ce2e-4440-8b43-8d83f4a85485&term=leishmaniasis.

46. Lira, R., et al., *Evidence that the high incidence of treatment failures in Indian kala-azar is due to the emergence of antimony-resistant strains of Leishmania donovani.* J Infect Dis, 1999. **180**(2): p. 564-7.

47. Sundar, S., et al., *Failure of pentavalent antimony in visceral leishmaniasis in India: report from the center of the Indian epidemic.* Clin Infect Dis, 2000. **31**(4): p. 1104-7.

48. Sundar, S., *Drug resistance in Indian visceral leishmaniasis.* Trop Med Int Health, 2001. **6**(11): p. 849-54.

49. Gradoni, L., et al., *Drug regimens for visceral leishmaniasis in Mediterranean countries.* Trop Med Int Health, 2008. **13**(10): p. 1272-6.

50. Ephros, M., et al., *Stage-specific activity of pentavalent antimony against Leishmania donovani axenic amastigotes.* Antimicrob Agents Chemother, 1999. **43**(2): p. 278-82.

51. Wyllie, S., M.L. Cunningham, and A.H. Fairlamb, *Dual action of antimonial drugs on thiol redox metabolism in the human pathogen Leishmania donovani.* J Biol Chem, 2004. **279**(38): p. 39925-32.

52. Baiocco, P., et al., *Molecular basis of antimony treatment in leishmaniasis.* J Med Chem, 2009. **52**(8): p. 2603-12.

53. Perry, M.R., et al., *Visceral leishmaniasis and arsenic: an ancient poison contributing to antimonial treatment failure in the Indian subcontinent?* PLoS Negl Trop Dis, 2011. **5**(9): p. e1227.

54. Dutcher JD, G.W., Pagano JF, John V, *Amphotericin b, its production, and its salts*. 1959.

55. Sampaio, S.A., et al., *The treatment of American (mucocutaneous) leishmaniasis with amphotericin B.* Arch Dermatol, 1960. **82**: p. 627-35.

56. Prata, A., *Treatment of Kala-Azar with Amphotericin B.* Trans R Soc Trop Med Hyg, 1963. **57**: p. 266-8.

57. Ramos, H., et al., *Amphotericin B kills unicellular leishmanias by forming aqueous pores permeable to small cations and anions.* J Membr Biol, 1996. **152**(1): p. 65-75.

58. Saha, A.K., T. Mukherjee, and A. Bhaduri, *Mechanism of action of amphotericin B on Leishmania donovani promastigotes.* Mol Biochem Parasitol, 1986. **19**(3): p. 195-200.

59. Laniado-Laborin, R. and M.N. Cabrales-Vargas, *Amphotericin B: side effects and toxicity.* Rev Iberoam Micol, 2009. **26**(4): p. 223-7.

60. Ghorbani, M. and R. Farhoudi, *Leishmaniasis in humans: drug or vaccine therapy?* Drug Des Devel Ther, 2018. **12**: p. 25-40.

61. Proffitt, R.T., et al., *Pharmacology and toxicology of a liposomal formulation of amphotericin B (AmBisome) in rodents.* J Antimicrob Chemother, 1991. **28 Suppl B**: p. 49-61.

62. Janoff, A.S., et al., *Unusual lipid structures selectively reduce the toxicity of amphotericin B.* Proc Natl Acad Sci U S A, 1988. **85**(16): p. 6122-6.

63. Guo L.S.S., et al., *Novel antifungal drug delivery: stable amphotericin B-cholesteryl sulfate discs.* International Journal of Pharmaceutics 1991. **75**(1): p. 45-54.

64. Aronson, N., et al., *Diagnosis and Treatment of Leishmaniasis: Clinical Practice Guidelines by the Infectious Diseases Society of America (IDSA) and the American Society of Tropical Medicine and Hygiene (ASTMH).* Am J Trop Med Hyg, 2017. **96**(1): p. 24-45.

65. Eldbouni, O., et al., *Visceral leishmaniasis in Lebanon a report of four cases: case series and review.* J Infect Dev Ctries, 2018. **12**(2.1): p. 31S.

66. KÖSE, Ş., et al., *Case Report: Treatment of Kala-Azar by Amphotericin B Lipid Complex (ABELCET®)* Türkiye Parazitoloji Dergisi, 2004. **28**(2): p. 126-128.

67. Dietze, R., et al., *Treatment of Brazilian kala-azar with a short course of amphocil (amphotericin B cholesterol dispersion).* Clin Infect Dis, 1993. **17**(6): p. 981-6.

68. Croft, S.L. and P. Olliaro, *Leishmaniasis chemotherapy–challenges and opportunities.* Clin Microbiol Infect, 2011. **17**(10): p. 1478-83.

69. World Health, O. *WHO and Gilead Sciences extend collaborative agreement to enhance access to treatment for visceral leishmaniasis*. 2023 Accessed on April 2023]; Available from: https://www.who.int/news/item/26-01-2023-who-and-gilead-sciences-extend-collaborative-agreement-to-enhance-access-to-treatment-for-visceral-leishmaniasis#:~:text=The%20World%20Health%20Organization%20(WHO,their%20previous%20agreement%20to%202025.

70. Meyerhoff, A., *U.S. Food and Drug Administration approval of AmBisome (liposomal amphotericin B) for treatment of visceral leishmaniasis.* Clin Infect Dis, 1999. **28**(1): p. 42-8; discussion 49-51.

71. Bern, C., et al., *Liposomal amphotericin B for the treatment of visceral leishmaniasis.* Clin Infect Dis, 2006. **43**(7): p. 917-24.

72. Musa, A.M., et al., *Efficacy of liposomal amphotericin B (AmBisome) in the treatment of persistent post-kala-azar dermal leishmaniasis (PKDL).* Ann Trop Med Parasitol, 2005. **99**(6): p. 563-9.

73. Croft, S.L., D. Snowdon, and V. Yardley, *The activities of four anticancer alkyllysophospholipids against Leishmania donovani, Trypanosoma cruzi and Trypanosoma brucei.* J Antimicrob Chemother, 1996. **38**(6): p. 1041-7.

74. Kuhlencord, A., et al., *Hexadecylphosphocholine: oral treatment of visceral leishmaniasis in mice.* Antimicrob Agents Chemother, 1992. **36**(8): p. 1630-4.

75. Sindermann, H. and J. Engel, *Development of miltefosine as an oral treatment for leishmaniasis.* Trans R Soc Trop Med Hyg, 2006. **100 Suppl 1**: p. S17-20.

76. Croft, S.L., et al., *The activity of alkyl phosphorylcholines and related derivatives against Leishmania donovani.* Biochem Pharmacol, 1987. **36**(16): p. 2633-6.

77. Berman, J., *Miltefosine to treat leishmaniasis.* Expert Opin Pharmacother, 2005. **6**(8): p. 1381-8.

78. Sindermann, H., et al., *Miltefosine (Impavido): the first oral treatment against leishmaniasis.* Med Microbiol Immunol, 2004. **193**(4): p. 173-80.

79. Sundar, S., et al., *Oral miltefosine for Indian visceral leishmaniasis.* N Engl J Med, 2002. **347**(22): p. 1739-46.

80. FDA. *CDER Rare Disease And Orphan Drug Designated Approvals*. 2014 Accessed on February 2020]; Available from: https://www.fda.gov/media/116659/download.

81. Rakotomanga, M., et al., *Miltefosine affects lipid metabolism in Leishmania donovani promastigotes.* Antimicrob Agents Chemother, 2007. **51**(4): p. 1425-30.

82. Luque-Ortega, J.R. and L. Rivas, *Miltefosine (hexadecylphosphocholine) inhibits cytochrome c oxidase in Leishmania donovani promastigotes.* Antimicrob Agents Chemother, 2007. **51**(4): p. 1327-32.

83. Paris, C., et al., *Miltefosine induces apoptosis-like death in Leishmania donovani promastigotes.* Antimicrob Agents Chemother, 2004. **48**(3): p. 852-9.

84. Palic, S., et al., *Systematic Review of Host-Mediated Activity of Miltefosine in Leishmaniasis through Immunomodulation.* Antimicrob Agents Chemother, 2019. **63**(7).

85. Carnielli, J.B.T., et al., *Natural Resistance of Leishmania infantum to Miltefosine Contributes to the Low Efficacy in the Treatment of Visceral Leishmaniasis in Brazil.* Am J Trop Med Hyg, 2019. **101**(4): p. 789-794.

86. Gonçalves, G., et al., *Increased Leishmania infantum resistance to miltefosine and amphotericin B after treatment of a dog with miltefosine and allopurinol.* Parasites & Vectors, 2021. **14**(1): p. 599.

87. Monge-Maillo, B. and R. Lopez-Velez, *Miltefosine for visceral and cutaneous leishmaniasis: drug characteristics and evidence-based treatment recommendations.* Clin Infect Dis, 2015. **60**(9): p. 1398-404.

88. van Thiel, P.P., et al., *Miltefosine treatment of Leishmania major infection: an observational study involving Dutch military personnel returning from northern Afghanistan.* Clin Infect Dis, 2010. **50**(1): p. 80-3.

89. El-On, J., et al., *Topical treatment of cutaneous leishmaniasis.* J Invest Dermatol, 1986. **87**(2): p. 284-8.

90. Sundar, S., et al., *Injectable paromomycin for Visceral leishmaniasis in India.* N Engl J Med, 2007. **356**(25): p. 2571-81.

91. Hailu, A., et al., *Geographical variation in the response of visceral leishmaniasis to paromomycin in East Africa: a multicentre, open-label, randomized trial.* PLoS Negl Trop Dis, 2010. **4**(10): p. e709.

92. Musa, A.M., et al., *Paromomycin for the treatment of visceral leishmaniasis in Sudan: a randomized, open-label, dose-finding study.* PLoS Negl Trop Dis, 2010. **4**(10): p. e855.

93. Bhandari, V., et al., *Elucidation of cellular mechanisms involved in experimental paromomycin resistance in Leishmania donovani.* Antimicrob Agents Chemother, 2014. **58**(5): p. 2580-5.

94. Singh, K., G. Garg, and V. Ali, *Current Therapeutics, Their Problems and Thiol Metabolism as Potential Drug Targets in Leishmaniasis.* Curr Drug Metab, 2016. **17**(9): p. 897-919.

95. Olias-Molero, A.I., et al., *Antileishmanial Drug Discovery and Development: Time to Reset the Model?* Microorganisms, 2021. **9**(12).

96. Gradoni, L., López-Vélez R., Mokni M., *Manual on case managment and surveillance of the leishmaniases in the WHO European Region*. 2017, WHO.

97. DNDi. *New hope for leishmaniasis: DNDi R&D and access programmes in focus*. 2022; Available from: https://dndi.org/wp-content/uploads/2022/07/DNDi-Leishmaniasis-EN.pdf.

98. Sundar, S., et al., *A phase II, non-comparative randomised trial of two treatments involving liposomal amphotericin B and miltefosine for post-kala-azar dermal leishmaniasis in India and Bangladesh.* PLoS Negl Trop Dis, 2024. **18**(6): p. e0012242.

99. Parvez, S., et al., *Modified solid lipid nanoparticles encapsulated with Amphotericin B and Paromomycin: an effective oral combination against experimental murine visceral leishmaniasis.* Sci Rep, 2020. **10**(1): p. 12243.

100. DNDi. *2023 R&D portfolio in review: Leishmaniasis*. 2024 On May 2024]; Available from: https://dndi.org/news/2024/2023-rd-portfolio-in-review-leishmaniasis/.

101. Nagle, A., et al., *Discovery and Characterization of Clinical Candidate LXE408 as a Kinetoplastid-Selective Proteasome Inhibitor for the Treatment of Leishmaniases.* J Med Chem, 2020. **63**(19): p. 10773-10781.

102. World Health, O., *Promising patient-friendly oral drug against visceral leishmaniasis enters Phase II clinical trial in Ethiopia*. 2024: https://www.who.int/news/item/23-04-2024-promising-patient-friendly-oral-drug-against-visceral-leishmaniasis-enters-phase-ii-clinical-trial-in-ethiopia.

103. Wijnant, G.J., et al., *Pharmacokinetics and Pharmacodynamics of the Nitroimidazole DNDI-0690 in Mouse Models of Cutaneous Leishmaniasis.* Antimicrob Agents Chemother, 2019. **63**(9).

104. Mowbray, C.E., et al., *DNDI-6148: A Novel Benzoxaborole Preclinical Candidate for the Treatment of Visceral Leishmaniasis.* Journal of Medicinal Chemistry, 2021. **64**(21): p. 16159-16176.

105. Wyllie, S., et al., *Preclinical candidate for the treatment of visceral leishmaniasis that acts through proteasome inhibition.* Proc Natl Acad Sci U S A, 2019. **116**(19): p. 9318-9323.

106. Thomas, M.G., et al., *Identification of GSK3186899/DDD853651 as a Preclinical Development Candidate for the Treatment of Visceral Leishmaniasis.* J Med Chem, 2019. **62**(3): p. 1180-1202.

107. Braillard, S., et al., *DNDI-6174 is a preclinical candidate for visceral leishmaniasis that targets the cytochrome bc(1).* Sci Transl Med, 2023. **15**(726): p. eadh9902.

108. Van den Kerkhof, M., et al., *In vitro and in vivo pharmacodynamics of three novel antileishmanial lead series.* Int J Parasitol Drugs Drug Resist, 2018. **8**(1): p. 81-86.

109. Wyllie, S., et al., *Cyclin-dependent kinase 12 is a drug target for visceral leishmaniasis.* Nature, 2018. **560**(7717): p. 192-197.

110. Thacker, S.G., et al., *CpG ODN D35 improves the response to abbreviated low-dose pentavalent antimonial treatment in non-human primate model of cutaneous leishmaniasis.* PLoS Negl Trop Dis, 2020. **14**(2): p. e0008050.

111. Maheshwari, K.K. and D. Bandyopadhyay, *Heterocycles in the Treatment of Neglected Tropical Diseases.* Curr Med Chem, 2021. **28**(3): p. 472-495.

112. Rocha, V.P.C., et al., *Activity of antimalarial drugs in vitro and in a murine model of cutaneous leishmaniasis.* J Med Microbiol, 2013. **62**(Pt 7): p. 1001-1010.

113. Rodrigues, J.M., Jr., et al., *The activity and ultrastructural localization of primaquine-loaded poly (d,l-lactide) nanoparticles in Leishmania donovani infected mice.* Trop Med Parasitol, 1994. **45**(3): p. 223-8.

114. Carvalho, L., et al., *Tafenoquine, an antiplasmodial 8-aminoquinoline, targets leishmania respiratory complex III and induces apoptosis.* Antimicrob Agents Chemother, 2010. **54**(12): p. 5344-51.

115. Carvalho, L., et al., *The 8-aminoquinoline analogue sitamaquine causes oxidative stress in Leishmania donovani promastigotes by targeting succinate dehydrogenase.* Antimicrob Agents Chemother, 2011. **55**(9): p. 4204-10.

116. Loiseau, P.M., S. Cojean, and J. Schrevel, *Sitamaquine as a putative antileishmanial drug candidate: from the mechanism of action to the risk of drug resistance.* Parasite, 2011. **18**(2): p. 115-9.

117. Costa Duarte, M., et al., *An effective in vitro and in vivo antileishmanial activity and mechanism of action of 8-hydroxyquinoline against Leishmania species causing visceral and tegumentary leishmaniasis.* Veterinary Parasitology, 2016. **217**: p. 81-88.

118. Prachayasittikul, V., et al., *8-Hydroxyquinolines: a review of their metal chelating properties and medicinal applications.* Drug Des Devel Ther, 2013. **7**: p. 1157-78.

119. Ben-Othman, R., et al., *Leishmania-mediated inhibition of iron export promotes parasite replication in macrophages.* PLoS Pathog, 2014. **10**(1): p. e1003901.

120. Riehemann, K., et al., *Nanomedicine–challenge and perspectives.* Angew Chem Int Ed Engl, 2009. **48**(5): p. 872-97.

121. Mitchell, M.J., et al., *Engineering precision nanoparticles for drug delivery.* Nat Rev Drug Discov, 2021. **20**(2): p. 101-124.

122. Pandian, S.R.K., et al., *Nano Based Approach for the Treatment of Neglected Tropical Diseases.* Frontiers in Nanotechnology, 2021. **3**.

123. Santos-Valle, A.B.C., et al., *Nanomedicine strategies for addressing major needs in neglected tropical diseases.* Annual Reviews in Control, 2019. **48**: p. 423-441.

124. Mehtani, D., et al., *Chapter 4 - Biomaterials for Sustained and Controlled Delivery of Small Drug Molecules*, in *Biomaterials and Bionanotechnology*, R.K. Tekade, Editor. 2019, Academic Press. p. 89-152.

125. Anselmo, A.C. and S. Mitragotri, *Nanoparticles in the clinic.* Bioeng Transl Med, 2016. **1**(1): p. 10-29.

126. Hotez, P., et al., *The neglected tropical diseases: the ancient afflictions of stigma and poverty and the prospects for their control and elimination.* Adv Exp Med Biol, 2006. **582**: p. 23-33.

127. Verrest, L. and T.P.C. Dorlo, *Lack of Clinical Pharmacokinetic Studies to Optimize the Treatment of Neglected Tropical Diseases: A Systematic Review.* Clin Pharmacokinet, 2017. **56**(6): p. 583-606.

128. Wijnant, G.-J., et al., *Tackling Drug Resistance and Other Causes of Treatment Failure in Leishmaniasis.* Frontiers in Tropical Diseases, 2022. **3**.

129. De Rycker, M., et al., *Anti-trypanosomatid drug discovery: progress and challenges.* Nat Rev Microbiol, 2023. **21**(1): p. 35-50.

130. *Policy Cures Research, G-FINDER - NEGLECTED DISEASE RESEARCH AND DEVELOPMENT: THE HIGHER COST OF LOWER FUNDING*. 2023.

131. *Policy Cures Research, G-FINDER - Neglected Diseases*. on May 2024; Available from: https://gfinderdata.policycuresresearch.org/pages/data-visualisations/allNeglectedDiseases.

132. Blanco, E., H. Shen, and M. Ferrari, *Principles of nanoparticle design for overcoming biological barriers to drug delivery.* Nat Biotechnol, 2015. **33**(9): p. 941-51.

133. Gutierrez, V., et al., *New approaches from nanomedicine for treating leishmaniasis.* Chem Soc Rev, 2016. **45**(1): p. 152-68.

134. Gustafson, H.H., et al., *Nanoparticle Uptake: The Phagocyte Problem.* Nano Today, 2015. **10**(4): p. 487-510.

135. Thakur, C., et al., *Chapter 9 - Treating blood cancer with nanotechnology: A paradigm shift*, in *Nano Drug Delivery Strategies for the Treatment of Cancers*, A.K. Yadav, U. Gupta, and R. Sharma, Editors. 2021, Academic Press. p. 225-243.

136. Azevedo, E.G., et al., *Mixed formulation of conventional and pegylated liposomes as a novel drug delivery strategy for improved treatment of visceral leishmaniasis.* Expert Opin Drug Deliv, 2014. **11**(10): p. 1551-60.

137. Jamshaid, H., F.U. Din, and G.M. Khan, *Nanotechnology based solutions for anti-leishmanial impediments: a detailed insight.* J Nanobiotechnology, 2021. **19**(1): p. 106.

138. de Souza, R.M., et al., *Lipid nanoparticles for amphotericin delivery in the treatment of American tegumentary leishmaniasis.* Drug Deliv Transl Res, 2020. **10**(2): p. 403-412.

139. Saqib, M., et al., *Amphotericin B Loaded Polymeric Nanoparticles for Treatment of Leishmania Infections.* Nanomaterials (Basel), 2020. **10**(6).

140. Ramos, G.S., et al., *Formulation of Amphotericin B in PEGylated Liposomes for Improved Treatment of Cutaneous Leishmaniasis by Parenteral and Oral Routes.* Pharmaceutics, 2022. **14**(5).

141. Mukherjee, S., et al., *Short-Course Treatment With Imipramine Entrapped in Squalene Liposomes Results in Sterile Cure of Experimental Visceral Leishmaniasis Induced by Antimony Resistant Leishmania donovani With Increased Efficacy.* Front Cell Infect Microbiol, 2020. **10**: p. 595415.

142. Saleem, K., et al., *Applications of Nanomaterials in Leishmaniasis: A Focus on Recent Advances and Challenges.* Nanomaterials (Basel), 2019. **9**(12).

143. Prasanna, P., et al., *Current status of nanoscale drug delivery and the future of nano-vaccine development for leishmaniasis - A review.* Biomed Pharmacother, 2021. **141**: p. 111920.

144. Tuon, F.F., et al., *Liposomal drug delivery systems for the treatment of leishmaniasis.* Parasitol Res, 2022. **121**(11): p. 3073-3082.

145. Akbarzadeh, A., et al., *Liposome: classification, preparation, and applications.* Nanoscale Res Lett, 2013. **8**(1): p. 102.

146. van der Meel, R., et al., *Ligand-targeted particulate nanomedicines undergoing clinical evaluation: current status.* Adv Drug Deliv Rev, 2013. **65**(10): p. 1284-98.

147. Alharthi, S., et al., *Enhancing the therapeutic landscape of cutaneous leishmaniasis: pegylated liposomal delivery of miltefosine for controlled release and improved efficacy.* Journal of Drug Delivery Science and Technology, 2024. **96**: p. 105735.

148. Romanelli, M.M., et al., *Sertraline Delivered in Phosphatidylserine Liposomes Is Effective in an Experimental Model of Visceral Leishmaniasis.* Front Cell Infect Microbiol, 2019. **9**: p. 353.

149. Andrade-Neto, V.V., et al., *Imipramine alters the sterol profile in Leishmania amazonensis and increases its sensitivity to miconazole.* Parasites & Vectors, 2016. **9**(1): p. 183.

150. Mukherjee, S., et al., *Imipramine is an orally active drug against both antimony sensitive and resistant Leishmania donovani clinical isolates in experimental infection.* PLoS Negl Trop Dis, 2012. **6**(12): p. e1987.

151. Kaplum, V., et al., *In Vitro and In Vivo Activities of 2,3-Diarylsubstituted Quinoxaline Derivatives against Leishmania amazonensis.* Antimicrob Agents Chemother, 2016. **60**(6): p. 3433-44.

152. de Oliveira, J.K., et al., *Liposome-based nanocarrier loaded with a new quinoxaline derivative for the treatment of cutaneous leishmaniasis.* Mater Sci Eng C Mater Biol Appl, 2020. **110**: p. 110720.

153. Tenchov, R., et al., *Lipid Nanoparticles - From Liposomes to mRNA Vaccine Delivery, a Landscape of Research Diversity and Advancement.* ACS Nano, 2021. **15**(11): p. 16982-17015.

154. Scioli Montoto, S., G. Muraca, and M.E. Ruiz, *Solid Lipid Nanoparticles for Drug Delivery: Pharmacological and Biopharmaceutical Aspects.* Frontiers in Molecular Biosciences, 2020. **7**.

155. Singh, A., et al., *Formulation, characterization and in vitro anti-leishmanial evaluation of amphotericin B loaded solid lipid nanoparticles coated with vitamin B(12)-stearic acid conjugate.* Mater Sci Eng C Mater Biol Appl, 2020. **117**: p. 111279.

156. Parvez, S., et al., *Coalition of Biological Agent (Melatonin) With Chemotherapeutic Agent (Amphotericin B) for Combating Visceral Leishmaniasis via Oral Administration of Modified Solid Lipid Nanoparticles.* ACS Biomater Sci Eng, 2021.

157. Tavares, J., et al., *Anti-leishmanial activity of the bisnaphthalimidopropyl derivatives.* Parasitol Int, 2012. **61**(2): p. 360-3.

158. Islek, Z., et al., *Antileishmanial Activity of BNIPDaoct- and BNIPDanon-loaded Emulsomes on Leishmania infantum Parasites.* Frontiers in Nanotechnology, 2022. **3**.

159. Guerra, R.O., et al., *Metallic Nanoparticles: A New Frontier in the Fight Against Leishmaniasis.* Curr Med Chem, 2022. **29**(26): p. 4547-4573.

160. Awad, M.A., et al., *Antileishmanial effect of silver nanoparticles: Green synthesis, characterization, in vivo and in vitro assessment.* Biomed Pharmacother, 2021. **137**: p. 111294.

161. Osorno, L.L., et al., *Review of Contemporary Self-Assembled Systems for the Controlled Delivery of Therapeutics in Medicine.* Nanomaterials (Basel), 2021. **11**(2).

162. Kumari, A., S.K. Yadav, and S.C. Yadav, *Biodegradable polymeric nanoparticles based drug delivery systems.* Colloids Surf B Biointerfaces, 2010. **75**(1): p. 1-18.

163. Kumar, R., et al., *Development of PLGA-PEG encapsulated miltefosine based drug delivery system against visceral leishmaniasis.* Mater Sci Eng C Mater Biol Appl, 2016. **59**: p. 748-753.

164. Costa Lima, S.A., et al., *Characterization and evaluation of BNIPDaoct-loaded PLGA nanoparticles for visceral leishmaniasis: in vitro and in vivo studies.* Nanomedicine (Lond), 2012. **7**(12): p. 1839-49.

165. Ghosh, S., et al., *Amphotericin B-loaded mannose modified poly(d,l-lactide-co-glycolide) polymeric nanoparticles for the treatment of visceral leishmaniasis: in vitro and in vivo approaches.* RSC Advances, 2017. **7**(47): p. 29575-29590.

166. Jarak, I., et al., *Multifunctional polymeric micelle-based nucleic acid delivery: Current advances and future perspectives.* Applied Materials Today, 2021. **25**: p. 101217.

167. Perumal, S., R. Atchudan, and W. Lee *A Review of Polymeric Micelles and Their Applications*. Polymers, 2022. **14**, DOI: 10.3390/polym14122510.

168. Cabral, H., et al., *Block Copolymer Micelles in Nanomedicine Applications.* Chem Rev, 2018. **118**(14): p. 6844-6892.

169. Shukla, A., et al., *A comprehensive review on polymeric micelles: a promising drug delivery carrier.* J Anal Pharm Res., 2021. **10**(3): p. 102-107.

170. Yokoyama, M., *Clinical Applications of Polymeric Micelle Carrier Systems in Chemotherapy and Image Diagnosis of Solid Tumors.* Journal of Experimental & Clinical Medicine, 2011. **3**(4): p. 151-158.

171. Houdaihed, L., J.C. Evans, and C. Allen, *Overcoming the Road Blocks: Advancement of Block Copolymer Micelles for Cancer Therapy in the Clinic.* Mol Pharm, 2017. **14**(8): p. 2503-2517.

172. Shi, Y., et al., *Physico-Chemical Strategies to Enhance Stability and Drug Retention of Polymeric Micelles for Tumor-Targeted Drug Delivery.* Macromol Biosci, 2017. **17**(1).

173. Beach, M.A., et al., *Polymeric Nanoparticles for Drug Delivery.* Chemical Reviews, 2024. **124**(9): p. 5505-5616.

174. Varela-Moreira, A., et al., *Clinical application of polymeric micelles for the treatment of cancer.* Materials Chemistry Frontiers, 2017. **1**(8): p. 1485-1501.

175. Talelli, M., et al., *Nanobody-shell functionalized thermosensitive core-crosslinked polymeric micelles for active drug targeting.* J Control Release, 2011. **151**(2): p. 183-92.

176. Hwang, D., J.D. Ramsey, and A.V. Kabanov, *Polymeric micelles for the delivery of poorly soluble drugs: From nanoformulation to clinical approval.* Adv Drug Deliv Rev, 2020. **156**: p. 80-118.

177. Lage, L.M., et al., *An 8-hydroxyquinoline-containing polymeric micelle system is effective for the treatment of murine tegumentary leishmaniasis.* Parasitol Res, 2016. **115**(11): p. 4083-4095.

178. Duarte, M.C., et al., *Treatment of murine visceral leishmaniasis using an 8-hydroxyquinoline-containing polymeric micelle system.* Parasitol Int, 2016. **65**(6 Pt A): p. 728-736.

179. Joaquim, A.R., et al., *Novel Antimicrobial 8-Hydroxyquinoline-Based Agents: Current Development, Structure–Activity Relationships, and Perspectives.* Journal of Medicinal Chemistry, 2021. **64**(22): p. 16349-16379.

180. Ghezzi, M., et al., *Polymeric micelles in drug delivery: An insight of the techniques for their characterization and assessment in biorelevant conditions.* J Control Release, 2021. **332**: p. 312-336.

181. van Nostrum, C.F., *Covalently cross-linked amphiphilic block copolymer micelles.* Soft Matter, 2011. **7**(7): p. 3246-3259.

182. Yokoyama, M., et al., *Characterization of physical entrapment and chemical conjugation of adriamycin in polymeric micelles and their design for in vivo delivery to a solid tumor.* J Control Release, 1998. **50**(1-3): p. 79-92.

183. Zhuang, W.-R., et al., *Applications of π-π stacking interactions in the design of drug-delivery systems.* Journal of Controlled Release, 2019. **294**: p. 311-326.

184. Shi, Y., et al., *Complete Regression of Xenograft Tumors upon Targeted Delivery of Paclitaxel via Pi-Pi Stacking Stabilized Polymeric Micelles.* ACS Nano, 2015. **9**(4): p. 3740-52.

185. Shi, Y., et al., *Pi-pi stacking increases the stability and loading capacity of thermosensitive polymeric micelles for chemotherapeutic drugs.* Biomacromolecules, 2013. **14**(6): p. 1826-37.

186. Bagheri, M., et al., *Effect of Formulation and Processing Parameters on the Size of mPEG- b-p(HPMA-Bz) Polymeric Micelles.* Langmuir, 2018. **34**(50): p. 15495-15506.

187. Etrych, T., et al., *HPMA copolymer-doxorubicin conjugates: The effects of molecular weight and architecture on biodistribution and in vivo activity.* Journal of Controlled Release, 2012. **164**(3): p. 346-354.

188. Seymour, L.W., et al., *Effect of molecular weight (Mw) of N-(2-hydroxypropyl)methacrylamide copolymers on body distribution and rate of excretion after subcutaneous, intraperitoneal, and intravenous administration to rats.* J Biomed Mater Res, 1987. **21**(11): p. 1341-58.

CHAPTER II. Development of an automated image analysis protocol for quantification of intracellular forms of *Leishmania* spp.

Gomes-Alves AG et al. *PLoS One* 2018. 13:e0201747

1. Abstract

Leishmania parasites cause a set of neglected tropical diseases with considerable public health impact, the leishmaniases, which are often fatal if left untreated. Since current treatments for the leishmaniases exhibit high toxicity, low efficacy and prohibitive prices, many laboratories throughout the world are engaged in research for the discovery of novel chemotherapeutics. This entails the necessity of screening large numbers of compounds against the clinically relevant form of the parasite, the obligatory intracellular amastigote, a procedure that in many laboratories is still carried out by manual inspection. To overcome this well-known bottleneck in *Leishmania* drug development, several studies have recently attempted to automate this process. Here we implemented an image-based high content triage assay for *Leishmania* which has the added advantages of using primary macrophages instead of macrophage cell lines and of enabling identification of active compounds against parasite species developing both in small individual phagolysosomes (such as *L. infantum*) and in large communal vacuoles (such as *L. amazonensis*). The automated image analysis protocol is made available for IN Cell Analyzer systems, and, importantly, also for the opensource CellProfiler software, in this way extending its implementation to any laboratory involved in drug development as well as in other aspects of Leishmania research requiring analysis of *in vitro* infected macrophages.

2. Introduction

Trypanosomatid protozoan parasites of the genus Leishmania are the causative agents of some of the most significant neglected tropical diseases, the leishmaniases. There are over 20 species of *Leishmania* which, together with the particular genetics and immune characteristics of infected individuals, can cause a variety of clinical manifestations, including cutaneous and mucocutaneous forms and a fatal visceral condition [1]. The leishmaniases are present in 98 tropical and subtropical countries, where approximately 1 billion people are at risk of infection [1,2]. One alarming reality in such a scenario is the lack of adequate anti-*Leishmania* drugs, as current therapeutics exhibit important drawbacks like high toxicity, low efficacy, difficult administration and prohibitive prices [3]. Furthermore, the long treatment regimens of most drugs together with the side effects they cause bring about low medication compliance which, in turn, promotes disease relapse and emergence of drug resistant parasite strains [4]. Even though combination therapy, as encouraged by World Health Organization, circumvents some of those problems, the development of novel and more adequate anti-*Leishmania* treatments remains urgent [5]. Whatever the exact strategy followed in drug discovery [6], this process is much facilitated by the capacity to rapidly screen *in vitro* many compound library series against

Leishmania parasites through automated platforms. To reproduce the physiological conditions encountered *in vivo*, such high-throughput screening (HTS) assays should use the clinically relevant parasite stages and host cells.

Infection by *Leishmania* takes place when female sandflies inoculate promastigotes into a mammalian host during a blood meal. Promastigotes are phagocytosed by mononuclear phagocytic cells, mainly macrophages, and differentiate into amastigotes; after replication in phagolysosomes, the latter infect new cells [7,8]. The intracellular amastigote is therefore the disease-causing stage of *Leishmania* and, as such, the target that high throughput campaigns must aim at. Although *Leishmania* can invade different phagocytic cells, only macrophages support replication. Previously developed screening assays often used the human monocytic leukemia THP-1 and other cell lines as models as these are easy to handle and have high proliferative rates providing an unlimited source of material [9]. Nevertheless, usage of cell lines for screening purposes is not without concerns. Apart from cross-contamination with other cell lines and with mycoplasma [10], the genotypic and phenotypic changes that can arise due to continuous passages *in vitro* may lead to important differences relative to the primary cells that they represent [9], affecting overall results. An alternative option is the use of primary macrophages that, despite having a limited lifespan, maintain most *in vivo* physiological characteristics and functions.

The purpose of this study was twofold. First, to implement a high content analysis (HCA) protocol that used primary macrophages as host cells for *Leishmania* amastigotes, to identify new therapeutic drug candidates for all types of leishmaniases and facilitate other studies requiring parasite enumeration in *in vitro* macrophage infections. Second, to make available high throughput quantification of infection assays using microscopy images obtained by any kind of fluorescence microscope and without the need of expensive image analysis software. For this, we provide the image-analysis pipeline developed during this work on the free opensource cell image analysis software, CellProfiler [11].

3. Materials and methods

3.1. Parasites

Promastigotes of *L. infantum* (MHOM/MA/67/ITMAP-263) and *L. amazonensis* (MHOM/BR/LTB0016) were cultured at 25˚C in RPMI 1640 Glutamax supplemented with 10% (v/v) heat inactivated fetal bovine serum (iFBS), 50 U ml^{-1} penicillin, 50 μg ml^{-1} streptomycin (from Gibco) and 20 mM HEPES pH 7.4 (Sigma) and in Schneider's Insect medium (Sigma) supplemented with 10% (v/v) iFBS, 100 U ml^{-1} penicillin, 100 μg ml^{-1} streptomycin, 5mM HEPES pH 7.4 and 5μg ml^{-1} phenol-red (Sigma) media, respectively. Promastigotes of both species were passaged through mice in order to ensure infectivity.

Axenic amastigotes of *L. infantum* were differentiated from parasites recently recovered from the spleen of infected mice, as described before [12], and maintained at 37˚C, 5% CO2, in MAA medium supplemented with 20% (v/v) iFBS, 2 mM Glutamax (Gibco), and 0.023 mM hemin (Sigma).

3.2. Macrophages

Bone marrow-derived macrophages (BMDM) were generated by adapting the protocol described by Gomes et al. [13]. Briefly, bone-marrow cells, collected by flushing femurs and tibia of BALB/c mice with Hank's Balanced Salt Solution (HBSS), were centrifuged and suspended in Dulbecco's Modified Eagle's Medium (DMEM) supplemented with 1% (v/v) Minimum Essential Medium Non-Essential (MEM) amino acids solution (from Gibco), 10% (v/v) iFBS, 50 U ml^{-1} penicillin, 50 μg ml^{-1} streptomycin (cDMEM) and 10% (v/v) L929 cell conditioned medium (LCCM) as a source of macrophage colony-stimulating factor. Bone-marrow cells were placed in Petri dishes and incubated at 37˚C with 5% CO2. Twenty four hours later, non-adherent cells were collected, counted, plated in 96-well plates (2.5 to $3x10^4$ cells per well) and incubated at 37˚C with 5% CO_2 for 10 days, with cDMEM+10%LCCM renewal on the 4th and 7th days.

3.3. Infections and drug assessment

Bone marrow-derived macrophages, in 96 well plates, were infected with *L. infantum* axenic amastigotes (3-days culture) or *L. amazonensis* stationary promastigotes (5-days culture) at a multiplicity of infection (MOI) of 10. After 3 hours of contact with macrophages, non-phagocytosed parasites were removed by washing twice with cDMEM. Internalized parasites were allowed to differentiate into amastigotes for 24 hours prior to being challenged with serially diluted Amphotericin B (Sigma) or vehicle (DMSO). Twenty four hours after addition of the compounds, cultures were fixed with paraformaldehyde and processed for HCA.

3.4. Identification of parasites and macrophages in infection assays

Intramacrophagic *Leishmania* amastigotes were identified upon staining of their DNA with 4',6-diamidino-2-phenylindole (DAPI; Sigma). Macrophages were labelled with high-content screening (HCS) CellMask™ Deep Red stain (Invitrogen) which labels both nucleus and cytoplasm, hence providing a means to delineate the cell boundary. Both, DAPI and HCS Cell-Mask™ were added together to cells previously fixed with 4% paraformaldehyde (w/v) and permeabilized with 0.1% (v/v) Triton X-100 (Sigma), at room temperature for 30 minutes. For visualization of intracellular parasites with an indirect

fluorescent antibody test (IFAT), fixed and permeabilized cultures were blocked with 1% (w/v) BSA and then incubated with a mixture of anti-cTXNPx1 [14] and anti-mTPx [14] as primary antibodies, and an Alexa Fluor 568 anti-rabbit IgG (Molecular Probes) as secondary antibody, all used at 1:2000 dilution at room temperature for 2hrs.

3.5. Image acquisition

Images were acquired in an IN Cell Analyzer 2000 microscope (GE Healthcare) with a Nikon 20x/0.45 NA Plan Fluor objective (binning 1X1), using a large chip CCD Camera (CoolSNAP K4) with a pixel array of 2048x2048 (7.40 μm^2 pixel). Image field of view (FOV) x-y for this objective is 0.76x0.76 mm. With these settings and an approximate 70–80% cell confluence, 1500–2000 macrophages per well were imaged (per 4 FOV), a number we consider reasonable for the quantifications as it is 15 to 20–fold higher than that used with manual counting [15–17]. The excitation and emission filters used to detect DAPI, Alexa Fluor 568 and HCS Cell-Mask™ were DAPI, Texas Red, and Cy5, respectively.

3.6. Image analysis using the IN Cell Investigator Developer Toolbox

Original images were analyzed with the IN Cell Investigator Developer Toolbox v. 1.9.2 (GE Healthcare) (Fig 1A and 1B). This image analysis workflow allows the identification of the host cell nuclei (a DAPI stained structure with a size greater than 50 μm^2) and cytoplasm, as well as of the DNA content of parasites. For macrophage nuclei identification we used the DAPI channel (Fig 1A) and applied a pre-defined nuclear segmentation algorithm. This operation uses a variation of the '*top-hat*' approach to segmentation followed by a binary opening procedure to smooth the contours of the segmented nuclei and by a hole filling procedure. We then applied a slight expansion (dilation) of the nuclear mask in order to avoid incorrect detection of parasites (Fig 1C). The cell cytoplasm was segmented from the HCS CellMask™ raw image (Fig 1B) using an intensity segmentation operation. This operation employs simple

multilevel global thresholding to classify a pixel as either belonging, or not, to a target set. In order to separate adjacent touching cells, we executed a `clump breaking' procedure consisting of approximate cellular boundaries using the Voronoi tessellation generated from a `seed' point, in this case a segmented nuclear image (Fig 1D). Parasites were also segmented from the DAPI raw image using a pre-defined granular segmentation algorithm. This operation uses a multi-scale 'top-hat' approach based on a minimum (0.25μm) and a maximum granule size (1.00μm), hence being easily distinguishable from macrophage nuclei. Only parasites located inside the cells were counted. Due to

heterochromatin heterogeneity, macrophage nuclei often present a granular aspect and these granules can occasionally be confused with parasites. To avoid such "false positives", the nuclear mask (Fig 1C) was subtracted from the parasite segmentation mask (Fig 1E). The final processed image is shown in Fig 1F, where macrophage nuclei, macrophage boundary and parasites are outlined in blue, yellow and green, respectively. Every segmentation algorithm used here can be fine-tuned through sensitivity adjustment to optimize the analysis of the images. Upon segmentation of all objects of interest, quantitative data were extracted. Accordingly, we obtained the total number of macrophages and parasites, the number of infected macrophages and the number of parasites per infected macrophage.

3.7. Image analysis using CellProfiler

The following specifications were used to analyze images with CellProfiler (2.2.0) (Fig 2A and 2B). For nuclei segmentation we applied a Global thresholding strategy followed by an Otsu thresholding method. Adjacent merged nuclei were separated into individual objects of interest by identification of a central single peak of brightness on each nucleus. Next, we did a slight expansion (dilation) of the nuclear mask in order to avoid false positive detection of parasites in the vicinity of the nuclei (Fig 2C). After this, the cell cytoplasm was segmented from the HCS CellMask™ raw image through a propagation algorithm of the mask starting from the previously identified nucleus until the edges of the staining using the same thresholding method as for nuclei segmentation (Fig 2D). Parasites were segmented using a similar methodology, based on a typical diameter of the parasites between 4–12 pixel units. Adjacent merged parasites were separated into individual objects through the identification of a central single peak of brightness on each organism (Fig 2E). Next, the number of amastigotes in the cytoplasm mask was calculated. The final processed image is shown in Fig 2F. The algorithm can be modified to optimize image analysis through fine-tuning of threshold correction factors. CellProfiler analysis provides the total number of macrophages and parasites, the number of infected macrophages and the number of parasites per infected macrophage.

3.8. Ethical statement

BALB/c mice were obtained from the i3S animal facility. Animal procedures were approved by the Local Animal Ethics Committee of i3S, licensed by DGAV (Direção Geral de Alimentação e Veterinária, Govt. of Portugal – DGAV). Animals were handled in strict accordance with good animal practice as defined by national authorities (DGAV, directive 113/2013 from 7th August) and European legislation (directive

2010/63/EU, revising directive 86/609/EEC). The i3S animal house is certified by DGAV. Mice were euthanized by an overdose of isoflurane inhalation followed by cervical dislocation.

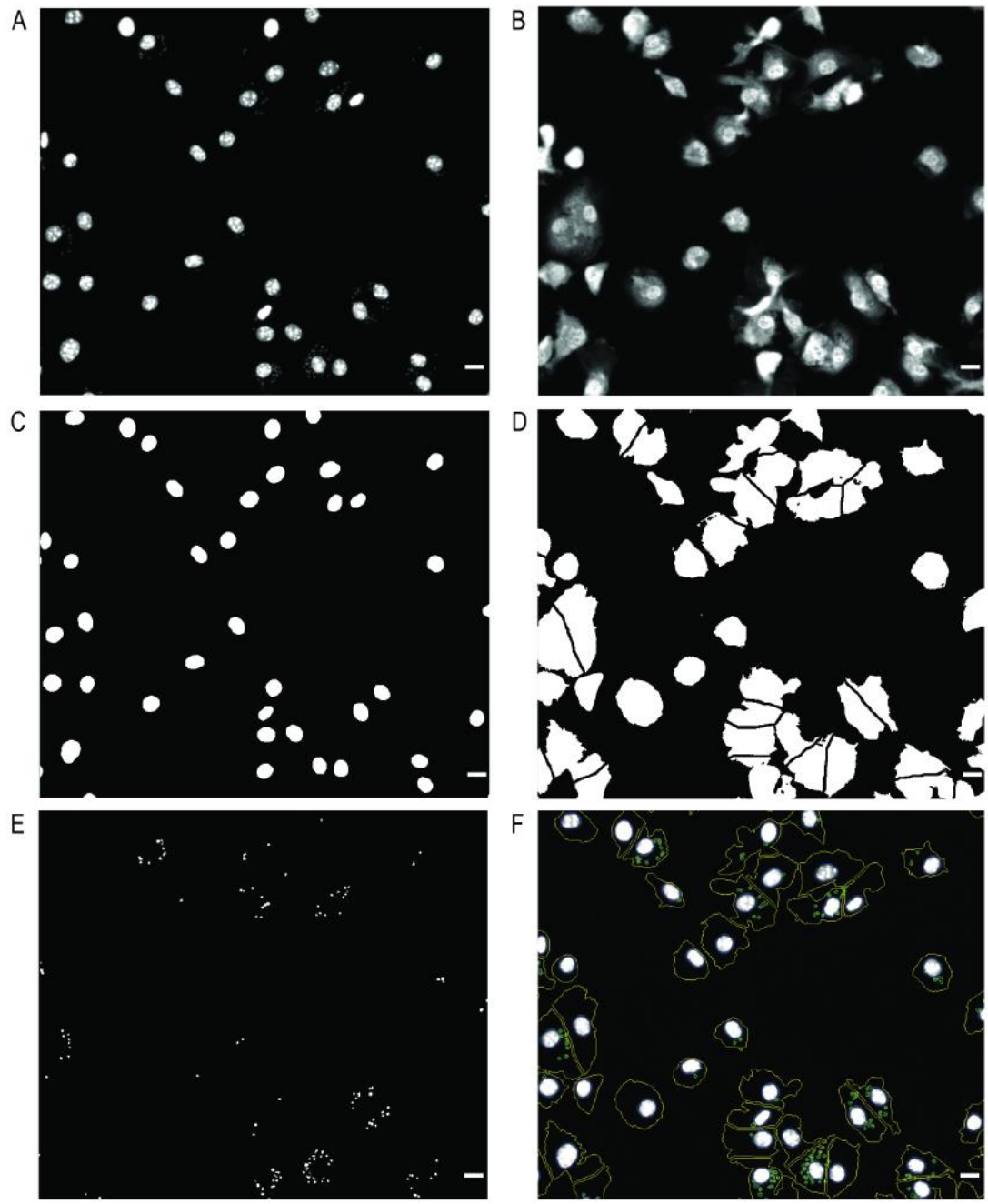

Fig 1. Detection of intramacrophagic parasites using IN Cell Investigator Developer Toolbox. Raw image from (A) DAPI and (B) HCS CellMask™ Deep Red channels acquired with IN Cell Analyzer 2000 microscope. (C) Nuclei of macrophages identified by a predefined nuclear segmentation for objects stained with DAPI larger than 50μm^2. (D) Cytoplasm of macrophages recognized by HCS CellMask™ Deep Red staining. (E) Parasites are objects stained with DAPI localized inside cytoplasm and with sizes between 0.25–1μm. (F) Final processed image showing macrophage nuclei (blue line), cell boundaries (yellow line) and parasites (green line). Scale bar, 10μm.

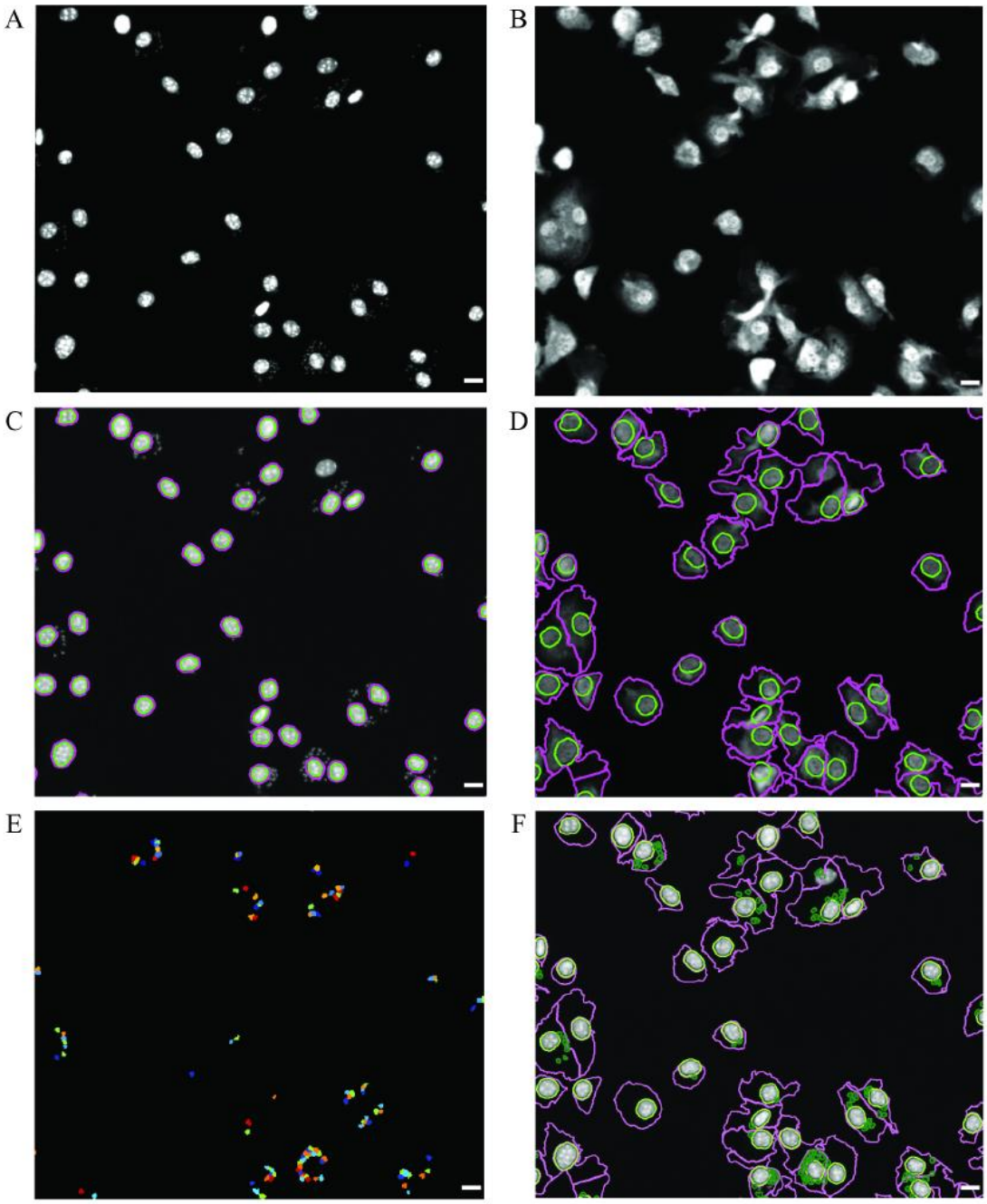

Fig 2. Detection of intramacrophagic parasites using Cell Profiler. Raw image from (A) DAPI and (B) HCS CellMask™ Deep Red imaging channels acquired with IN Cell Analyzer 2000 microscope. (C) BMDM nuclei identified as DAPI-positive objects with a size range of 18–50 pixels (green line); also depicted is the nuclear expansion applied to avoid false positive detection of parasites in the vicinity of the nuclei (pink line). (D) Macrophages detected by a propagation algorithm of the HCS CellMask™ Deep Red staining which starts in the nucleus (green line) and ends in the BMDM cell boundaries (pink line). (E) Parasites identified as DAPI-staining objects with 4–12 pixels located within the cytoplasm of BMDMs. (F) Final processed image showing BMDM nuclei expansion (light green line), cell boundary (pink line) and parasites (dark green line). Scale bar, 10μm.

3.9. Statistical analysis

Statistical analysis (One way ANOVA) to compare data extracted from CellProfiler and IN Cell Investigator Developer Toolbox with that obtained by manual counting was performed using GraphPad Prism Software 5.02. This same software was also used to calculate amphotericin B half maximal inhibitory concentrations (IC_{50}).

4. Results

4.1. Parasite and infected cell labelling

In this work, we implemented HCS assays for quantification of intracellular *Leishmania* using primary murine macrophages as the parasite host cells. A crucial step in microscopy-based high content methodologies is the capacity to detect and discriminate between the different image elements accurately, in this case intracellular parasites and macrophages. Amastigote identification was achieved employing DAPI staining, as described previously [18–20]. The suitability of this stain was confirmed by labelling intracellular *L. infantum* with DAPI and with anti-parasite antibodies by IFAT (Fig 3). We used the anti-cTXNPx and anti-mTXNPx antibodies (Fig 3A), which recognize proteins located in the parasite cytoplasm and mitochondria, respectively. This approach showed that all structures detected with DAPI co-localized

with the antibody-staining (Fig 3B and 3C). For macrophage detection both nuclei and the cytoplasm were taken into account. The former were identified with DAPI, the second by delimiting their contour. Some HCA studies have defined the macrophage boundary by computation based on the position of the nucleus [18,20]. This approach, that assumes that nuclei are consistently located in the center of the cell, can lead to inaccurate results especially when using primary macrophages such as BMDMs. Indeed, the morphology of these is not as homogeneous as that of macrophage cell lines, in many instances presenting protrusions that expand away from the nucleus (Fig 4). To overcome this issue, we have defined BMDM contour, as described by Manu De Rycker et al. [21], taking advantage of the HCS CellMask™, a cell delineation tool for HCS assays. As shown in Fig 4, this mask clearly labels the cell cytoplasm facilitating macrophage identification even in cultures with heterogeneous morphologies.

4.2. IN Cell Investigator Developer Toolbox and CellProfiler image analysis

The first image protocol developed here used the IN Cell Investigator Developer Toolbox. The program identifies individual macrophages, by the association of a nucleus with a well-delimited cytoplasm, and the parasites within each of them. Two important algorithm features should be outlined. First, parasites

that do not co-localize inside macrophage boundaries are not taken into account to calculate the percentage of infected macrophages and the number of intracellular parasites. Second, even though DAPI staining labels two different structures in each parasite, one corresponding to nuclear DNA and the other to the mitochondrial kinetoplast DNA (kDNA), the segmentation applied ensures that only the latter, which is brighter, is identified by the software algorithm as a parasite (Fig 1E). The ability of the software to correctly detect macrophages and intracellular *L. infantum* amastigotes is illustrated in Fig 1F and S1C Fig. Unlike *L. infantum*, that replicates in tight-fitting, individual phagolysosomes, some *Leishmania* species propagate within giant vacuoles hosting many parasites, a phenotypic characteristic that can reflect on the morphology of the macrophage. Using *L. amazonensis*, a representative of such species, we ensured that the type of phagolysosome parasitized by *Leishmania* does not interfere with the capacity of the program to correctly identify macrophages and parasites (S1C Fig), in this way validating the use of the algorithm to any *Leishmania* species. Fig 5, showing that the estimated infection rates augment as the multiplicity of infection (MOI) increases, also suggests that the system is adequate for intramacrophage amastigote quantification.

The IN Cell Investigator Developer Toolbox is a commercial, expensive, software that may not be available to all research groups. In order to enable usage of our framework by other labs working on *Leishmania*, we have adapted our image analysis workflow to an open-source software, CellProfiler [11], which permits analysis of images acquired by any kind of fluorescence microscope, including of high throughput. CellProfiler identifies macrophages and parasites similarly and as effectively as the IN Cell Investigator Developer Toolbox, as demonstrated for *L. infantum* (Fig 2F) and *L. amazonensis* (S1D Fig).

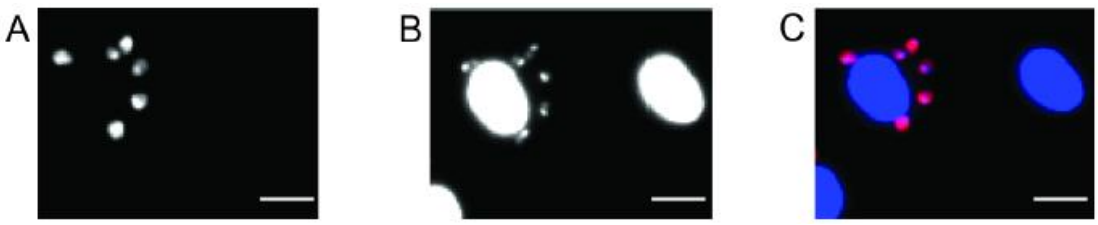

Fig 3. Intracellular *L. infantum* labeled with anti-parasite antibodies by IFAT and with DAPI. *Leishmania infantum*-infected BMDM stained with (A) anti-cTXNPx and anti-mTXNPx and with (B) DAPI (arrows identify intracellular parasites). (C) Merged image showing co-localization of DAPI-stained (blue) parasites with antibody labeling (red). Images were acquired with an IN Cell Analyzer 2000 microscope. Scale bar, 10μm.

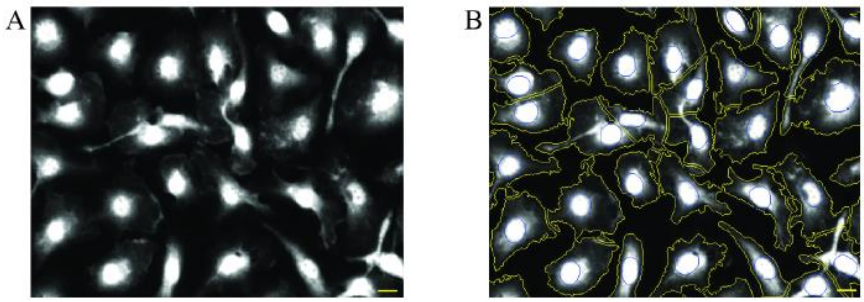

Fig 4. Heterogeneous morphology of BMDM. (A) HCS CellMask™ Deep Red raw image acquired with an IN Cell Analyzer 2000 microscope (B) Cytoplasm boundary defined by IN Cell Investigator Developer Toolbox (yellow line). Blue lines represents cell nucleus. Scale bar, 10μm.

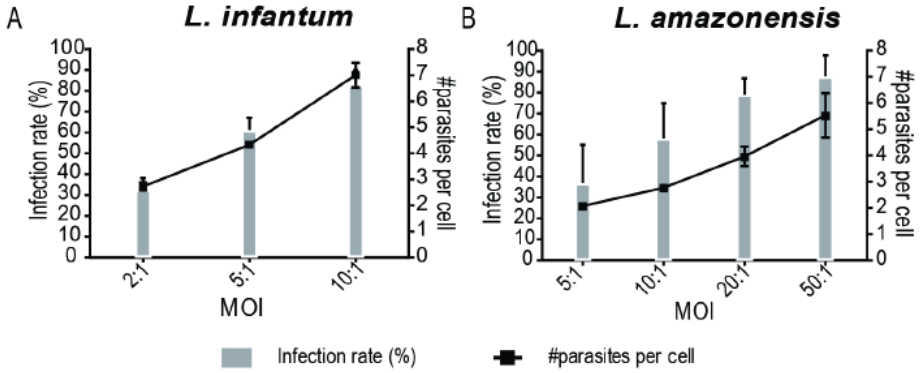

Fig 5. IN Cell Investigator Developer Toolbox infectivity parameters depends on the MOI. Infection rate and the number of intracellular amastigotes by (A) *L. infantum*, (B) *L. amazonensis* using different parasite:BMDM ratios (MOI), as detected by IN Cell Investigator Developer Toolbox. Values represent the mean and standard deviation of three independent experiments.

4.3.Comparison of Cell Profiler with IN Cell Investigator Developer Toolbox

Validation of CellProfiler and IN Cell Investigator Developer Toolbox image analysis workflows was performed by comparing their data output with that obtained by manual counting (i.e., upon eye enumeration of macrophage and parasite numbers on the acquired images). For this purpose, the number of parasites detected in each case in approximately 900 *L. infantum*-infected macrophages (300 representative of each MOI) was registered. Using these data, we calculated the infection rate and the number of parasites per macrophage (Fig 6). We found that the former parameter was similar in all three methodologies (Fig 6A). As for the number of parasites per macrophage, this also compared well in the MOI of 2 and 5 but was found lower when using automated analysis in the MOI of 10 (Fig 6B).

This occurs due to a greater number of highly infected macrophages in this condition making discrimination of single parasites less accurate.

The CellProfiler image analysis pipeline was additionally compared with the IN Cell Investigator Developer Toolbox protocol. Analysis of 382 images with both workflows indicated a high degree of correlation between them (Fig 7). The infection rate (Fig 7A), the number of parasites per macrophage (Fig 7B), as well as the total number of macrophages (Fig 7C) were similar in both outputs (R^2>0.97).

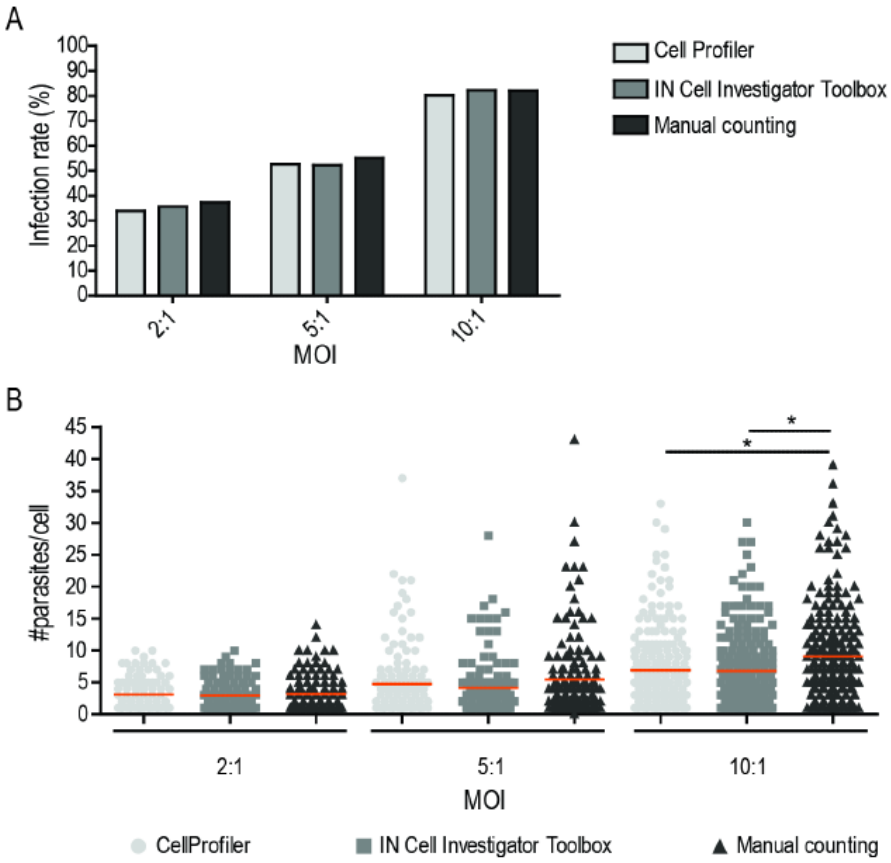

Fig 6. Comparison of IN Cell Investigator Developer Toolbox and CellProfiler image analysis protocols with manual counting. BMDMs were infected with *L. infantum* axenic amastigotes at different MOI. (A) Infection rate. (B) Number of parasites per infected cell obtained with each automated protocol was compared with manual counting. Each dot represents the number of parasites in a single host cell and horizontal lines show the mean. Around 300 cells counted in each MOI condition. Statistical analysis was performed using the One-Way ANOVA. P-values correspond to *p<0.05.

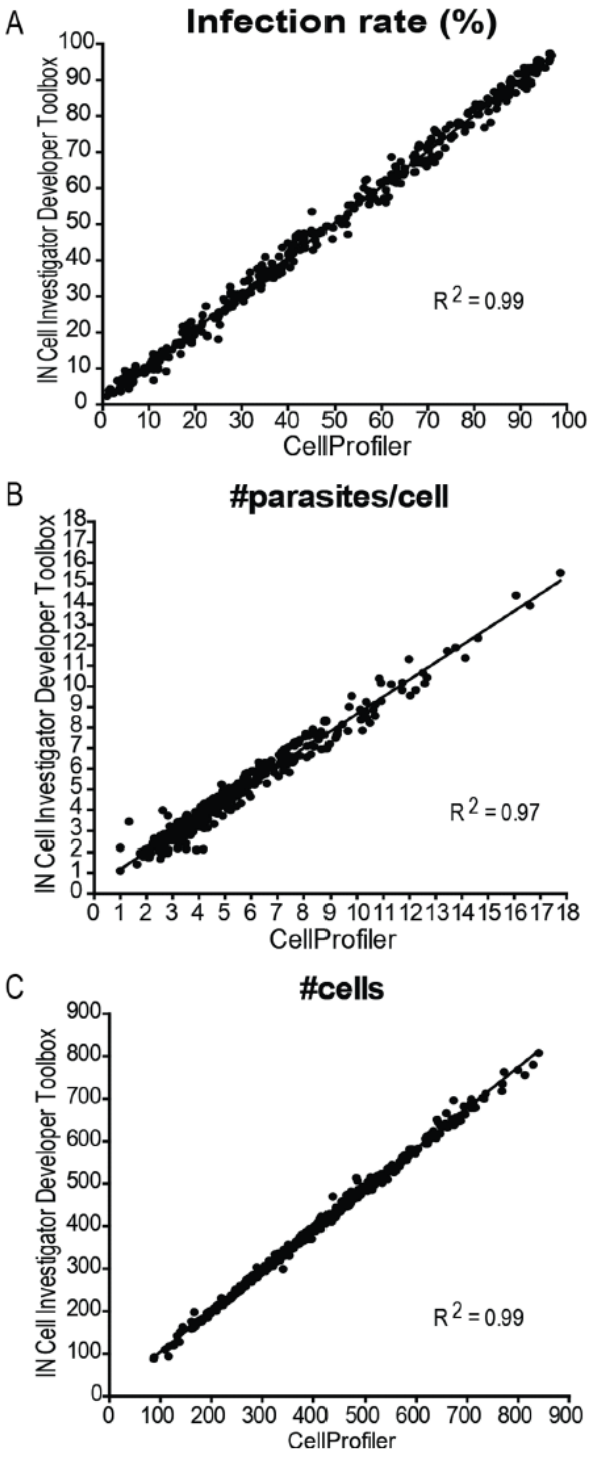

Fig 7. Correlation between IN Cell Investigator Developer Toolbox and CellProfiler image analysis protocols. (A) Infection rate, (B) number of parasites per infected cell, and (C) the total number of cells as compared using both image analysis protocol. Each dot represents the result of a single image.

4.4. Pharmacological validation of IN Cell Investigator Developer Toolbox and Cell Profiler workflows

Since facilitating anti-*Leishmania* drug testing was a major driving force towards implementation of the IN Cell Investigator Developer Toolbox and CellProfiler protocols, we evaluated their pharmacological relevance. For this, we infected BMDM with *L. infantum* and *L. amazonensis* and treated the monolayers with amphotericin B, an anti-*Leishmania* reference drug that acts by disrupting parasite membranes and, hence, translates in a rapid decrease in amastigote number [18,19,22,23]. Images acquired at the end of the experiments were then analyzed following both methodologies, extracting both the percentages of infection and the number of amastigotes per infected macrophage. The results, obtained for both *Leishmania* species, are depicted in Fig 8. The IC_{50} values calculated from those data (0.037±0.012 and 0.024±0.010μM for *L. infantum* according to IN Cell Investigator Developer Toolbox and CellProfiler, respectively, and 0.037±0.012 and 0.039±0.004μM for *L. amazonensis* in the same situations) were in concordance with published results [24].

In short, the image analysis protocols developed using the IN Cell Investigator Developer Toolbox and the CellProfiler software enable high throughput and reliable determination of the number of infected macrophages and of parasites per infected macrophage, independently of the *Leishmania* species used.

Both image analysis workflows, IN Cell Investigator Developer Toolbox protocol (S1 Appendix) and CellProfiler pipeline (S2 Appendix), can be freely downloaded from https://github.com/andrefilipemaia/intramacrophagic_parasites_counter.

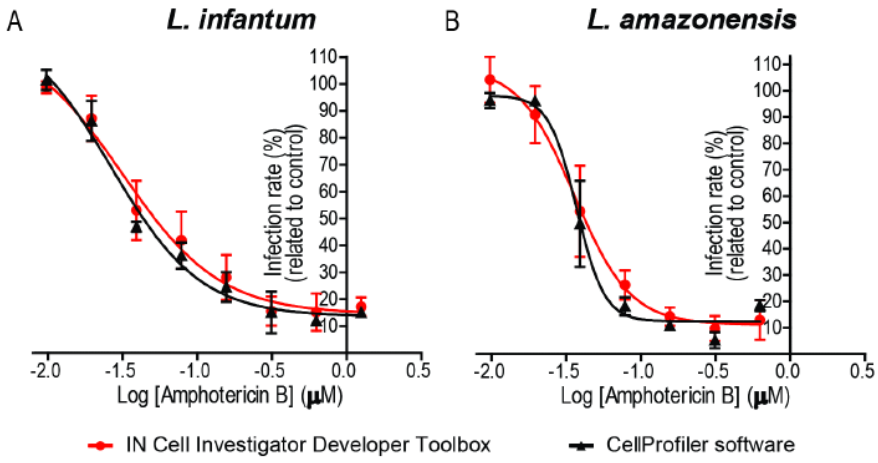

Fig 8. Anti-*Leishmania* activity of amphotericin B assessed with IN Cell Investigator Developer Toolbox and CellProfiler. Dose response curves of (A) *L. infantum* or (B) *L. amazonensis*. IN Cell Investigator Developer Toolbox (red line) and CellProfiler (black line). Values represent the mean and standard deviation of at least two independent experiments.

5. Discussion

Drug discovery for infectious diseases inevitably requires the capacity to triage large numbers of chemical compounds against microbial pathogens, a process simplified by the existence of adequate high throughput phenotypic methodologies. In the case of diseases caused by *Leishmania* parasites, previously developed HTS assays often used promastigotes and axenic amastigotes [22,25–27]. However, in spite of enabling cheap, fast and simple protocols, screening against these parasite forms in many instances lead to false positive and negative hits [18,21,28]. For instance, apparent leishmanicidal compounds will in fact lack clinical relevance if unable to cross host cell membranes or if their target molecule is not expressed by intracellular amastigotes [29–31]. Triage based on axenic parasite forms will exclude chemicals of interest whenever these require host cell metabolism for activity, or when their parasiticidal capacity is promoted not by the compound itself but by its ability to induce an inflammatory state in infected macrophages. For these reasons, recent HTS assays have favored the use of the more physiologically relevant intracellular amastigotes, albeit, with two exceptions [19,32], resorting to macrophage cell lines [18,20,21,23]. In order to mimic as closely as possible an *in vivo* infection, the present assay was established using primary macrophages derived from murine bone marrow. Although optimized here for 96-well plates, with appropriate equipment, the BMDM differentiation protocol can be adapted to 384 or 1536 well plates allowing screening of larger libraries with a relatively low number of animals. The methodology developed in this report is, in addition, a high content analysis (HCA) procedure that quantifies intracellular amastigotes based on optical microscopy. An important feature of microscopy based methods, when compared to indirect methodologies like luminescence/fluorescence plate reading approaches, is that they enable visualization and determination of the actual parasite number. Previous studies [21,32] employed genetically modified parasites expressing a reporter gene such as green fluorescence protein (GFP) or DsRed2 molecule to facilitate parasite identification. However, this approach has the immediate drawback that such organisms are no longer wild-type and the reporter genes may interfere with drug screening output by decreasing strain virulence [18,33]. Furthermore, genetic manipulation steps would be required every time a new species or strain is used. The protocol developed in this study overcomes these limitations and can also be used in functional analysis studies of *Leishmania* requiring transgenic or knockout mutants.

Determination of the number of macrophages and intracellular amastigotes was first automated with the IN Cell Investigator Developer Toolbox, a proprietary software accompanying our high content microscope, IN Cell Analyzer 2000. However, many laboratories performing *Leishmania* drug

development studies do not have easy access to HCS-microscopes and this specific software. In such cases, drug screening ability is limited by the time required for image acquisition and analysis. In order to simplify the latter, we proposed the CellProfiler image analysis pipeline whose correlation with IN Cell Investigator Developer protocol was very high (R^2>0.97). Since the activity of some drugs (*eg* miltefosine) can differ between *Leishmania* spp., candidate compounds ought to be screened *in vitro* against several species [34,35]. Both software workflows employed in this study are suitable for addressing this issue as they were optimized and validated with *L. infantum* and *L. amazonensis*. The former parasite is representative of species maturing in small individual parasitophorous vacuoles, while *L. amazonensis* represents *Leishmania* spp. inhabiting communal vacuoles housing several amastigotes, a factor that dramatically changes host cell morphology. The use of *L. infantum* axenic amastigotes to infect BMDM relates to the high infection rates that are possible to obtain with this parasite form. Unfortunately, we are not able to cultivate *L. amazonensis* axenic amastigotes and, as such, resorted to stationary phase promastigotes. Both image analysis workflows are comparable in terms of performance with manual counting; however, in some circumstances, adjustment of specific image analysis settings might be required for maximum performance. This is the case, for instance, when analyzing compounds affecting host cell nucleus morphology.

In conclusion, this work presents a new methodology for identification of novel therapeutic drugs for leishmaniasis in two image analysis platforms, IN Cell Investigator Developer Toolbox and the free open source Cell Profiler. This workflow should enable fast and standardized analysis of microscopy images from *Leishmania*-infected macrophages in any laboratory.

6. References

1. World Health Organization. Leishmaniasis in high-burden countries: an epidemiological update based on data reported in 2014. Relev Epidemiol Hebd. 2016; 91: 287–96.

2. Alvar J, VeÂlez ID, Bern C, Herrero M, Desjeux P, Cano J, et al. Leishmaniasis worldwide and global estimates of its incidence. PLoS One. 2012; 7: e35671. https://doi.org/10.1371/journal.pone.0035671 PMID: 22693548

3. Field MC, Horn D, Fairlamb AH, Ferguson MAJ, Gray DW, Read KD, et al. Anti-trypanosomatid drug discovery: an ongoing challenge and a continuing need. Nat Rev Microbiol. 2017; 15: 217–231. https://doi.org/10.1038/nrmicro.2016.193 PMID: 28239154

4. Alvar J, Croft S, Olliaro P. Chemotherapy in the Treatment and Control of Leishmaniasis. Adv Parasitol. 2006; 61: 223–274. https://doi.org/10.1016/S0065-308X(05)61006-8 PMID: 16735166

5. World Health Organization. Control of the leishmaniases. World Health Organ Tech Rep Ser. 2010; xii–xiii, 1–186, back cover. https://doi.org/10.1038/nrmicro1766

6. Field MC, Horn D, Fairlamb AH, Ferguson MAJ, Gray DW, Read KD, et al. Anti-trypanosomatid drug discovery: An ongoing challenge and a continuing need. Nature Reviews Microbiology. 2017. pp. 217–231. https://doi.org/10.1038/nrmicro.2016.193 PMID: 28239154

7. Handman E, Bullen DVR. Interaction of Leishmania with the host macrophage. Trends in Parasitology. 2002. pp. 332–334. https://doi.org/10.1016/S1471-4922(02)02352-8 PMID: 12377273

8. Kaye P, Scott P. Leishmaniasis: complexity at the host-pathogen interface. Nat Rev Microbiol. 2011; 9: 604–615. https://doi.org/10.1038/nrmicro2608 PMID: 21747391

9. Kaur G, Dufour JM. Cell lines: Valuable tools or useless artifacts. Spermatogenesis. 2012; 2: 1–5. https://doi.org/10.4161/spmg.19885 PMID: 22553484

10. Capes-Davis A, Theodosopoulos G, Atkin I, Drexler HG, Kohara A, MacLeod RAF, et al. Check your cultures! A list of cross-contaminated or misidentified cell lines. Int J Cancer. 2010; 127: 1–8. https://doi.org/10.1002/ijc.25242 PMID: 20143388

11. Carpenter AE, Jones TR, Lamprecht MR, Clarke C, Kang IH, Friman O, et al. CellProfiler: image analysis software for identifying and quantifying cell phenotypes. Genome Biol. 2006; 7: R100. https://doi.org/10.1186/gb-2006-7-10-r100 PMID: 17076895

12. Sereno D, Lemesre JL. Axenically cultured amastigote forms as an in vitro model for investigation of antileishmanial agents. Antimicrob Agents Chemother. 1997; 41: 972–976. PMID: 9145854

13. Salomé Gomes M, Fernandes SS, Cordeiro J V., Gomes SS, Vieira A, Appelberg R. Engagement of Toll-like receptor 2 in mouse macrophages infected with Mycobacterium avium induces non-oxidative and TNF-independent anti-mycobacterial activity. Eur J Immunol. 2008; 38: 2180–2189. https://doi.org/10.1002/eji.200737954 PMID: 18624355

14. Castro H, Teixeira F, Romao S, Santos M, Cruz T, Flórido M, et al. Leishmania mitochondrial peroxiredoxin plays a crucial peroxidase-unrelated role during infection: Insight into its novel chaperone activity. PLoS Pathog. 2011; 7: e1002325. https://doi.org/10.1371/journal.ppat.1002325 PMID: 22046130

15. Shokri A, Abastabar M, Keighobadi M, Emami S, Fakhar M, Hosseini Teshnizi S, et al. Promising antileishmanial activity of novel imidazole antifungal drug Luliconazole against Leishmania major: in vitro and in silico studies. J Glob Antimicrob Resist. 2018; https://doi.org/10.1016/j.jgar.2018.05.007 PMID:29793051

16. Isaac-Márquez AP, TalamaÂs-Rohana P, Galindo-Sevilla N, Gaitan-Puch SE, Diaz-Diaz NA, Hernández-Ballina GA, et al. Decanethiol functionalized silver nanoparticles are new powerful leishmanicidals in vitro. World J Microbiol Biotechnol. 2018; https://doi.org/10.1007/s11274-018-2420-0 PMID: 29460068

17. Monzote L, GarcõÂa M, Pastor J, Gil L, Scull R, Maes L, et al. Essential oil from Chenopodium ambrosioides and main components: Activity against Leishmania, their mitochondria and other microorganisms. Exp Parasitol. 2014; https://doi.org/10.1016/j.exppara.2013.10.007 PMID: 24184772

18. Siqueira-Neto JL, Moon S, Jang J, Yang G, Lee C, Moon HK, et al. An image-based high-content screening assay for compounds targeting intracellular Leishmania donovani amastigotes in human macrophages. PLoS Negl Trop Dis. 2012; 6: e1671. https://doi.org/10.1371/journal.pntd.0001671 PMID: 22720099

19. Eren RO, Kopelyanskiy D, Moreau D, Chapalay JB, Chambon M, Turcatti G, et al. Development of a semi-automated image-based high-throughput drug screening system. Front Biosci (Elite Ed). 2018; 1: 242–253.

20. De Muylder G, Ang KKH, Chen S, Arkin MR, Engel JC, McKerrow JH. A screen against Leishmania intracellular amastigotes: Comparison to a promastigote screen and identification of a host cell-specific hit. PLoS Negl Trop Dis. 2011; 5: e1253. https://doi.org/10.1371/journal.pntd.0001253 PMID: 21811648

21. De Rycker M, Hallyburton I, Thomas J, Campbell L, Wyllie S, Joshi D, et al. Comparison of a highthroughput high-content intracellular Leishmania donovani assay with an axenic amastigote assay. Antimicrob Agents Chemother. 2013; 57: 2913–2922. https://doi.org/10.1128/AAC.02398-12 PMID: 23571538

22. Siqueira-Neto JL, Song OR, Oh H, Sohn JH, Yang G, Nam J, et al. Antileishmanial high-throughput drug screening reveals drug candidates with new scaffolds. PLoS Negl Trop Dis. 2010; 4: e675. https://doi.org/10.1371/journal.pntd.0000675 PMID: 20454559

23. Dagley MJ, Saunders EC, Simpson KJ, McConville MJ. High-Content Assay for Measuring Intracellular Growth of Leishmania in Human Macrophages. Assay Drug Dev Technol. 2015; 13: 389±401. https://doi.org/10.1089/adt.2015.652 PMID: 26247370

24. Seifert K, Escobar P, Croft SL. In vitro activity of anti-leishmanial drugs against Leishmania donovani is host cell dependent. J Antimicrob Chemother. 2010; 65: 508–511. https://doi.org/10.1093/jac/dkp500 PMID: 20089542

25. Mikus J, Steverding D. A simple colorimetric method to screen drug cytotoxicity against Leishmania using the dye Alamar Blue. Parasitol Int. 2000; 48: 265–269. https://doi.org/10.1016/S1383-5769(99)00020-3 PMID: 11227767

26. Sharlow ER, Close D, Shun T, Leimgruber S, Reed R, Mustata G, et al. Identification of potent chemotypes targeting Leishmania major using a high-throughput, low-stringency, computationally enhanced, small molecule screen. PLoS Negl Trop Dis. 2009; 3: e540. https://doi.org/10.1371/journal.pntd.0000540 PMID: 19888337

27. Shimony O, Jaffe CL. Rapid fluorescent assay for screening drugs on Leishmania amastigotes. J Microbiol Methods. 2008; 75: 196–200. https://doi.org/10.1016/j.mimet.2008.05.026 PMID: 18573286

28. Vermeersch M, Da Luz RI, ToteÂ K, Timmermans JP, Cos P, Maes L. In vitro susceptibilities of Leishmania donovani promastigote and amastigote stages to antileishmanial reference drugs: Practical relevance of stage-specific differences. Antimicrob Agents Chemother. 2009; 53: 3855–3859. https://doi.org/10.1128/AAC.00548-09 PMID: 19546361

29. Pescher P, Blisnick T, Bastin P, SpaÈth GF. Quantitative proteome profiling informs on phenotypic traits that adapt Leishmania donovani for axenic and intracellular proliferation. Cell Microbiol. 2011; 13: 978–991. https://doi.org/10.1111/j.1462-5822.2011.01593.x PMID: 21501362

30. Rochette A, Raymond F, Ubeda J-M, Smith M, Messier N, Boisvert S, et al. Genome-wide gene expression profiling analysis of Leishmania major and Leishmania infantum developmental stages reveals substantial differences between the two species. BMC Genomics. 2008; 9: 255. https://doi.org/10.1186/1471-2164-9-255 PMID: 18510761

31. Rochette A, Raymond F, Corbeil J, Ouellette M, Papadopoulou B. Whole-genome comparative RNA expression profiling of axenic and intracellular amastigote forms of Leishmania infantum. Mol Biochem Parasitol. 2009; 165: 32–47. https://doi.org/10.1016/j.molbiopara.2008.12.012 PMID: 19393160

32. Aulner N, Danckaert A, Rouault-Hardoin E, Desrivot J, Helynck O, Commere PH, et al. High Content Analysis of Primary Macrophages Hosting Proliferating Leishmania Amastigotes: Application to Antileishmanial Drug Discovery. PLoS Negl Trop Dis. 2013; 7: e2154. https://doi.org/10.1371/journal.pntd.0002154 PMID: 23593521

33. de Toledo JS, Junqueira dos Santos AF, Rodrigues de Moura T, Antoniazi SA, Brodskyn C, Indiani de Oliveira C, et al. Leishmania (Viannia) braziliensis transfectants overexpressing the miniexon gene lose virulence in vivo. Parasitol Int. Elsevier Ireland Ltd; 2009; 58: 45–50. https://doi.org/10.1016/j.parint.2008.09.006 PMID: 18992366

34. Dorlo TPC, Balasegaram M, Beijnen JH, de vries PJ. Miltefosine: A review of its pharmacology and therapeutic efficacy in the treatment of leishmaniasis. J Antimicrob Chemother. 2012; 67: 2576–2597. https://doi.org/10.1093/jac/dks275 PMID: 22833634

35. Croft SL, Sundar S, Fairlamb AH. Drug resistance in leishmaniasis. Clin Microbiol Rev. 2006; 19: 111–26. https://doi.org/10.1128/CMR.19.1.111-126.2006 PMID: 16418526

7. Supporting information

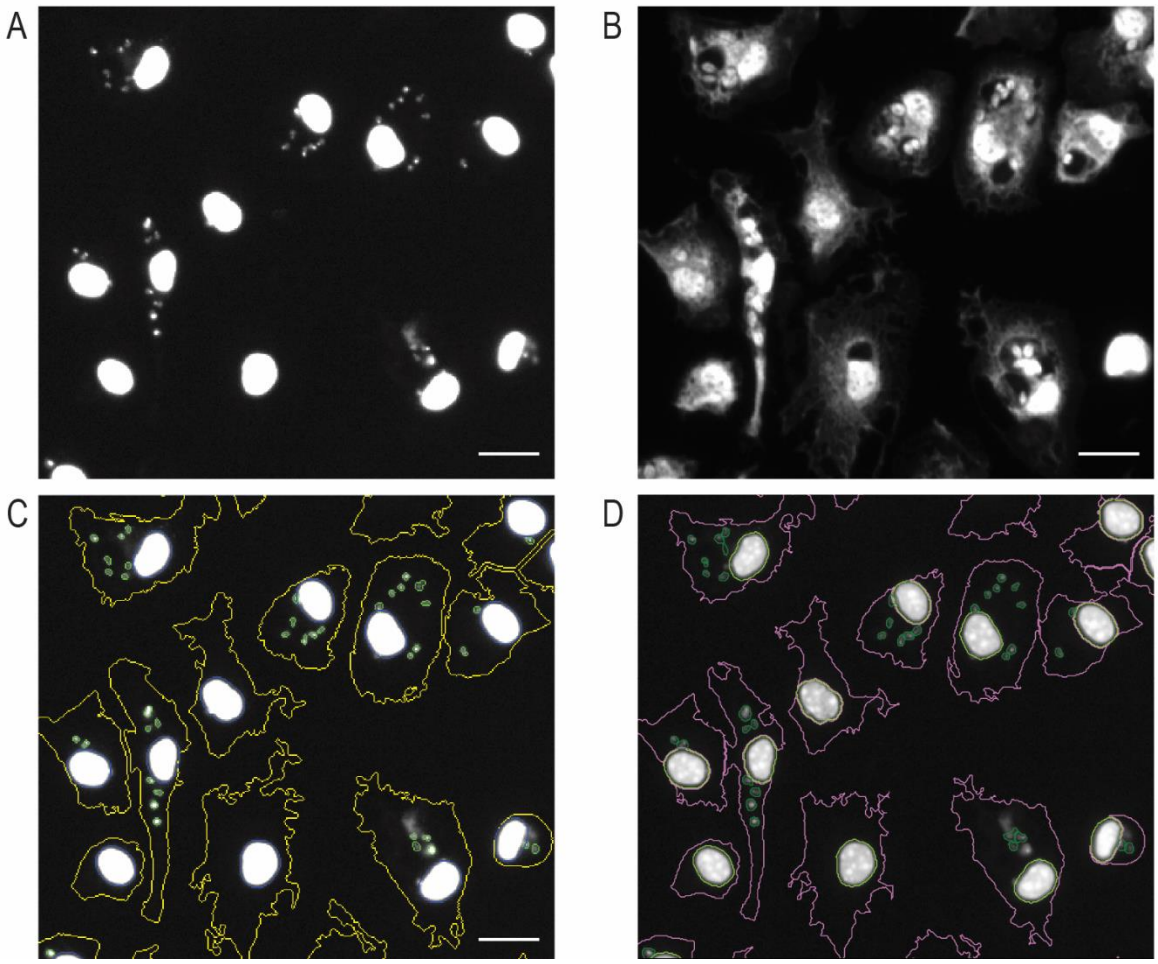

S1 Fig. Detection of intramacrophagic L. amazonensis parasites using IN Cell Investigator Developer Toolbox and CellProfiler. Raw image from (A) DAPI and (B) HCS CellMask™ Deep Red imaging channels acquired with IN Cell Analyzer 2000 microscope. (C) Final processed image obtained from IN Cell Investigator Developer Toolbox, showing macrophage nuclei (blue line), cell boundaries (yellow line) and parasites (green line). (D) CellProfiler final processed image showing BMDM nuclei expansion (light green line), cell boundary (pink line) and parasites (dark green line). Scale bar, 20μm. (TIF)

S1 Appendix. IN Cell Investigator Developer Toolbox protocol.
(XEAP)

S2 Appendix. CellProfiler pipeline.
(CPPIPE)

CHAPTER III. Biological Evaluation and Mechanistic Studies of Quinolin-(1*H*)-imines as a New Chemotype against Leishmaniasis

Gomes-Alves AG et al. *Antimicrob Agents Chemother*. 2021;65(7):e0151320.

1. Abstract

Leishmaniasis is one of the most challenging neglected tropical diseases and remains a global threat to public health. Currently available therapies for leishmaniases present significant drawbacks and are rendered increasingly inefficient due to parasite resistance, making the need for more effective, safer, and less expensive drugs an urgent one. In our efforts to identify novel chemical scaffolds for the development of antileishmanial agents, we have screened in-house antiplasmodial libraries against axenic and intracellular forms of *Leishmania infantum*, *Leishmania amazonensis*, and *Leishmania major*. Several of the screened compounds showed half-maximal inhibitory concentrations (IC_{50}s) against intracellular *L. infantum* parasites in the submicromolar range (compounds 1h, IC_{50} = 0.9 μM, and 1n, IC_{50} = 0.7 μM) and selectivity indexes of 11 and 9.7, respectively. Compounds also displayed activity against *L. amazonensis* and *L. major* parasites, albeit in the low micromolar range. Mechanistic studies revealed that compound 1n efficiently inhibits oxygen consumption and significantly decreases the mitochondrial membrane potential in *L. infantum* axenic amastigotes, suggesting that this chemotype acts, at least in part, by interfering with mitochondrial function. Structure-activity analysis suggests that compound 1n is a promising antileishmanial lead and emphasizes the potential of the quinoline-(1*H*)-imine chemotype for the future development of new antileishmanial agents.

2. Introduction

Leishmaniases are a group of neglected diseases caused by trypanosomatid parasites of the genus *Leishmania* that manifest in several clinical forms, including cutaneous leishmaniasis, the most common form, mucocutaneous leishmaniasis, a highly disfiguring and debilitating condition, and visceral leishmaniasis, a life-threatening disorder. According to the latest reports, the World Health Organization (WHO) estimates that approximately 1 billion people, mainly from the poorest communities in tropical and subtropical countries, live at risk of developing these illnesses (1). In the absence of a human vaccine or a prophylactic drug, control of leishmaniases is largely based on chemotherapy of infected individuals. Current available medicines include first-line agents, such as pentavalent antimonials (sodium stibogluconate and meglumine antimoniate), which are administered daily over the course of 20 to 30 days, and second-line agents (amphotericin B, pentamidine, miltefosine, and paromomycin), which are often used in unresponsive or resistant cases (2). However, none of these drugs has even close to optimal performance, and their use in leishmaniasis treatment is compromised by several factors: high costs, prolonged administration over multiple weeks, and poor safety indexes, presenting important adverse effects (2). Miltefosine, for instance, the only available oral

drug for treatment of leishmaniasis, is unsuitable for pregnant patients due to fetotoxic and teratogenic risks (3). A further problem limiting the efficacy of therapy in areas of endemicity is the gradual emergence of parasite strains resistant to antileishmanial drugs (4).

The multiple drawbacks associated with current leishmaniasis therapeutics, together with the worldwide public health impact of these diseases, prompts the scientific community to identify new chemotypes for developing effective, safe, and accessible antileishmanial drugs (5). Quinolines and structurally related heterocycles are privileged scaffolds found in several natural products that exhibit a wide range of biological properties, including activity against different *Leishmania* spp. (in both *in vitro* and *in vivo* models), as well as against other protozoa (6). The antiplasmodial 8-aminoquinolines sitamaquine (SQ) and tafenoquine (TFQ), for example, have been extensively studied as potential treatments for visceral leishmaniasis. From a mechanistic point of view, TFQ appears to suppress the parasite's respiratory chain through cytochrome *c* reductase (complex III) inhibition, inducing a rapid drop in intracellular ATP and depolarization of mitochondrial membrane potential (7). SQ, on the other hand, was reported to inhibit succinate dehydrogenase (complex II), an essential enzyme for *Leishmania* (8). Quinolin-4(1*H*)-imines, which can be considered tautomeric analogues of quinolines, were previously reported by some of us as potent dual-stage antiplasmodials, displaying potential to bind to the Q_o ubiquinone oxidation site of cytochrome bc_1 from *Plasmodium falciparum* (9, 10). More recently, quinolin-4(1*H*)-imines were also disclosed as efficient antitrypanosomal agents, endowed with excellent pharmacokinetic profiles (11). Additionally, a high-throughput phenotypic screen of roughly 600,000 small molecules against *Leishmania mexicana* promastigotes identified a quinolin-4(1*H*)-imine derivative as one of the top hits (12), further highlighting the potential of this chemotype against parasitic diseases. In this paper, we report the screening of a set of quinolin-4(1*H*)-imines from in-house antiplasmodial libraries against promastigotes and amastigotes of three different *Leishmania* species. Our results show that several compounds inhibit parasitic growth within mammalian host macrophages and that the mechanism of action can be explained, to some extent, by their ability to interfere with *Leishmania* parasites' mitochondrial function.

3. Materials and methods

3.1. Cells and parasites

Leishmania infantum promastigotes (MHOM/MA/67/ITMAP-263) were cultured at 25°C in RPMI 1640 GlutaMax supplemented with 10% (vol/vol) heat-inactivated fetal bovine serum (iFBS), 50 U ml^{-1} penicillin, 50 µg ml^{-1} streptomycin (from Gibco), and 20 mM HEPES sodium salt, pH 7.4 (Sigma).

Leishmania major and *Leishmania amazonensis* promastigotes (MHOM/SA/85/JISH 118 and MHOM/BR/LTB0016, respectively) were maintained at 25°C in Schneider's insect medium (Sigma) supplemented with 10% (vol/vol) iFBS, 100 U ml^{-1} penicillin, 100 µg ml^{-1} streptomycin, 5mM HEPES sodium salt, pH 7.4, and 5 µg ml^{-1} phenol red (Sigma). *L. infantum* axenic amastigotes were maintained at 37°C and 5% CO_2 in MAA20 medium, as described previously (26). Briefly, MAA consisted of media 199 with Hanks' salts (Gibco) supplemented with 15 mM D-glucose, 4 mM $NaHCO_3$, 0.5% trypto-casein-soy (Biorad) and 25 mM HEPES at a final pH of 6.5. Afterward, MAA20 was obtained by supplementing MAA medium with 20% (vol/vol) iFBS, 2 mM GlutaMax (Gibco), and 0.023 mM hemin.

3.2. Compound synthesis

The synthesis and characterization of all compounds screened has been previously reported (9, 10, 13, 14). Stock solutions with concentrations between 10 and 20 mM were prepared by dissolving the compounds in dimethyl sulfoxide (DMSO) at room temperature and were stored at -20°C.

3.3. Evaluation of compound activity against promastigotes of different *Leishmania* species and axenic amastigotes of *L. infantum*

Promastigotes in the late exponential phase ($3x10^6$ cells/ml) were seeded in 96-well plates in a final volume of 100 µl of either RPMI (*L. infantum*) or Schneider's medium (*L. major* and *L. amazonensis*); *L. infantum* axenic amastigotes were seeded ($1.5x10^5$ cells/ml) in 100 µl of MAA20, also in 96-well plates. Stock solutions of test compounds were prepared in 100% DMSO. Parasites were then incubated with different concentrations (between 0.2 and 30 µM) of the compounds dissolved in medium (DMSO concentrations in wells never exceeded 0.5%). DMSO (0.5%) and amphotericin B were used as the negative and positive control, respectively. Parasite viability was evaluated upon 24 h of exposure to each compound and was assessed using resazurin (Sigma) to a final concentration of 0.1 mM as described in Vale-Costa et al. (27). Fluorescence intensity (excitation at 530nm and emission at 590 nm) was measured in a Synergy Mx microplate reader (BioTek Instruments). The half-maximal inhibitory concentrations (IC_{50}s) were determined with GraphPad Prism 7 software (GraphPad Software, Inc., La Jolla, CA).

3.4. Generation of BMDM

Bone marrow-derived macrophages (BMDM) were obtained following a previously described protocol (28). Briefly, bone-marrow (BM) cells were isolated by flushing femurs and tibias of BALB/c mice with

Dulbecco's modified Eagle's medium (DMEM; Gibco). Cells were collected, centrifuged, and suspended in DMEM supplemented with 10% iFBS, 1% minimum essential medium-nonessential amino acids solution (MEM; Gibco), 50 U ml^{-1} penicillin, 50 µg ml^{-1} streptomycin (complete DMEM medium [cDMEM]), and 10% L929 cell-conditioned medium (LCCM) as a source of macrophage-colony stimulating factor (M-CSF). BM cells were placed in petri dishes for 24 h at 37°C with 5% CO_2. Nonadherent cells were then collected, counted, plated in 96-well plates (2.5 to $3x10^4$ cells per well), and incubated at 37°C with 5% CO_2 for 10 days, with cDMEM plus 10% LCCM renewal on the fourth and seventh days.

3.5. Determination of IC_{50}s against intramacrophagic *L. infantum*, *L. major*, and *L. amazonensis*

The activities of the compounds against intracellular amastigotes were determined in *in vitro* cultures of BMDM, in 96-well plates. Differentiated BMDM were infected with *L. infantum* axenic amastigotes or with *L. major* and *L. amazonensis* stationary-phase promastigotes at a multiplicity of infection (MOI) of 10. After 3 h of contact with macrophages, noninternalized parasites were removed by washing twice with DMEM and internalized parasites allowed to differentiate into amastigotes for 24 h prior to the addition of the compounds (at concentrations of 0.3 to 5 µM). Twenty-four hours later, cells were fixed with 4% paraformaldehyde, permeabilized with 0.1% Triton X-100, and stained with HCS CellMask deep red (Invitrogen) and DAPI (4',6-diamidino-2-phenylindole) (Sigma) for 30 min at room temperature. Cultures were imaged using the IN Cell Analyzer 2000 microscope (GE Healthcare) and analyzed with the IN Cell Investigator Developer Toolbox version 1.9.2 (GE Healthcare) for determination of the percentage of infection as previously described (28). Half-maximal inhibitory concentrations (IC_{50}s) were calculated using GraphPad Prism 7 software.

3.6. Cytotoxicity on BMDM

The cytotoxicity of the compounds against mammalian cells was evaluated in BMDM isolated as described above. Macrophages were incubated with serial dilutions of the compounds (between 0.6 and 20 µM) for 24 h at 37°C with 5% CO_2. Cell viability was determined with the resazurin assay as described above. The percentages of viable BMDM were calculated in relation to control cultures to which only vehicle (0.5% DMSO) was added. Data were analyzed with GraphPad Prism 7 software, and the 50% cytotoxic concentration (CC_{50}) for each compound determined.

3.7. Determination of oxygen consumption in parasites

Oxygen consumption in stationary-phase promastigotes of *L. infantum*, *L. major*, and *L. amazonensis*, as well as in axenic amastigotes of *L. infantum*, was measured in a Clark-type oxygen electrode (Hansatech) at 25°C in respiration buffer (300 mM sucrose, 10 mM potassium phosphate, pH 7.2, 5 mM $MgCl_2$, 10 mM KCl, 0.02% [wt/vol] bovine serum albumin [BSA], 1 mM EGTA and 4 µM carbonyl cyanide m-chlorophenyl hydrazine [CCCP]). For each reaction mixture, 100 µl of a suspension of $3x10^8$ parasites/ml in PBS was used. Oxygen consumption was monitored continuously for 5 min as follows: basal oxygen consumption was read during 2 min, compounds were added (at twice the IC_{50}), and measurements were taken for 3 more minutes. One millimolar KCN, a complex IV inhibitor, was used as a control (complete inhibition of oxygen consumption). Results were evaluated with O2view software (Hansatech) (29).

3.8. Evaluation of mitochondrial membrane potential

Variation of the mitochondrial membrane potential ($\Delta\Psi_m$) in treated parasites was evaluated using the potential-sensitive probe tetramethylrhodamine ethyl ester (TMRE; Sigma). For this, $1x10^7$ *L. infantum*, *L. major*, or *L. amazonensis* stationary-phase promastigotes or *L. infantum* axenic amastigotes were treated with the different compounds at concentrations of 2 to 5 times their IC_{50}s for 45 min and then incubated with 500 nM TMRE for a further 30 min. Treatments were carried out in the media (without iFBS) and temperature conditions described above. Upon two washes in medium (without iFBS), the $\Delta\Psi_m$ was determined by monitoring fluorescence in a BioTek Synergy Mx microplate reader with excitation and emission wavelengths of 540nm and 590nm, respectively. The mitochondrial oxidative phosphorylation uncoupler CCCP was used as a positive control.

3.9. Analysis of ROS production

Reactive oxygen species (ROS) production was determined using MitoTracker red CM-H_2XRos (Molecular Probes) according to the manufacturer's instructions. Briefly, $1x10^7$ stationary-phase promastigotes of *L. infantum*, *L. major*, or *L. amazonensis* or $1x10^7$ axenic amastigotes of *L. infantum* were treated with selected compounds (at concentrations of 2 to 5 times the IC_{50}s) for 45 min and then incubated with 200 nM MitoTracker red CM-H_2XRos for 30 min. Subsequently, parasites were washed twice in their respective culture medium (without iFBS) and fluorescence quantified in a BioTek Synergy Mx microplate reader with excitation and emission wavelengths of 579nm and 599 nm, respectively. Antimycin A (AA) (10 µM) was used as the positive control.

3.10. Ethical statement

The use of BALB/c mice was approved by the Local Animal Ethics Committee of i3S, licensed by DGAV (Direção Geral de Alimentação e Veterinária, Government of Portugal). Animals were handled in accordance with good animal practice as defined by national authorities (DGAV; Decree 113/2013 from 7th August) (30) and European legislation (Directive 2010/63/EU, revising Directive 86/609/EEC) (31).

4. Results

4.1. Effect of chemical libraries on *L. infantum* proliferation: structure-activity relationships (SARs)

The leishmanicidal potential of 38 compounds was initially assessed at a single concentration against *L. infantum* promastigotes (10 or 20 μM) and axenic amastigotes (10 μM). With the purpose of increasing the chemical diversity of our initial screening, besides the main family of quinolin-4(1*H*)-imines (compounds 1a to -n and 2a to -m), we also evaluated the structurally related pyridon-4(1*H*)-imines (compounds 3a to -c), as well as flavones (compounds 4a to -h), bioisosteres of the quinolonimine core scaffold (13, 14).

Inspection of the activity data presented in Table 1 reveals that pyridon-4(1*H*)-imines and flavones are not effective against *L. infantum* promastigotes and are poorly active against axenic amastigotes (inhibition of <30% at 10 μM). In contrast, the vast majority of quinolin-4(1*H*)-imines tested were found to be active against the promastigote stage of the parasite (inhibition of ≥90% at 10 or 20 μM), with several compounds also exhibiting good activity against axenic amastigotes (inhibition of ≥30% at 10 μM). Among the quinolin-4(1*H*)-imine family, preliminary structure-activity relationships indicate that the size and nature of the *N*-linked side chain is important for activity in both stages of the parasite. With the exception of compound 2c, quinolin-4(1*H*)-imines belonging to class 1 (X = methyl or ethyl) are more potent against axenic amastigotes than compounds containing a basic alkylamino side chain at the N-1 nitrogen atom of the quinolonimine scaffold (class 2). Therefore, quinolin-4(1*H*)-imines 1e to -n, presenting good inhibition profiles (promastigotes, ≥90%, and axenic amastigotes, ≥30%) were selected for IC_{50} determination for the same parasite forms, as well as for intramacrophagic amastigotes. Quinolin-4(1*H*)-imines 1d and 2c were also included for comparative purposes. The cytotoxicities of the different molecules to BMDM were evaluated in parallel (Table 2). We found that the IC_{50}s were dependent on the parasite stage. Axenic amastigotes were the less susceptible forms (IC_{50}s varying between 5.9 and 19.4 μM), promastigotes ranked second (IC_{50}s ranging from 1.4 to 4.5 μM), and intracellular amastigotes were the most susceptible forms (IC_{50}s between 0.7 and 2.2 μM). The 12

quinolin-4(1*H*)-imines analyzed exhibited selectivity indexes (SIs) ranging between 5.7 and 11.1 (Table 2).

Table 1. Anti-*Leishmania* activities of chemical libraries against *L. infantum* promastigotes and axenic amastigotes[a].

Quinolin-4(1*H*)-imine libraries[refs]

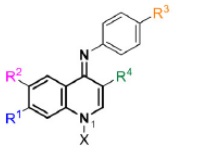

Class 1, X = OH, Me or Et: 1a-n
Class 2, X = alkylamino: 2a-m

Pyridon-4(1*H*)-imine libraries[refs]

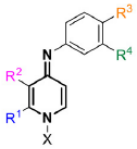

X = Me or Et
3a-c

Flavone libraries[ref]

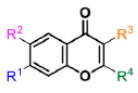

4a-h

Compounds						% Inhibition		
						Promastigotes		Axenic amastigotes
	R^1	R^2	R^3	R^4	X	10 µM	20 µM	10 µM
1a	Cl	H	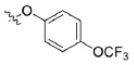	H	OH	53	----	9
1b	H	F		CO_2Et	Me	----	NA	24
1c	H	F		CO_2Et	Et	94	----	26
1d	Cl	H		H	Et	94	----	6
1e	CF_3	H	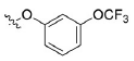	H	Et	92	----	51
1f	CF_3	H	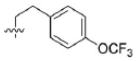	H	Et	93	----	64
1g	Cl	H	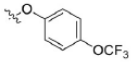	H	Et	99	----	59
1h	Cl	H		H	Et	98	----	41
1i	Cl	H	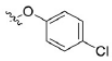	H	Et	99	----	64
1j	Cl	H	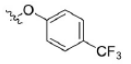	H	Et	100	----	53
1k	Cl	H	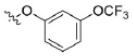	H	Et	98	----	51
1l	Cl	H	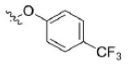	H	Me	100	----	30
1m	Cl	H		H	Et	100	----	41
1n	Cl	H	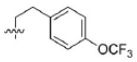	H	Et	100	----	92
2a	Cl	H	Cl	H	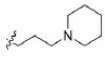	----	>90	NA
2b	Cl	H	Br	H	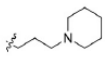	----	>90	8
2c		H		H	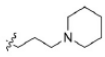	----	>90	99

(Continued on next page)

Table 1 (continued)

2d	Cl	H	Me	H	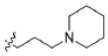	----	>90	12
2e	Cl	H		H	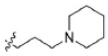	90	----	20
2f	Cl	H		H	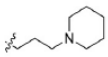	100	----	NA
2g	CF_3	H		H		100	----	NA
2h	CF_3	H		H		100	----	23
2i	Cl	H		H	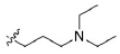	100	----	21
2j	H	CF_3		H	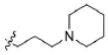	100	----	33
2k	CF_3	H		H	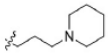	100	----	26
2l	Cl	H		H	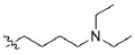	100	----	NA
2m	Cl	H		H		100	----	25
3a	H	H	OMe	H	Me	NA	----	15
3b	H	H	OH	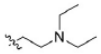	Me	NA	----	5
3c	H	NH_2		H	----	45	----	79
4a	H	H	H	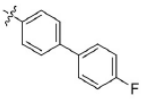	----	----	NA	22
4b	H	H	H		----	NA	----	32
4c	H	H	I	H	----	NA	----	29
4d	Me	Cl	H	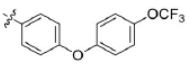	----	22	----	20
4e	Me	Cl	H	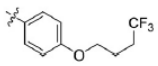	----	NA	----	24
4f	CH_2Br	Cl	Br	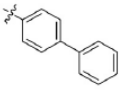	----	NA	----	9
4g	H	H		H	----	NA	----	12
4h	Cl	H	H	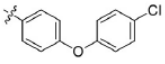	----	NA	----	15

[a] Parasites were incubated for 24 h with different compounds. NA, not active.

In a second step of the analysis, we tested compounds 1d, 1g, 1h, and 1n against *L. major* and *L. amazonensis*, two species causing cutaneous leishmaniasis. As shown in Table 3, intracellular amastigotes of *L. major* and *L. amazonensis* showed IC_{50}s between 2.3 and 3.9 μM, indicating that,

although these species are less sensitive to the tested quinolin-4(1*H*)-imines than *L. infantum*, the chemotype has therapeutic potential for both types of leishmaniasis. Curiously, when the screening was carried out on promastigotes, a different result was found, as in this case, *L. major* was more susceptible than the other two species.

Table 2. Leishmanicidal activities for different forms of *L. infantum* and cytotoxicities of quinolin-4(1*H*)-imine derivatives.

	Mean value ± SD for[a]:				
	IC_{50} (μM) against:				
Compound	Promastigotes	Axenic amastigotes	Intramacrophagic amastigotes	CC_{50} (μM) in BMDM	SI[b]
1d	2.8 ± 0.6	19.4 ± 1.4	1.3 ± 0.5	10.1 ± 3.4	7.8
1e	ND	11.3 ± 1.1	2.2 ± 0.6	14.4 ± 1.9	6.5
1f	4.5 ± 0.3	12.2 ± 1.9	1.7 ± 0.4	10.8 ± 0.9	6.4
1g	2.3 ± 0.2	11.4 ± 0.8	1.4 ± 0.6	9.6 ± 0.9	6.9
1h	1.5 ± 0.3	10.9 ± 0.5	0.9 ± 0.1	10.0 ± 1.8	11.1
1i	1.4 ± 0.1	5.8 ± 2.8	1.1 ± 0.3	9.1 ± 1.4	8.3
1j	1.9 ± 0.1	14.1 ± 4.2	1.4 ± 0.3	9.5 ± 1.0	6.8
1k	2.50 ± 0.01	11.0 ± 1.7	1.9 ± 0.5	10.9 ± 1.5	5.7
1l	2.42 ± 0.02	15.8 ± 2.3	1.9 ± 0.2	10.8 ± 1.0	5.7
1m	1.7 ± 0.2	13.4 ± 3.0	1.3 ± 0.2	8.4 ± 2.1	6.5
1n	1.9 ± 0.2	6.5 ± 2.8	0.7 ± 0.2	6.8 ± 0.8	9.7
2c	ND	ND	>0.5	<0.5	
AMB[c]	0.17 ± 0.09	0.39 ± 0.24	0.06 ± 0.01	3.1 ± 0.6	52

[a] *L. infantum* promastigotes, axenic amastigotes, and intramacrophagic amastigotes, as well as BALB/c mouse BMDM, were incubated for 24 h with different concentrations of the different compounds. IC50, half-maximal inhibitory concentration; CC_{50}, 50% cytotoxic concentration; ND, not determined.

[b] SI, selectivity index (ratio between CC_{50} and IC_{50} values for intramacrophagic amastigotes).

[c] AMB, amphotericin B, used as a positive control.

Table 3. Effects of selected quinolin-4(1*H*)-imines against promastigotes and intramacrophagic amastigotes of *L. major* and *L. amazonensis*.

	Mean IC_{50} ± SD (μM) (SI) against[a]:			
	Promastigotes		Intramacrophagic amastigotes	
Compound	*L. major*	*L. amazonensis*	*L. major*	*L. amazonensis*
1d	0.5 ± 0.1	8.7 ± 1.6	3.9 ± 1.1 (2.6)	2.8 ± 1.1 (3.6)
1g	0.8 ± 0.1	3.4 ± 0.8	3.4 ± 0.9 (2.8)	3.5 ± 1.3 (2.7)
1h	0.6 ± 0.2	4.9 ± 1.4	2.6 ± 0.9 (3.8)	2.7 ± 0.9 (3.7)
1n	0.75 ± 0.01	2.4 ± 0.6	2.3 ± 1.1 (2.9)	2.3 ± 0.4 (2.9)

[a] *L. major* and *L. amazonensis* promastigotes and intramacrophagic amastigotes were incubated for 24 h with serial dilutions of selected quinolin-4(1*H*)-imines. IC_{50}, half-maximal inhibitory concentration; SI, selectivity index (ratio between CC_{50} and IC_{50} values).

4.2. Effect of quinolin-4(1*H*)-imines on mitochondrial functions

Quinolin-4(1*H*)-imines were originally designed to inhibit *Plasmodium* mitochondrial respiration, more particularly the cytochrome bc_1 complex, also known as complex III. To investigate whether the mitochondrial activity of *Leishmania* was altered by these compounds, we analyzed the effects of the compounds with better selectivity indexes on basal oxygen consumption, mitochondrial membrane potential, and reactive oxygen species (ROS) production.

4.3. Quinolin-4(1*H*)-imines inhibit oxygen consumption in *Leishmania*

The basal oxygen consumption of intact promastigotes and of axenic amastigotes was evaluated upon incubation of parasites with twice the IC_{50} of selected quinolin-4(1*H*)-imines. We found that all compounds inhibit oxygen consumption in both promastigote and axenic amastigote forms, with higher efficiency in the latter (Fig. 1). Compound 1n was the most effective, decreasing oxygen consumption by around 65% in *L. amazonensis* promastigotes and by 85% in *L. infantum* axenic amastigotes. In contrast, compound 1h showed milder effects on all species analyzed. In this case, oxygen consumption inhibition varied from 18% in *L. amazonensis* promastigotes to 39% in *L. infantum* axenic amastigotes. These results are consistent with the hypothesis that quinolin-4(1*H*)-imines may affect *Leishmania* respiratory complexes.

4.4. Quinolin-4(1*H*)-imines alter the mitochondrial membrane potential

Impairment of the electron transfer chain following inhibition of respiratory complexes (such as complex III) is often associated with the collapse of the mitochondrial membrane potential ($\Delta\Psi_m$) (9). We used TMRE to investigate changes in $\Delta\Psi_m$ upon treatment of parasites with selected quinolin-4(1*H*)-imines. When incubated with cells, TMRE accumulates inside the negative environment of mitochondria, but after $\Delta\Psi_m$ collapse, the probe diffuses out of the organelle, resulting in dissipation of the signal. We found that the $\Delta\Psi_m$ of *L. amazonensis* (promastigotes) and *L. infantum* (promastigotes and axenic amastigotes) parasites was significantly decreased after incubation with quinolin-4(1*H*)-imines, similarly to incubation with CCCP, a potent uncoupler of the mitochondrial oxidative phosphorylation, used as a positive control (Fig. 2). In contrast, *L. major* (promastigotes) $\Delta\Psi_m$ was not altered during the time frame of the analysis.

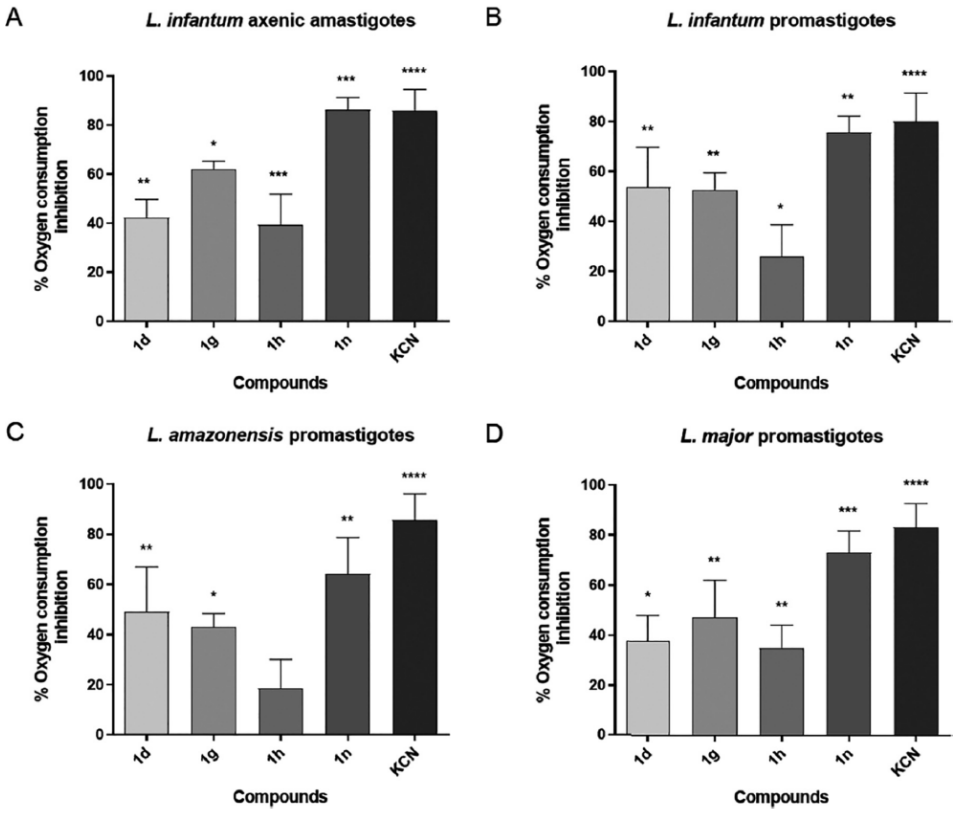

Fig 1. Effects of selected quinolin-4(1*H*)-imines on oxygen consumption of *Leishmania* parasites. *L. infantum* axenic amastigote (A) and *L. infantum* (B), *L. amazonensis* (C), and *L. major* (D) promastigotes were treated with 2-fold the IC_{50}s of each selected quinolin-4(1*H*)-imine. Percentages of inhibition are relative to the oxygen consumption values obtained at basal levels. The graphs show the mean values and standard deviations (error bars) from 3 independent experiments. KCN was used as the positive control. Statistical significance was determined using a paired *t* test. *, $p<0.05$; **, $p<0.005$; ***, $p<0.0005$; ****, $p<0.0001$.

4.5. Quinolin-4(1*H*)-imines do not induce ROS production

We next evaluated ROS levels in parasites treated with selected quinolin-4(1*H*)-imines, finding that none of the compounds triggered ROS generation (Fig. 3). This result is not inconsistent with activity of the compounds on one of the respiratory complexes, as the production of ROS depends on the exact site of the enzymatic complex that is targeted. In the case of complex III, for instance, inhibition of its Q_i site (e.g., with antimycin A) generates reactive oxygen species, while interference with electron flow through the Q_o site is not generally associated with the production of these species (15–17).

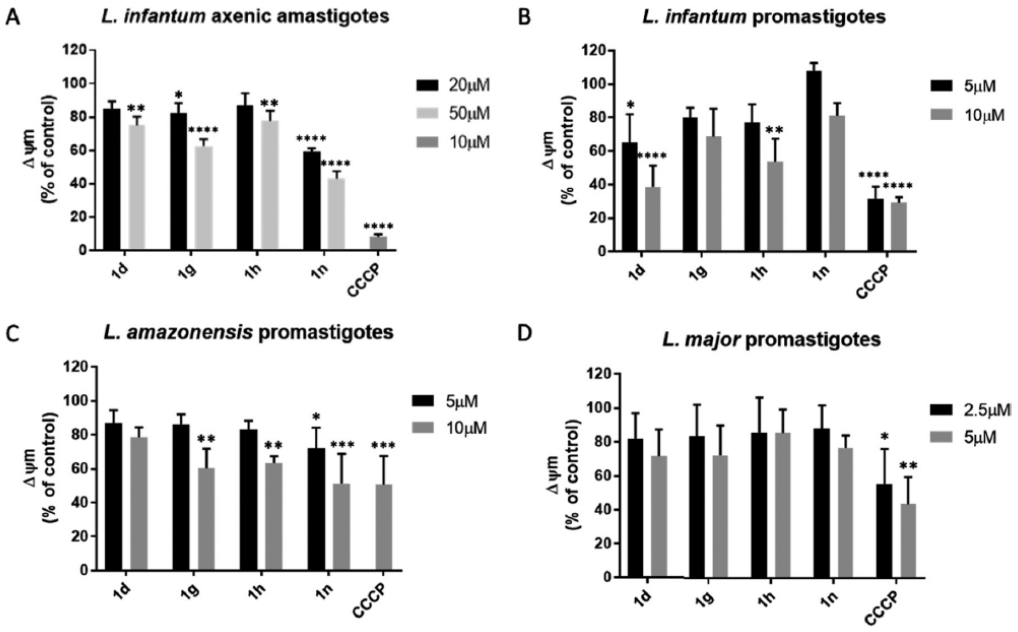

Fig 2. Effect of selected quinolin-4(1H)-imines on mitochondrial membrane potential ($\Delta\Psi_m$) of *Leishmania* parasites. *L. infantum* axenic amastigotes (A) and *L. infantum* (B), *L. amazonensis* (C), and *L. major* (D) promastigotes were treated for 45 min with different concentrations of selected quinolin-4(1*H*)-imines. CCCP, carbonyl cyanide m-chlorophenyl hydrazine, uncoupler of the $\Delta\Psi_m$, was used as the positive control. Graphs represent the mean fold change in treated parasites relative to control cells (treated with DMSO) and standard deviations (error bars) from 3 independent experiments. Statistical significance was determined using 2-way analysis of variance (ANOVA) with Sidak's multiple-comparison test. *, $p<0.05$; **, $p<0.005$; ***, $p<0.0005$; ****, $p<0.0001$.

5. Discussion

Current treatments for leishmaniases are based on chemotherapeutics that show important limitations in terms of efficacy, specificity, and administration regimens, rendering the development of new drugs a compelling necessity (4). Unfortunately, this faces significant challenges. First, *Leishmania* parasites in the disease-causing stage inhabit specific compartments within their mammalian host cells, which implies that, to reach the parasites, drugs must overcome two membrane barriers (18). Second, *Leishmania* parasites display an enormous capacity to adapt to the presence of exogenous compounds (4). Third, there is insufficient and unsustained investment by pharmaceutical companies in the development of drugs to treat leishmaniases, with much of the effort toward this objective remaining academia driven (19). The present work, which represents an example of the latter studies, is aimed at assessing the

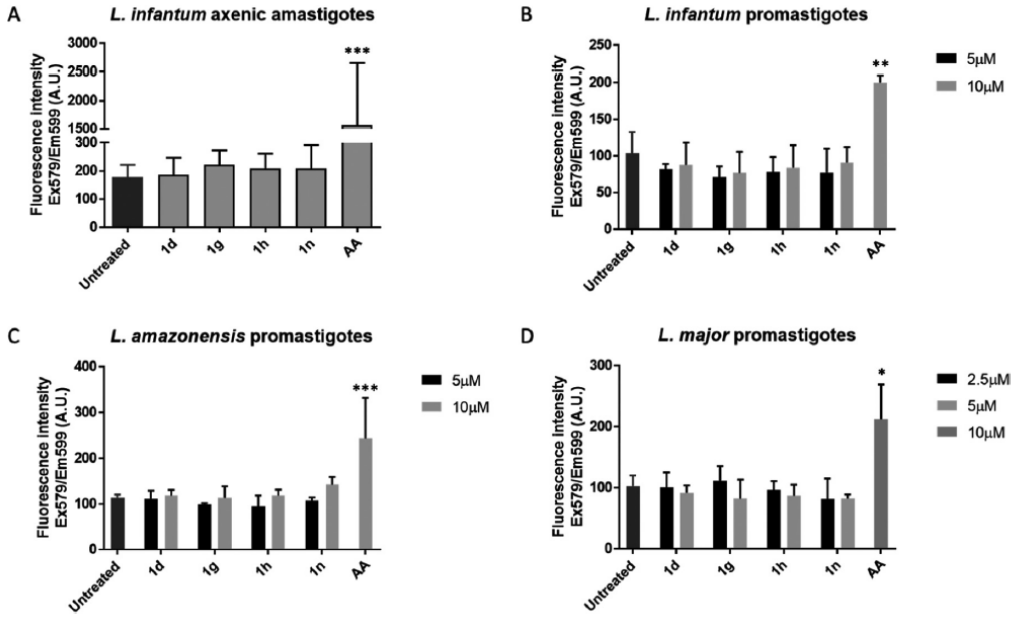

Fig 3. Analysis of ROS production in *Leishmania* parasites after the addition of selected quinolin-4(1*H*)-imines. *L. infantum* axenic amastigotes (A) and *L. infantum* (B), *L. amazonensis* (C), and *L. major* (D) promastigotes were treated with different concentrations of the selected quinolin-4(1*H*)-imines for 45 min. AA, antimycin A, was used as the positive control for ROS production. Graphs show the mean values and standard deviations (error bars) from 3 independent experiments. Statistical significance was determined using 2-way ANOVA with Sidak's multiple-comparison test. *, $p<0.05$; **, $p<0.005$; ***, $p<0.0005$; ****, $p<0.0001$.

antileishmanial value of a series of quinolin-4(1*H*)-imine derivatives previously developed for inhibition of malaria parasites (8, 9).

The screening performed indicated that the quinolin-4(1*H*)-imine scaffold is an interesting and novel chemotype for leishmaniasis drug development. Several of the compounds tested showed IC_{50}s toward intracellular *L. infantum* parasites in the low micromolar range, with two of them exhibiting IC_{50}s in the submicromolar range (compound 1h, IC_{50} = 0.9 μM, and compound 1n, IC_{50} = 0.7 μM) and selectivity indexes of 11.1 and 9.7, respectively. Structure-activity relationships revealed that enhanced activity and selectivity are obtained with an ethyl group linked at the N-1 nitrogen of the quinolonimine scaffold and that basic alkylamino side chains at this position are detrimental for activity (Table 1). Regarding the substituents at the imine moiety, groups with alkyl linkers between the two phenyl rings are, in general, beneficial for activity, although oxygen linkers are also tolerated. Inspection of the activity data against intramacrophagic amastigotes presented in Table 2 also reveals that compounds containing a chloro as an R1 group are more potent than their trifluoromethyl derivatives (e.g., compound 1k versus

1e and 1n versus 1f). These findings suggest that the electronic nature of the group at the 7 position of the quinolonimine scaffold can be further explored in order to generate analogues with improved selectivity and physicochemical properties. Therefore, the future generation of quinolin-4(1*H*)-imine libraries will explore the introduction of electron-donating groups and water-solubilizing groups at this position. Future work will also test the possibility of using specific systems to deliver those compounds in experimental settings.

While screening the different *L. infantum* forms, we observed that intramacrophagic amastigotes were more susceptible than axenic amastigotes to the quinolin-4(1*H*)-imines tested. Several explanations can account for this finding: (i) the compounds might display an inherent capacity to directly activate macrophages, (ii) drug metabolism within macrophages might induce the formation of a derivative more potent against intramacrophagic *Leishmania* than against axenic amastigotes, and (iii) there might be metabolic differences between the two parasite forms that render intramacrophagic amastigotes particularly prone to inhibition. Although we did not identify the mechanism responsible for the higher drug sensitivity of intracellular *L. infantum* parasites, our data, showing important differences in activity between different parasite forms, support studies advising for drug testing to be preferentially carried out on intramacrophagic amastigotes, a more physiological form of the parasite (20, 21).

Originally, the quinolin-4(1*H*)-imines tested were designed to favor hydrophobic interactions at the Q_o binding pocket of the *Plasmodium* cytochrome bc_1 complex (9). However, it has been reported that the structurally related 4(1*H*)-pyridone (22) and quinolone (23) antimalarials bind to the Q_i site, suggesting that this binding site can accommodate a broader range of chemotypes than initially anticipated. As a means to approach the physiological target of the compounds under study in *Leishmania* parasites, we investigated their effect on parasite mitochondrial function. The robust inhibition of oxygen consumption observed suggests that in *Leishmania* parasites, the mechanism of action also involves inhibition of the mitochondrial electron transport chain. This is consistent with the alterations in $\Delta\Psi_m$ observed in *L. infantum* and *L. amazonensis* parasites (albeit these were not detected in *L. major* parasites). Future investigations are required to confirm whether respiratory complexes, and specifically the complex III Q_o site, are the primary targets of quinolin-4(1*H*)-imines in *Leishmania* parasites. In this respect, it is interesting to notice that the compounds did not trigger ROS production, which is in line with what would be expected for a Q_o inhibitor. Indeed, it is well established that, while drugs targeting the complex III Q_i site (e.g., antimycin A) enhance superoxide production (15–17), Q_o inhibitors (stigmatellin and myxothiazol) abolish or reduce ROS generation (15).

In conclusion, we have disclosed a new chemotype that expands the current toolbox of antileishmanial compounds with activity against intramacrophagic amastigotes. Despite the structural similarity between quinolin-(1*H*)-imines and their quinoline counterparts, our previous research revealed that this particular chemotype displays low metabolic susceptibility. This contrasts with 8-aminoquinolines, such as primaquine and sitamaquine, which are metabolized by cytochrome P450 2D6 (24, 25) and generate hydroxyquinoline metabolites that have been associated with toxicity issues and glucose-6-phosphate dehydrogenase (G6PD) liability. Importantly, quinolin-4(1*H*)-imines exert their effect, at least partially, by inhibiting mitochondrial respiration, a mechanism that remains underexplored in the context of antileishmanial therapy.

6. References

1. World Health Organization. 2016. Leishmaniasis in high-burden countries: an epidemiological update based on data reported in 2014. Wkly Epidemiol Rec 91:287–296.

2. Uliana SRB, Trinconi CT, Coelho AC. 2018. Chemotherapy of leishmaniasis: present challenges. Parasitology 145:464–480. https://doi.org/10.1017/S0031182016002523.

3. Monge-Maillo B, Lopez-Velez R. 2015. Miltefosine for visceral and cutaneous leishmaniasis: drug characteristics and evidence-based treatment recommendations. Clin Infect Dis 60:1398–1404. https://doi.org/10.1093/cid/civ004.

4. Ponte-Sucre A, Gamarro F, Dujardin JC, Barrett MP, Lopez-Velez R, Garcia-Hernandez R, Pountain AW, Mwenechanya R, Papadopoulou B. 2017. Drug resistance and treatment failure in leishmaniasis: a 21st century challenge. PLoS Negl Trop Dis 11:e0006052. https://doi.org/10.1371/journal.pntd.0006052.

5. Burrows JN, Elliott RL, Kaneko T, Mowbray CE, Waterson D. 2014. The role of modern drug discovery in the fight against neglected and tropical diseases. MedChemCommun 5:688–700. https://doi.org/10.1039/c4md00011k.

6. Bongarzone S, Bolognesi ML. 2011. The concept of privileged structures in rational drug design: focus on acridine and quinoline scaffolds in neurodegenerative and protozoan diseases. Expert Opin Drug Discov 6:251–268. https://doi.org/10.1517/17460441.2011.550914.

7. Carvalho L, Luque-Ortega JR, Manzano JI, Castanys S, Rivas L, Gamarro F. 2010. Tafenoquine, an antiplasmodial 8-aminoquinoline, targets Leishmania respiratory complex III and induces apoptosis. Antimicrob Agents Chemother 54:5344–5351. https://doi.org/10.1128/AAC.00790-10.

8. Carvalho L, Luque-Ortega JR, Lopez-Martin C, Castanys S, Rivas L, Gamarro F. 2011. The 8-aminoquinoline analogue sitamaquine causes oxidative stress in Leishmania donovani promastigotes by targeting succinate dehydrogenase. Antimicrob Agents Chemother 55:4204–4210. https://doi.org/10.1128/AAC.00520-11.

9. Rodrigues T, da Cruz FP, Lafuente-Monasterio MJ, Goncalves D, Ressurreicao AS, Sitoe AR, Bronze MR, Gut J, Schneider G, Mota MM, Rosenthal PJ, Prudencio M, Gamo FJ, Lopes F, Moreira R. 2013. Quinolin-4(1H)-imines are potent antiplasmodial drugs targeting the liver stage of malaria. J Med Chem 56:4811–4815. https://doi.org/10.1021/jm400246e.

10. Ressurreicao AS, Goncalves D, Sitoe AR, Albuquerque IS, Gut J, Gois A, Goncalves LM, Bronze MR, Hanscheid T, Biagini GA, Rosenthal PJ, Prudencio M, O'Neill P, Mota MM, Lopes F, Moreira R. 2013. Structural optimization of quinolon-4(1H)-imines as dual-stage antimalarials: toward increased potency and metabolic stability. J Med Chem 56:7679–7690. https://doi.org/10.1021/jm4011466.

11. Bachovchin KA, Sharma A, Bag S, Klug DM, Schneider KM, Singh B, Jalani HB, Buskes MJ, Mehta N, Tanghe S, Momper JD, Sciotti RJ, Rodriguez A, Mensa-Wilmot K, Pollastri MP, Ferrins L. 2019. Improvement of aqueous solubility of lapatinib-derived analogues: identification of a quinolinimine lead for human African Trypanosomiasis drug development. J Med Chem 62:665–687. https://doi.org/10.1021/acs.jmedchem.8b01365.

12. Ortiz D, Guiguemde WA, Hammill JT, Carrillo AK, Chen Y, Connelly M, Stalheim K, Elya C, Johnson A, Min J, Shelat A, Smithson DC, Yang L, Zhu F, Guy RK, Landfear SM. 2017. Discovery of novel, orally bioavailable, antileishmanial compounds using phenotypic screening. PLoS Negl Trop Dis 11:e0006157. https://doi.org/10.1371/journal.pntd.0006157.

13. Rodrigues T, Ressurreicao AS, da Cruz FP, Albuquerque IS, Gut J, Carrasco MP, Goncalves D, Guedes RC, dos Santos DJ, Mota MM, Rosenthal PJ, Moreira R, Prudencio M, Lopes F. 2013. Flavones as isosteres of 4(1H)-quinolones: discovery of ligand efficient and dual stage antimalarial lead compounds. Eur J Med Chem 69:872–880. https://doi.org/10.1016/j.ejmech.2013.09.008.

14. Rodrigues T, Guedes RC, dos Santos DJ, Carrasco M, Gut J, Rosenthal PJ, Moreira R, Lopes F. 2009. Design, synthesis and structure-activity relationships of (1H-pyridin-4-ylidene)amines as potential antimalarials. Bioorg Med Chem Lett 19:3476–3480. https://doi.org/10.1016/j.bmcl.2009.05.017.

15. Bleier L, Drose S. 2013. Superoxide generation by complex III: from mechanistic rationales to functional consequences. Biochim Biophys Acta 1827:1320–1331. https://doi.org/10.1016/j.bbabio.2012.12.002.

16. Quinlan CL, Gerencser AA, Treberg JR, Brand MD. 2011. The mechanism of superoxide production by the antimycin-inhibited mitochondrial Q-cycle. J Biol Chem 286:31361–31372. https://doi.org/10.1074/jbc.M111.267898.

17. Zorov DB, Juhaszova M, Sollott SJ. 2014. Mitochondrial reactive oxygen species (ROS) and ROS-induced ROS release. Physiol Rev 94:909–950. https://doi.org/10.1152/physrev.00026.2013.

18. Shahnaz G, Sarwar HS, Yasinzai M. 2018. Crossing biological barriers for leishmaniasis therapy: from nanomedicinal targeting perspective. In Afrin F (ed), Leishmaniases are re-emerging diseases, IntechOpen Limited, London, UK. https://doi.org/10.5772/intechopen.75911.

19. Weng HB, Chen HX, Wang MW. 2018. Innovation in neglected tropical disease drug discovery and development. Infect Dis Poverty 7:67. https://doi.org/10.1186/s40249-018-0444-1.

20. Vermeersch M, da Luz RI, Tote K, Timmermans JP, Cos P, Maes L. 2009. In vitro susceptibilities of Leishmania donovani promastigote and amastigote stages to antileishmanial reference drugs: practical relevance of stage-specific differences. Antimicrob Agents Chemother 53:3855–3859. https://doi.org/10.1128/AAC.00548-09.

21. De Rycker M, Hallyburton I, Thomas J, Campbell L, Wyllie S, Joshi D, Cameron S, Gilbert IH, Wyatt PG, Frearson JA, Fairlamb AH, Gray DW. 2013. Comparison of a high-throughput high-content intracellular Leishmania donovani assay with an axenic amastigote assay. Antimicrob Agents Chemother 57:2913–2922. https://doi.org/10.1128/AAC.02398-12.

22. Capper MJ, O'Neill PM, Fisher N, Strange RW, Moss D, Ward SA, Berry NG, Lawrenson AS, Hasnain SS, Biagini GA, Antonyuk SV. 2015. Antimalarial 4(1H)-pyridones bind to the Qi site of cytochrome bc1. Proc Natl Acad Sci U S A 112:755–760. https://doi.org/10.1073/pnas.1416611112.

23. David Hong W, Leung SC, Amporndanai K, Davies J, Priestley RS, Nixon GL, Berry NG, Samar Hasnain S, Antonyuk S, Ward SA, Biagini GA, O'Neill PM. 2018. Potent antimalarial 2-pyrazolyl

quinolone bc 1 (Qi) inhibitors with improved drug-like properties. ACS Med Chem Lett 9:1205–1210. https://doi.org/10.1021/acsmedchemlett.8b00371.

24. Camarda G, Jirawatcharadech P, Priestley RS, Saif A, March S, Wong MHL, Leung S, Miller AB, Baker DA, Alano P, Paine MJI, Bhatia SN, O'Neill PM, Ward SA, Biagini GA. 2019. Antimalarial activity of primaquine operates via a two-step biochemical relay. Nat Commun 10:3226. https://doi.org/10.1038/s41467-019-11239-0.

25. Loiseau PM, Cojean S, Schrevel J. 2011. Sitamaquine as a putative antileishmanial drug candidate: from the mechanism of action to the risk of drug resistance. Parasite 18:115–119. https://doi.org/10.1051/parasite/2011182115.

26. Sereno D, Lemesre JL. 1997. Axenically cultured amastigote forms as an in vitro model for investigation of antileishmanial agents. Antimicrob Agents Chemother 41:972–976. https://doi.org/10.1128/AAC.41.5.972.

27. Vale-Costa S, Gomes-Pereira S, Teixeira CM, Rosa G, Rodrigues PN, Tomas A, Appelberg R, Gomes MS. 2013. Iron overload favors the elimination of Leishmania infantum from mouse tissues through interaction with reactive oxygen and nitrogen species. PLoS Negl Trop Dis 7:e2061. https://doi.org/10.1371/journal.pntd.0002061.

28. Gomes-Alves AG, Maia AF, Cruz T, Castro H, Tomas AM. 2018. Development of an automated image analysis protocol for quantification of intracellular forms of Leishmania spp. PLoS One 13:e0201747. https://doi.org/10.1371/journal.pone.0201747.

29. Melo AM, Duarte M, Moller IM, Prokisch H, Dolan PL, Pinto L, Nelson MA, Videira A. 2001. The external calcium-dependent NADPH dehydrogenase from Neurospora crassa mitochondria. J Biol Chem 276:3947–3951. https://doi.org/10.1074/jbc.M008199200.

30. Direção Geral de Alimentação e Veterinária, Ministério da Agricultura, do Mar, do Ambiente e do Ordenamento do Território. 2013. Decree-Law no. 113/2013 implementing EU Directive no. 2010/63 on animal protection for scientific purposes. Diário da República no. 151/2013, Série de 2013-8-7, p 4709–4739.

31. European Parliament and Council. 2010. Directive 2010/63/EU of the European Parliament and of the Council of 22 September 2010 on the protection of animals used for scientific purposes. Off J Eur Union L 276:33.

CHAPTER IV. Π-Π stacking stabilized polymeric micelles for hydrophobic drug delivery in the treatment of leishmaniasis

1. Abstract

Current strategies to control leishmaniases – a group of diseases caused by *Leishmania* parasites – rely on chemotherapy, which is associated with significant drawbacks, including severe side effects and limited drug efficacy. The public health impact of these diseases underscores the urgent need for new therapeutic approaches. A family of compounds, the quinoline-(1*H*)-imines, have emerged as promising lead compounds for antileishmanial drug development. However, their poor aqueous solubility poses a significant challenge. In the present study, quinoline-(1*H*)-imines were encapsulated into polymeric micelles (PMs) composed of block copolymer of methoxy poly(ethylene glycol)-*b*-poly(N-2-benzoyloxypropyl methacrylamide) [mPEG-*b*-p(HPMAm-Bz)]. These PMs are known to establish noncovalent π-π stacking interactions between the aromatic rings present in the p(HPMAm-Bz) block and the drug molecules, to enhance solubility. Encapsulation of quinoline-(1*H*)-imines resulted in comparable efficacy to the free drugs against *Leishmania* parasites, while significantly reducing toxicity toward primary macrophages *in vitro*. In a murine model of visceral leishmaniasis, the micellar formulation facilitated targeted drug accumulation in organs typically affected by the disease, as the liver, spleen and bone marrow. In contrast, the free drug was undetectable or present in markedly lower concentrations after 24 hours. These findings highlight the potential of mPEG-*b*-p(HPMAm-Bz) micelles as effective delivery systems for quinoline-(1*H*)-imines and potentially other antileishmanial agents. Nevertheless, encapsulated quinoline-(1*H*)-imines did not exhibit leishmanicidal effects in *L. infantum*-infected mice, despite significantly reduced toxicity compared to the free drug. Further studies are needed to optimize micellar stability and dosing regimens to fully harness their therapeutic potential.

2. Introduction

Leishmaniases belongs to a group of infectious diseases, defined by the World Health Organization (WHO) as neglected tropical diseases, with high impact in global public health, especially in poor communities from tropical and subtropical regions [1]. WHO estimates that around 700,000 to 1 million new cases of leishmaniases occur annually, resulting in 26,000 to 65,000 deaths. Leishmaniases are caused by more than 20 *Leishmania* species and transmitted between mammalian hosts through the bite of infected phlebotomine sandflies [1]. After being injected into the skin, *Leishmania* parasites survive and replicate inside macrophages, residing in phagolysosome-like compartments known as parasitophorous vacuoles (PVs) [2]. The exact location of the parasites and the clinical manifestation within the human host vary according, at least partially, to the *Leishmania* species. These manifestations range from self-curing cutaneous leishmaniasis (CL), the most common

form of the disease, to mucocutaneous leishmaniasis (MCL), a highly disfiguring and debilitating condition, and visceral leishmaniasis (VL), which is fatal if left untreated [3]. CL primarily affects the skin, MCL is characterized by a partial or total destruction of mucous membranes of the nose, mouth and throat, and VL affects mainly the liver, spleen and bone marrow [1].

Despite the scientific efforts made in leishmaniases research, there are still no effective human vaccines against these parasites and the control of leishmaniases relies on chemotherapy. Currently used drugs include pentavalent antimonials, amphotericin B (AmpB) deoxycholate, and its liposomal formulation (Ambisome®), miltefosine, paromomycin and pentamidine, but they all show important drawbacks concerning safety, administration (e.g., requiring multiple weeks of treatment in hospital settings), costs, and emergence of resistant parasite strains [4, 5]. Consequently, there is a need to develop new anti-*Leishmania* drugs and drug formulations.

Quinolines and structurally related heterocyclic compounds have been considered for their potential against *Leishmania* [6, 7]. Two examples are sitamaquine and tafenoquine (the latter recently approved by FDA for the treatment of *Plasmodium vivax*). In a previous study we reported that a series of quinolin-4(1*H*)-imines are capable of inhibiting the growth of different *Leishmania* species within macrophages *in vitro* [8-10]. Given the high hydrophobicity of these compounds, their intravenous administration would be hampered. While excipients, such as Cremophor, can effectively solubilize poorly-water soluble drugs they may also induce several side effects [11, 12]. The amount of excipient needed to solubilize a specific drug has been frequently linked to toxicity, thereby limiting the dosage of drug administered in clinical settings and hindering patient compliance with outcome of the treatment [13]. Nano-sized drug delivery systems have been employed to enhance the efficacy of drugs in the treatment of several diseases, including leishmaniases [14, 15]. These systems are known for their ability to solubilize hydrophobic drugs, deliver the compound to specific tissues, and provide sustained release, hence reducing the side effects and increasing the patient compliance to the treatment [16-18]. Some formulations using polymeric micelles (PMs), such as as Genexol® or Nanoxel® M, already used in clinic, or NK105, currently in clinical trials, enabled to increase drug dosage while providing improved drug safety profiles or enhanced pharmacokinetics when compared to drugs administered with other excipients [19-23].

In the present study we investigated whether PMs are suitable delivery systems for quinolin-4(1*H*)-imines that showed high toxicity when intravenously administered as free drug (data not shown). The selected nanocarrier is a polymeric micelle composed of block copolymer of methoxy poly(ethylene glycol)-b-poly(N-2-benzoyloxypropyl methacrylamide) [mPEG-*b*-p(HPMAm-Bz)] previously developed by

Shi et al. for the delivery of paclitaxel (PTX), a chemotherapeutic drug [24]. In that case, the PTX polymeric micelle formulation improved PTX solubility and circulation kinetics resulting in complete tumor regression in a mouse model. The study also demonstrated that the noncovalent π-π stacking interactions between the aromatic rings present on the p(HPMAm-Bz) block and the drug likely contribute to good drug retention in the carrier, resulting in favorable blood circulation kinetics and therapeutic effects [24].

The quinolin-4(1*H*)-imines contain aromatic structures and, therefore, likely establish π-π stacking interactions with the p(HPMAm-Bz) block. We investigated the loading and retention of quinolin-4(1H)-imines in mPEG-*b*-p(HPMAm-Bz) micelles and tested their *in vitro* efficacy against *L. amazonensis* and *L. infantum*, two causative agents of CL and VL, respectively. Subsequently, the blood circulation kinetics and tissue distribution of labeled PMs and the incorporated selected quinolin-4(1*H*)-imine were evaluated using healthy C57BL/6 mice. Finally, the therapeutic potential of this PM-drug formulation was assessed in the same mouse model infected with *L. infantum*.

3. Materials and Methods

3.1. Synthesis of quinolin-4(1*H*)-imine derivatives

The quinolin-4(1*H*)-imine derivatives were synthesized and characterized as previously reported [9, 10]. For *in vitro* experiments using the free drugs, stock solutions with concentrations of 20 mM were prepared in dimethyl sulfoxide (DMSO, Sigma Aldrich) and stored at -20 °C until further use.

3.2. Preparation and characterization of quinolin-4(1*H*)-imines-loaded polymeric micelles

Methoxy poly(ethylene glycol)-*b*-(N-(2-benzoyloxypropyl)-methacrylamide)) (mPEG-*b*-p(HPMAm-Bz) copolymer (M_n of 22 kDa) was synthesized via free radical polymerization, using HPMA-Bz as monomer and $mPEG_2$-ABCPA (mPEG of 5 kDa) as macroinitiator, as described previously [24]. PMs were prepared by a nanoprecipitation method adapted from Shi et al. [24]. Briefly, 10 mg of mPEG-*b*-p(HPMAm-Bz) block copolymer was dissolved in 1 mL of tetrahydrofuran (THF) and added dropwise to 1 mL of a phosphate-buffered saline (PBS) solution while stirring. The solution was maintained overnight in the fume hood at RT, to allow organic solvent evaporation, resulting in the formation of micelles. After incubation, the volume of the micellar dispersion was adjusted to 1 mL. Loaded PMs were prepared as described above with different concentrations of quinolin-4(1*H*)-imines dissolved in THF together with the polymer. The obtained micellar dispersions were subsequently filtrated through a 0.45 μm nylon membrane to remove nonencapsulated drug.

Polymer labeled with Cy7 or Cy3 was obtained as described before by Shi et al. [24]. Cy7 and Cy3 labelled micelles were prepared as described above by mixing non-labelled mPEG-*b*-p(HPMAm-Bz) with 1.5% (w/w) of Cy3/Cy7-labeled polymer [25].

Empty and drug-loaded mPEG-*b*-p(HPMAm-Bz) micelles were characterized for Z-average (Z_{ave}) particle size, polydispersity index (PDI), encapsulation efficiency (EE) and loading capacity (LC). The Z_{ave} particle size and PDI were measured at 25 °C, after a 10x dilution in PBS, by dynamic light scattering (DLS) using a Malvern ALV CGS-3 system. Encapsulation efficiency (EE) and loading capacity (LC) were calculated based on the amount of compound loaded in the polymeric micelles. To this end, after filtration, the formed particles were diluted 10 times in acetonitrile (ACN) and vortexed for 1 min to dissociate the micelles and dissolve the encapsulated compounds. Compound content was subsequently determined by ultra-performance liquid chromatography (UPLC), using a Waters Acquity system. Two eluents were used, eluent A containing 10% ACN in water and eluent B with 90% ACN in water, both with 0.1% trifluoroacetic acid (TFA). A gradient was run for 6 min, allowing eluent B to increase from 0 to 100% at a flow rate of 1 mL/min. A C18 column (ACQUITY UPLC® BEHC18™ 1.7 µm, 2.1 x 50mm Waters Corporation, Milford, MA) was used. Samples of 1 µL were injected and detection was done at a wavelength of 220 nm. Quinolin-4(1H)-imines concentrations in the different samples were determined using calibration curves of the compounds dissolved in ACN in a range of 4-500 µM. Analysis was performed using the Empower software. The EE and LC were calculated as follows:

EE (%) = amount loaded drug/total amount of added drug x 100%

LC (%) = mg loaded drug / (mg loaded drug + mg polymer) x 100%

3.3. Generation of bone marrow-derived macrophages

Differentiation of bone marrow-derived macrophages (BMDM) was performed as previously described [26]. Briefly, bone marrow cells were obtained by flushing tibia and femur from BALB/c mouse with Dulbecco's Modified Eagle's Medium (DMEM - Gibco). After centrifugation, cells were resuspended in DMEM supplemented with 10% iFBS, 1% of Minimum Essential Media Non-Essential Amino Acids Solution (MEM - Gibco), 50 U/mL penicillin, 50 µg/mL streptomycin (complete DMEM medium or cDMEM), and 10% L929 cell conditioned medium (LCCM) as source of Macrophage-Colony Stimulating Factor (M-CSF). After being seeded in Petri dishes and incubated for 24 h at 37 °C with 5% CO_2, non-adherent cells were recovered and counted. Subsequently, cells were plated in 96-well plates (2.5-3x10^4

cells per well) and incubated for 10 days at 37 °C with 5% CO_2, and cDMEM containing 10% LCCM was renewed on the 4th and 7th day.

3.4. *In vitro* activity

3.4.1. Parasite cultures

*Leishmania infa*ntum promastigotes (MHOM/MA/67/ITMAP-263) were cultured at 25 °C in RPMI 1640 GlutaMax supplemented with 10% (v/v) heat-inactivated fetal bovine serum (iFBS), 50 U/mL penicillin, 50 µg/mL streptomycin (from Gibco), and 20 mM HEPES sodium salt, pH 7.4 (Sigma). *Leishmania amazonensis* promastigotes (MHOM/BR/LTB0016) were maintained at 25 °C in Schneider's insect medium (Sigma) supplemented with 10% (v/v) iFBS, 100 U/mL penicillin, 100 µg/mL streptomycin, 5 mM HEPES sodium salt, pH 7.4, and 5 µg/mL phenol red (Sigma). *L. infantum* axenic amastigotes were maintained at 37 °C and 5% CO_2 in MAA20 medium, as described previously [27]. Briefly, MAA consisted of media 199 with Hanks' salts (Gibco) supplemented with 15 mM D-glucose, 4 mM NaHCO3, 0.5% trypto-casein-soy (Biorad) and 25 mM HEPES at a final pH of 6.5. Afterward, MAA20 was obtained by supplementing MAA medium with 20% (v/v) iFBS, 2 mM GlutaMax (Gibco), and 0.023 mM hemin.

3.4.2. Determination of IC_{50}s against intramacrophagic *L. infantum* and *L. amazonensis*

The leishmanicidal activity of free and encapsulated compounds was evaluated using intramacrophagic parasites in *in vitro* BMDM cultures, in 96-well plates. After differentiation, as described in section 2.3., BMDM were infected either with *Leishmania infantum* axenic amastigotes (MHOM/MA/67/ITMAP-263) or *L. amazonensis* stationary-phase promastigotes (MHOM/BR/LTB0016) at a multiplicity of infection (MOI) of 10. After 3 h incubation with BMDM, non-internalized parasites were removed by washing the cells twice with DMEM Subsequently, an incubation for 24 h prior the addition of compounds allowed the settlement and differentiation of amastigotes. The effect of free and encapsulated compounds – concentrations ranging from 0.15 to 5 µM and 0.15 to 10 µM, respectively – on elimination of intracellular parasites was assessed upon 48 h incubation with cultures at 37 °C and with 5% CO_2. The final polymer concentration added to cells varied from 6 to 567 µg/mL. Briefly, non-treated and treated BMDM were fixed in 4% paraformaldehyde, permeabilized with 0.1% Triton X-100 and stained with HCS CellMask™ Deep Red (Invitrogen) and DAPI (SIGMA), following manufacturer's instructions. Anti-*Leishmania* effect was evaluated by determination of the percentage of infected cells in the presence or absence of the different drugs, in images acquired using the IN Cell Analyzer 2000 microscope (GE

Healthcare) and later analyzed with the IN Cell Investigator Developer Toolbox v. 1.9.2 (GE Healthcare), as previously described [26]. Half maximal inhibitory concentrations (IC_{50}) were calculated using GraphPad Prism 7 software.

3.4.3. Cytotoxicity of free and encapsulated quinolin-4(1*H*)-imine derivatives on BMDM

The cytotoxicity effect of the different compounds on mammalian cells was evaluated using BMDM (obtained as described in section 3.3.), following protocol adapted from Vale-Costa et al. [28]. Briefly, BMDM were incubated with free and encapsulated compounds, concentrations ranging from 0.6 to 20 μM and 1.56 to 50 μM, respectively, for 48 h at 37 °C with 5% CO_2. The final polymer concentration added to cells varied from 61 to 2.8 mg/mL. After that, 0.1 mM of resazurin (Sigma) was added to each well and fluorescence intensity (excitation at 530 nm and emission at 590 nm) was measured after 3 h, using BioTek's Synergy™ Mx Microplate Reader. Cells were additionally incubated with vehicle (DMSO) as negative control. Data were analyzed with GraphPad Prism 7 software and 50% cytotoxic concentrations (CC_{50}) determined.

3.4.4. Localization of Cy3-labeled mPEG-*b*-p(HPMAm-Bz) micelles in infected BMDM

Intracellular localization of Cy3-labeled mPEG-*b*-p(HPMAm-Bz) micelles was assessed after 3 and 6 h incubation with *Leishmania*-infected BMDM. Macrophages differentiation and infection were performed as described in sections 3.3. and 3.4.2., respectively. The final polymer concentration added to cells was 6 mg/mL. Intracellular parasites were visualized using an indirect fluorescent antibody test (IFAT) [29]. Briefly, after fixation and permeabilization with 4% paraformaldehyde and 0.1 % Triton X-100, respectively, cultures were blocked with 1% (w/v) BSA. Next, cells were incubated with mouse monoclonal anti-α-tubulin TAT1 (diluted to 1:50) and 4',6-diamidino-2-phenylindole (DAPI). Secondary antibody was Alexa Fluor 488 anti-mouse IgG used at 1:2000 dilution. Images were acquired using the IN Cell Analyzer 2000 microscope.

3.5. *In vivo* studies

Due to ethical concerns regarding the use of animals, the pharmacokinetics, biodistribution and therapeutic efficacy of Cy7-labelled-mPEG-*b*-p(HPMAm-Bz) micelles, were investigated using only free and encapsulated 1n since this compound showed the most promising performance *in vitro*.

3.5.1. Pharmacokinetics and biodistribution

Pharmacokinetics (PK) and biodistribution studies of empty or 1n-loaded Cy7-labelled-mPEG-*b*-p(HPMAm-Bz) micelles, as well as free 1n, were performed using C57BL/6 mice (four per group). Empty PMs (20 mg/mL) and 1n-loaded in PMs (6.4 mM of 1n, and 20 mg/mL polymer) were prepared as described in section 2.2., and free 1n (5.5 mM) was solubilized in 0.5% DMSO (v/v) and 5% (w/v) Cremophor in PBS. Animals were injected via the tail vein with a 60-70 mL solution for a final concentration of 8 mg/kg of drug and 60 mg/kg of PMs. After 24 h, mice were sacrificed via isoflurane anesthesia followed by cervical dislocation.

For the PK studies, mice blood samples were withdrawn from the tail vein at several time points and collected in tubes with EDTA as anticoagulant. Samples were centrifuged at 2,000 g for 5 min, and the obtained plasma fraction was stored at -80 °C until further analysis.

To study the circulation kinetics of Cy7-labelled-mPEG-*b*-p(HPMAm-Bz) micelles, plasma samples were diluted with PBS, loaded in a 384-well plate, and then analyzed by fluorescence, using Odyssey® (LI-COR Westburg, the Netherlands), as described previously [25]. Calibration was performed using Cy7-labelled polymer diluted in mouse plasma at concentrations ranging from 0.1-40 mg/ml). To measure the concentration of the drug in the bloodstream, either injected as a micellar formulation or in its free form, plasma samples were ten times diluted with ACN, vortexed for 1 min followed by centrifugation at 12,000 g for 15 min. The obtained supernatants were subsequently analyzed for drug concentration by high-performance liquid chromatography (HPLC) using a Waters Acquity system. Two eluents were used, namely eluent A containing 10% ACN and eluent B with 80% ACN in water, both containing 0.1% trifluoroacetic acid (TFA). A gradient was run for 8 min allowing eluent B to increase from 0 to 100% at a flow rate of 1 mL/min. A C18 column (SunFire 5 μm 4.6 x 150 mm Waters Corporation, Milford, MA) was used and 20 μL samples were injected; detection was done at a wavelength of 220 nm. The analysis of HPLC results was performed using the Empower software. Calibration curve was performed with compound 1n dissolved in DMSO and diluted in plasma at concentrations ranging from 0.2-107 mM.

To study the biodistribution of empty or 1n-loaded Cy7-labelled-mPEG-*b*-p(HPMAm-Bz) micelles, as well as free 1n, different organs (heart, lungs, kidneys, liver, spleen, and bone marrow) were collected 24 h post-injection, snap-frozen in liquid nitrogen and stored at -80 °C until further use. To 100 mg of the different organ tissues, 200 μL of PBS pH 7.4 was added and the mixture grinded for 60 s at speed of 6000/s, using a Precellys 24 bead mill homogenizer (Bertin Instruments, France). The presence of

Cy7-labelled-mPEG-*b*-p(HPMAm-Bz) micelles was determined by loading 20 µL of the different organ samples in a 384-well plate and fluorescence measured, as described before in this section. The biodistribution of 1n (both in its free form and as micellar formulation) was evaluated by analyzing the amount of compound in the different organ samples by HPLC. The homogenized samples were diluted 3x in ACN and vortexed for 1 min. After a 15 min centrifugation, at 12,000 g, the supernatants were collected and analyzed by HPLC, as described above in this section. Calibrations curves were prepared with Cy7-labelled polymer or 1n dissolved in DMSO and diluted in PBS at concentrations ranging from 0.1-50 µg/mL and 0.05-107 µM, respectively.

3.5.2. *In vivo* therapeutic efficacy of 1n-loaded mPEG-*b*-p(HPMAm-Bz) micelles

C57BL/6 mice were infected with $2x10^7$ *L. infantum* stationary promastigotes and after 18 days, they were treated with empty (20 mg/mL polymer) or 1n-loaded mPEG-b-p(HPMAm-Bz) micelles (6 mM of 1n, and 20 mg/mL polymer) (prepared as described in section 2.2.). All formulations were administered intravenously (IV) via tail vein, once every other day, for a total of 6 injections of 100-200 µL solution. Each injected dose corresponded to 20 mg/kg of drug and around 145 mg/kg of PMs. Untreated mice were used as control. Four days after the last injection, mice were sacrificed via isoflurane anaesthesia followed by cervical dislocation. A limiting dilution technique was used and parasite burden was calculated as described by Buffet et al. [30]. For that, spleens and livers were recovered, weighed and homogenized in Schneider's medium (Sigma) supplemented with 10% (v/v) iFBS, 100 U/mL penicillin, 100 µg/mL streptomycin, 5 mM HEPES sodium salt, pH 7.4 (Sigma), 5 µg/mL phenol red (Sigma), and 2% (v/v) sterile human urine. Homogenates were then diluted to 10 mg/mL and each sample plated in quadruplicate across a 96-well plate in serial two-fold dilutions. After two weeks of incubation at 25 °C, the last dilution containing promastigotes was registered and the number of parasites per gram of organ was calculated.

3.6. Ethical statement

The use of BALB/c and C57BL/6 mice was approved by the Local Animal Ethics Committee of i3S, licensed by DGAV (Direção Geral de Alimentação e Veterinária, Government of Portugal). Animals were handled in accordance with good animal practice as defined by national authorities (DGAV; Decree 113/2013 from 7th August) [31] and European legislation (Directive 2010/63/EU, revising Directive 86/609/EEC) [32].

4. Results and Discussion

4.1. Characterization of empty and loaded mPEG-*b*-p(HPMAm-Bz) micelles

In a previous study, we reported on the *in vitro* efficacy of quinolin-4(1*H*)-imines derivatives against *in vitro* cultures of *Leishmania* [8]. According to our findings and the physicochemical properties of these drugs (Fig. 1), such as a log P > 1.6, they are able to cross cell membranes [8, 33]. However, in spite of this and the observed anti-parasite activities, the use of these compounds in animal models would most likely be hampered by their poor water-solubility. To overcome this drawback, we developed formulations of quinolin-4(1*H*)-imines loaded into mPEG-*b*-p(HPMAm-Bz) micelles. The selected polymeric micelle type was inspired by a previous study of Shi et al. [24] showing that noncovalent π-π stacking interaction between the polymer chains and aromatic groups of paclitaxel yielded PMs nanoparticles stable in the bloodstream with excellent drug retention.

To assess the ability of the PMs as carriers for quinolin-4(1*H*)-imines derivatives (Fig. 1), we loaded the four most active compounds found in a previous study [8] at increasing concentrations up to 7.5 mM, in mPEG-*b*-p(HPMAm-Bz) based micelles. The quinolin-4(1*H*)-imines selected for this study possess an aqueous solubility lower than 2.4 µg/mL. However, after encapsulation in PMs, it substantially improved and reached values of 3 mg/mL showing the excellent solubilization capacity of these PMs. The encapsulation efficiencies (EE) were around 80% for the different quinolin-4(1*H*)-imines investigated (Fig. 2). We further showed that the loading capacity (LC) increased with the feed amount of drug to up to 24 wt% (Fig. 2), a value similar to that reported for other compounds [24, 34]. Shi et al. [24] reported a maximum LC of these micelles of 23 wt% for paclitaxel, while Varela-Moreira et al. [34] tested several hydrophobic anti-cancer drugs with different physicochemical properties and observed values between 5 and 34 wt%. Beyond a certain threshold, the drug LC levels off, indicating saturation of the PMs core with the compound. According to our results, we did not reach the maximum LC of PMs for quinolin-4(1*H*)-imines. We did not attempt to reach higher loadings since this might result in overloading and insufficient drug retention in the micelles, as shown earlier [34].

DLS analysis showed that empty and loaded PMs had average diameters (Z_{ave}) ranging from 100 to 120 nm and a polydispersity index (PDI) below 0.2 (Fig. 2). The PMs were larger than previously reported (<100 nm) [24, 34], maybe because the micelles were formed in PBS as opposed to demi water as discussed by Bagheri et al. paper [35].

4.2. *In vitro* cytotoxicity and leishmanicidal activity of quinolin-4(1*H*)-imines-loaded mPEG-*b*-p(HPMAm-Bz) micelles

The properties of the PMs-drug complex such as size, PDI, EE and LC, were similar for the four quinolin-4(1*H*)-imines tested. Subsequent studies of efficacy and toxicity against *Leishmania* parasites and mammalian cells were performed using PMs loaded with compounds designated as 1h and 1n, the molecules with highest selectivity indexes (SI) in a previous study [8].

We observed that the IC_{50} of the encapsulated drugs on *L. infantum* and *L. amazonensis* were only slightly higher than that of the free drugs. Importantly, the toxicity of the formulations for mammalian cells was at least four times lower than that of the free drugs (Table I). The highest concentrations tested for the loaded 1h and 1n were 50 µM and 20 µM, respectively, and neither induced 50% death of bone marrow-derived macrophages (BMDM). Therefore, when encapsulated in PMs, these compounds have selectivity indexes at least 3 times higher than the corresponding free drug (Table I). DMSO (maximum 0.1%) and empty PMs, used as controls, showed no leishmanicidal activity or toxicity against BMDM, confirming that the effects of the PMs-drug result from the activity of the encapsulated quinolin-4(1*H*)-imines. In conclusion, the use of PMs can reduce the toxicity of compounds, as we observed both *in vitro* and *in vivo* (detailed below). This potentially enables the administration of a higher dose of the drug without adverse side effects, which could lead to better therapeutic outcomes and greater patient compliance and improved quality of life [21].

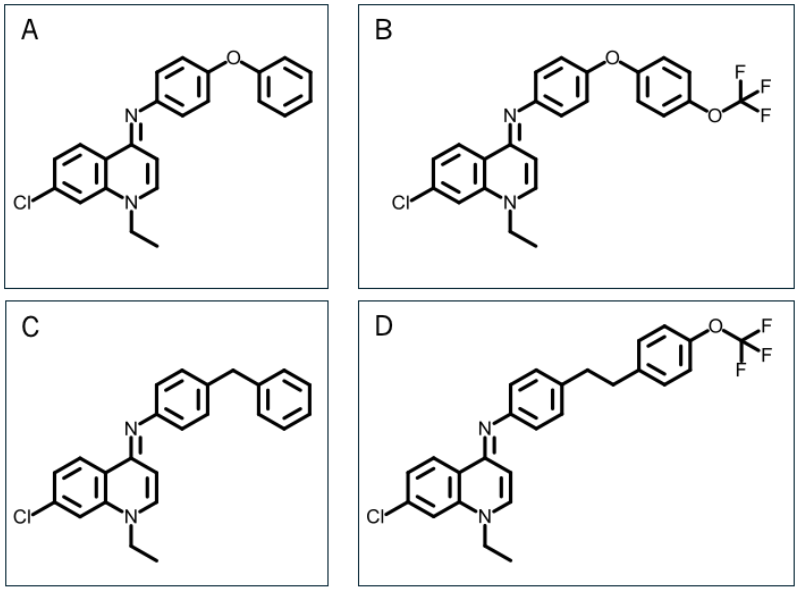

E

Name of the drug	MW (g/mol)	LogP[a]
1d	375	6.65
1g	459	7.62
1h	373	6.86
1n	471	7.85

Fig. 1 – Chemical structures (A-D) and physicochemical properties (E) of quinolin-4(1*H*)-imines used in this study and loaded in mPEG-*b*-p(HPMAm-Bz) micelles. (A) 1d, (B) 1g, (C) 1h and (D) 1n. MW – molecular weight. Properties retrieved from [a]http://www.molinspiration.com.

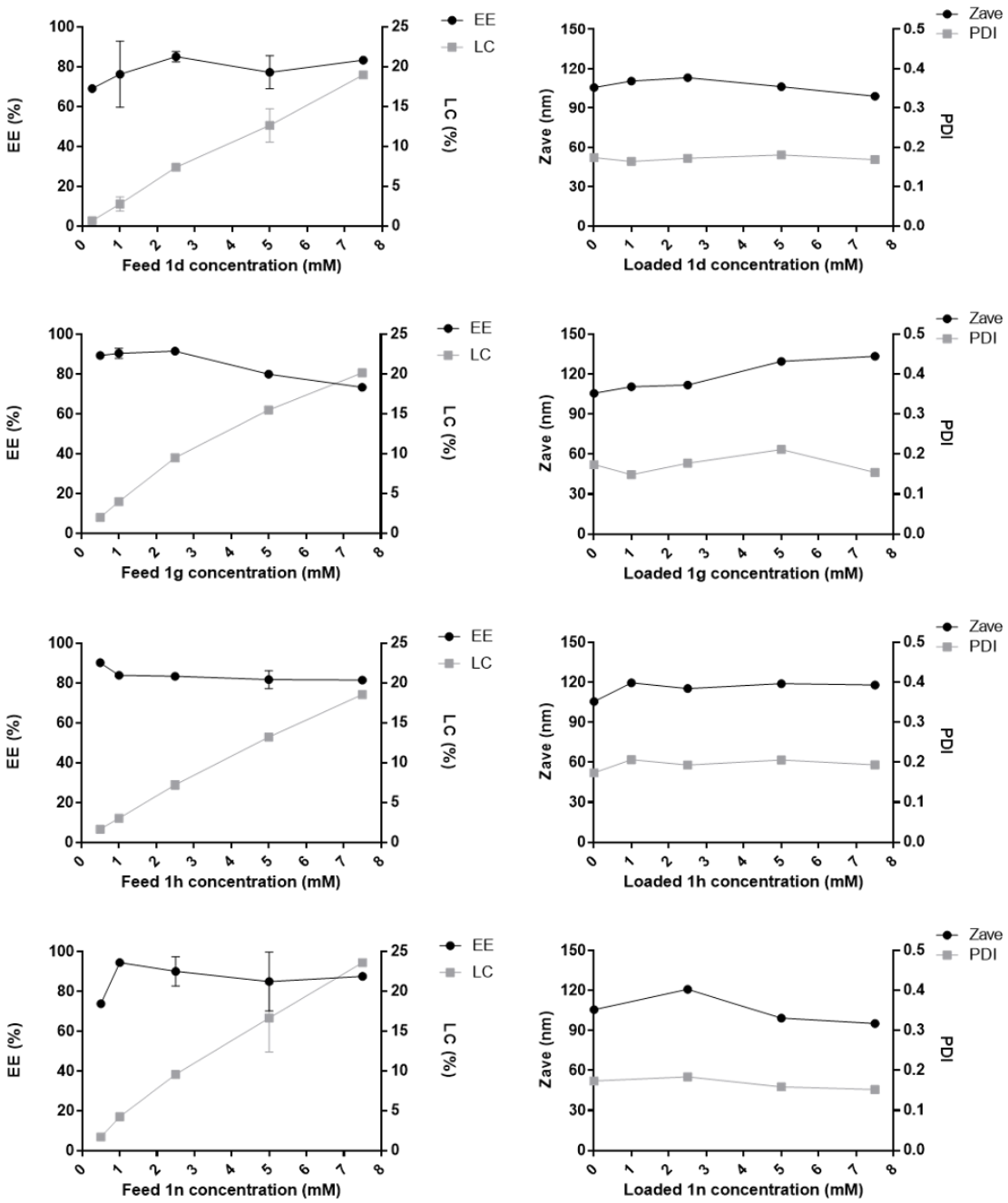

Fig. 2 – Characteristics of mPEG-*b*-p(HPMAm-Bz) micelles (10 mg/mL polymer) loaded with different amounts of quinolin-4(1*H*)-imines derivatives. (A) Encapsulation efficiency (% - EE) and loading capacity (% - LC), determined by UPLC; (B) Z_{ave} (nm – diameter) and polydispersity index (PDI) measured by DLS. Data are shown as mean ± SD, n = 3.

Table I – Leishmanicidal activities against *L. infantum* and *L. amazonensis* intramacrophagic amastigotes, and cytotoxicity of free and quinolin-4(1*H*)-imine loaded in mPEG-*b*-p(HPMAm-Bz) micelles (PMs).

Formulations	IC_{50} in intramacrophagic amastigotes (μM)		CC_{50} in BMDM (μM)	SI	
	L. infantum	*L. amazonensis*		*L. infantum*	*L. amazonensis*
Free 1h	0.98±0.33	1.29±0.37	8.8±2.5	8.98	6.82
Free 1n	1.08±0.26	1.76±0.37	5±2	4.63	2.84
1h-loaded PMs	1.83±0.57	2.31±1.11	>>50	>>27	>>22
1n-loaded PMs	1.55±0.69	2.24±1.04	>>20	>>13	>>9

L. infantum and *L. amazonensis* intramacrophagic amastigotes, as well as BALB/c mouse BMDM, were incubated for 48 h with increasing concentrations of free or encapsulated quinolin-4(1*H*)-imines. Data is presented as mean ± SD, n≥3.

IC_{50}, half-maximal inhibitory concentration; CC_{50}, 50% cytotoxic concentration; SI, selectivity index (ratio between CC_{50} and IC_{50} values).

4.3. Intracellular localization of mPEG-*b*-p(HPMAm-Bz) micelles in BMDM

As outlined previously, within infected macrophages, parasites inhabit parasitophorous vacuoles (PVs) of acidic nature, which can be small and contain one single amastigote (as in *L. infantum*), or large communal vacuoles housing several parasites (as in *L. amazonensis*) [2].

To investigate whether PMs were internalized by infected macrophages and reached parasites within PVs, we incubated infected cells with fluorescently Cy3 labelled mPEG-*b*-p(HPMAm-Bz) micelles (Z_{ave} of 155± 1 nm and a PDI of 0.25±0.01). These localization studies were carried out 3 and 6 h after incubation of PMs with cells (Fig. 3). Fluorescence microscopy showed the presence of PMs inside *L. infantum*/ *L. amazonensis*-infected cells indicating that macrophages hosting parasites retain the capacity to internalize micelles. This observation aligns with previous studies demonstrating that mPEG-*b*-p(HPMAm-Bz) micelles can be efficiently internalized by macrophages. [36]. Nonetheless, no co-localization with *Leishmania* was detected, indicating that PMs and parasites coexist in the same cells but are localized in different cell compartments (Fig. 3). It is generally accepted that cells internalize nanoparticles through endocytosis, leading to their accumulation in lysosomes [37]. When it comes to *Leishmania* parasites, macrophages internalize them through phagocytosis, forming an internal vesicle known as phagosome. Parasites possess the ability to manipulate the phagosome maturation process,

which involves the fusion of the phagosome with endosomes and lysosomes, leading to the formation of phagolysosome-like structures, called PVs [38]. Within PVs *Leishmania* spp. create a perfect niche to survive and replicate, acquiring nutrients from the host cell nutrients and evading host defense mechanisms [39]. Although our data suggest that PMs apparently lack the ability to cross the PV membrane, they can release the drug into infected cells, which likely crosses the PV membrane to reach the parasites.

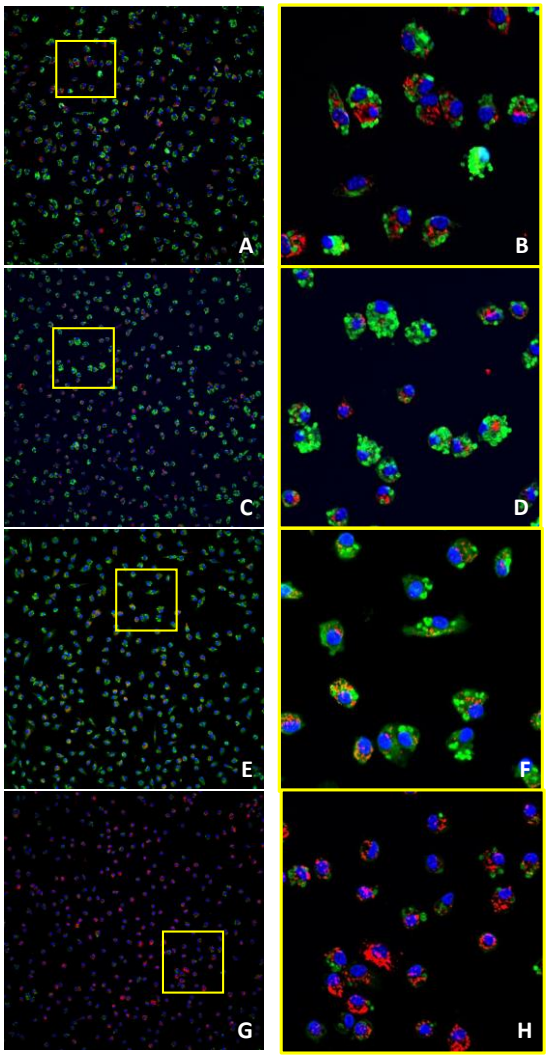

Fig. 3 – Representative images of BMDM infected with *L. infantum* (A-D) or *L. amazonensis* (E-G), incubated for 3h (A, B, E and F) and 6h (C, D, G and H) with Cy3-labeled mPEG-*b*-p(HPMAm-Bz) micelles. Parasites were visualized by indirect immunofluorescence incubated with mouse monoclonal anti-α-tubulin TAT1 (FITC; in green). DNA was stained with DAPI (in blue). Cy3-labeled mPEG-*b*-p(HPMAm-Bz) micelles were visualized with Cy3 channel (in red). Images were acquired using the IN Cell Analyzer 2000. Scale bar: 10 μm.

4.4. Pharmacokinetics and biodistribution of Cy7-labelled mPEG-*b*-p(HPMAm-Bz) micelles and 1n

An important feature of an efficient drug carrier system against leishmaniasis is its ability to accumulate in the infected target organ. In our disease model, the drug must reach macrophages in the organs most affected by VL, such as liver, spleen and bone marrow. To address whether this was the case, pharmacokinetics and biodistribution studies were performed. To this end, empty and 1n-loaded mPEG-*b*-p(HPMAm-Bz) micelles labelled with Cy7, as well as free 1n, were administered intravenously into C57BL/6 mice. The levels of drug-containing PMs were monitored in the bloodstream and several organs using fluorescence for the nanoparticles and HPLC for the incorporated drug. Preliminary analysis indicated that the maximum tolerated dose (MTD) of free quinolin-4(1*H*)-imines 1n and 1h after IV administration was 10 mg/kg, at which toxic effects were observed (data not shown). Therefore, in our experiments, C57BL/6 mice were injected with a lower PMs-1n dose of 8 mg/kg.

Cy7-labelled PMs loaded with 6.4 mM (3 mg/mL) of 1n exhibited a mean size of 108 nm, an EE of 100% and a LC of 13% (Table II). Empty Cy7-labelled mPEG-*b*-p(HPMAm-Bz) micelles were of about the same size and presented the same low PDI value (0.13).

Table II – Characteristics of Cy7-labelled mPEG-*b*-p(HPMAm-Bz) micelles empty or loaded with 1n.

Formulations	Z_{ave} (nm)[a]	PDI[a]	EE (%)[b]	LC (%)[b]
Cy7-labelled PMs	101	0.13	N/A	N/A
1n-loaded Cy7-labelled PMs	108	0.13	103	13.1

Polymeric micelles were obtained by a nanoprecipitation method. Twenty mg/ml of non-labelled mPEG-*b*-p(HPMAm-Bz) mixed with 1.5 % (w/w) of Cy7-labeled polymer was loaded with 3 mg/mL of 1n.

[a]Z_{ave} (size) and PDI (polydispersity index) determined by DLS; [b]EE (encapsulation efficiency) and LC (loading capacity) determined by UPLC.

Circulation kinetics of both the drug and PMs was addressed by blood collection from the tail, at different times points, from 2-5 min to 24 h after injection. C57BL/6 mice were then sacrificed, and the organs of interest collected for biodistribution analysis. The amount of Cy7 and 1n recovered in the blood, immediately after the intravenous (IV) injection was considered as 100% injected dose (ID). Quite unexpectedly, and in contrast with earlier findings on the pharmacokinetics of this type of PMs [24], we

observed that about 65% of the injected PMs dose (ID) was eliminated from circulation within the first hour after intravenous administration. Then, blood levels stabilized, declining slowly over time. The underlying cause for this biphasic pattern is unclear and needs further study. Prior research conducted by Shi [24] and Varela-Moreira [34] demonstrated a slightly higher percentage of micelles remaining in circulation after 24 h (20% and 28% ID, respectively) compared to our findings (13%). Nonetheless, it is important to note that Shi and Varela-Moreira administered polymer doses ranging from 120 to 240 mg/kg, whereas we used 60 mg/kg, which could potentially influence circulation kinetics of PMs. In fact, Bagheri injected 500 mg/kg of polymer and observed that more than 50% of the ID of micelles were still in the circulation after 24h [40].

Regarding the quinolin-4(1*H*)-imine 1n loaded in PMs, we observed a circulation kinetics similar to that of the free drug (Fig. 4 A and B). One hour upon injection of PMs-encapsulated drug, 8.9 ± 3.4% of the ID was detected, whereas the concentration of the free drug was below the detection limit (Fig. 4 B). This rapid elimination aligns with the unexpected fast clearance of the PMs within the first hour after administration, although it is also possible that the encapsulated drug is quickly released from the PMs structures following intravenous injection. In either case, a rapid decrease in drug concentration shortly after injection into the bloodstream is undesirable and may be related to micelle overloading and/or to poor retention of the drug in the micelle core. In the present study, the maximum LC tested for 1n in mPEG-*b*-p(HPMAm-Bz) micelles, without compromising the EE, was 24% (w/w) at a concentration of 7.5 mM. To avoid overloading of this micellar formulation, we loaded PMs with 13% (w/w) of 1n. Nonetheless, additional studies are required to determine the cause of the burst release.

The anticipated stability of these PMs is primarily attributed to π-π and hydrophobic interactions between the hydrophobic block of the mPEG-*b*-p(HPMAm-Bz) and the encapsulated drug. Previous studies aimed at enhancing retention of PTX and curcumin within mPEG-*b*-p(HPMAm-Bz) micelles, involved the use of different molecular weights of the hydrophobic HPMA-Bz block. In both cases, an increase in drug retention values were observed as the molecular weight of the hydrophobic block increased from the lowest to the highest tested [40, 41]. Additionally, the drug-to-polymer ratio played a significant role, with lower drug loading improving retention in the micelle core. The observed poor retention of 1n in mPEG-*b*-p(HPMAm-Bz) micelles suggests that the loading parameters should be adjusted, by decreasing the amount of drug or increasing the polymer concentration from 20 to 30 mg/mL [40, 41]. In follow up studies, the *in vitro* release assay developed by Varela-Moreira et al. [34] and Wang et al. [42], which uses media containing acceptor molecules like albumin for hydrophobic

compounds, or directly in mouse plasma or whole mouse blood, can be used to predict drug release kinetics more reliably. This approach could reduce the need for extensive PK studies in animals.

Most nanocarrier systems developed so far are designed for cancer treatment. In this context, surface decoration of NPs with PEG intends to enhance their pharmacokinetic properties and increase targeted biodistribution to diseased organs by preventing rapid clearance from circulation by the mononuclear phagocyte system (MPS) [43, 44]. The MPS is mainly composed of phagocytic cells, including circulating blood monocytes, tissue macrophages and dendritic cells, localized in organs such as the liver, spleen and bone marrow where they are responsible for the elimination of 'foreign invaders' from the bloodstream. Our biodistribution analysis showed much higher accumulation of 1n-loaded Cy7-labeled PMs in the liver and spleen, likely due to the uptake of intact micelles by MPS macrophages, compared to other organs investigated (lungs, heart, and BM) (Fig. 4 C and D). This finding is in line with previous studies using mPEG-*b*-p(HPMAm-Bz) micelles and is consistent with the well-established understanding of nanoparticle behavior following intravenous administration [24, 25, 40]. Of note, in mice injected with the free drug, the concentration of 1n in the bloodstream decreased below detection limit within 1h. Furthermore, after 24h, 1n was detect it in the kidney, suggesting clearance through glomerular filtration, and in the liver (Fig. 4 D). From this study, we can conclude that the highest drug levels in the liver, spleen and bone marrow are achieved when the drug is given in PMs-encapsulated form. This represents a significant advantage, considering that these organs are the most affected by VL. The targeted accumulation observed with mPEG-*b*-p(HPMAm-Bz) micelles could therefore enhance the efficacy of drugs against leishmaniasis.

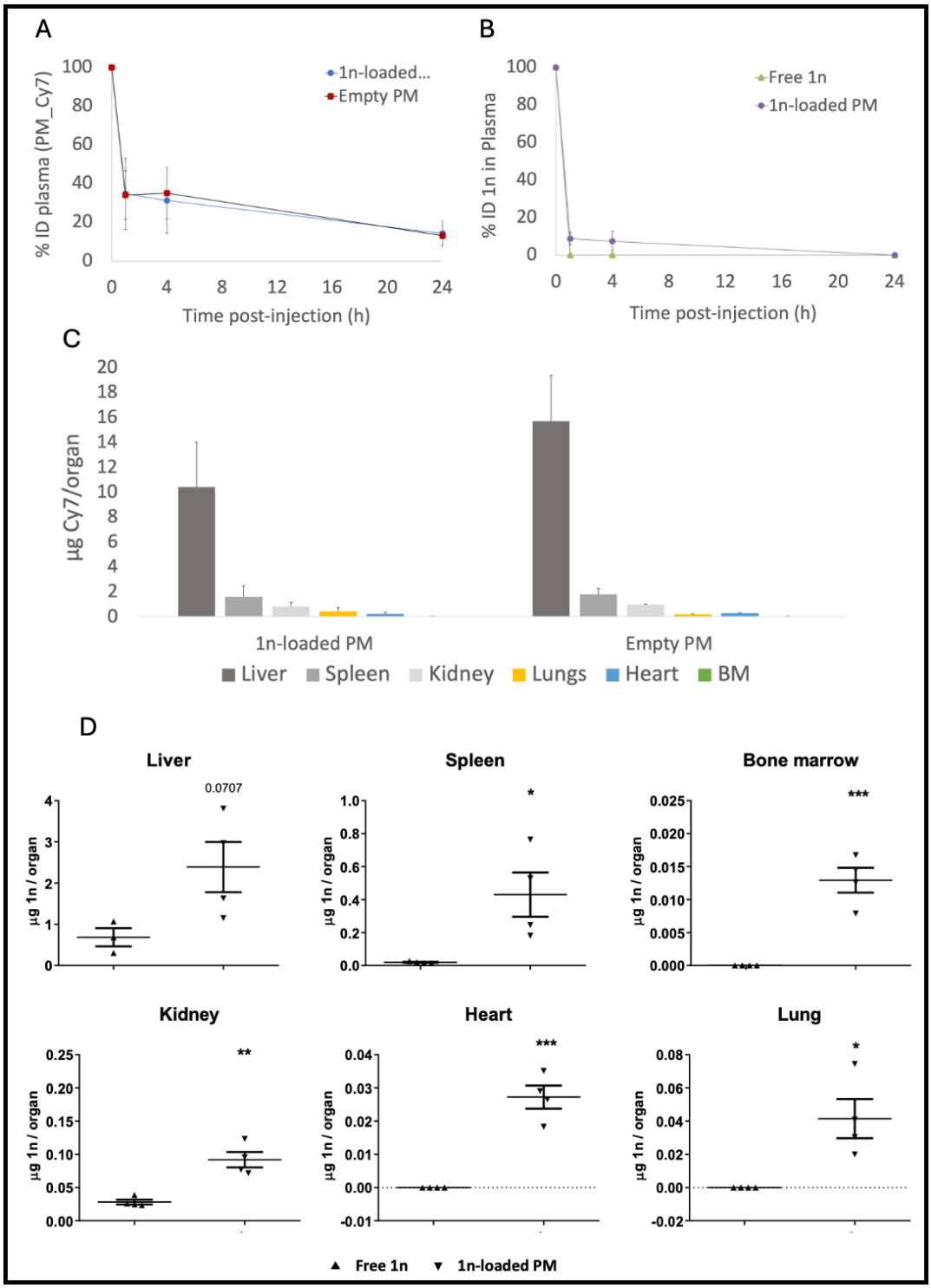

Fig.4 – Pharmacokinetics and biodistribution of Cy7-labeled mPEG-*b*-p(HPMAm-Bz) micelles and 1n (free and loaded in Cy7-labeled PMs). C57BL/6 mice were injected IV with Cy7-labeled mPEG-*b*-p(HPMAm-Bz) micelles, 1n-loaded Cy7-labeled PMs and free 1n. Blood samples were collected at different time points to quantify the amount of PMs (A) and 1n (B) in systemic circulation. Biodistribution of PMs (C) and 1n (D), in organs was analyzed 24h after IV injection. Graphs show the mean ± SD for 3 to 4 C57BL/6 mice. Statistical significance was determined using t-test *, P<0.05; **, P<0.005; ***, P<0.0005; ****, P<0.0001. PMs – polymeric micelles; BM – bone marrow.

4.5. Potential therapeutic effect of 1n-loaded mPEG-*b*-p(HPMAm-Bz) micelles

The therapeutic effect of 1n-loaded mPEG-*b*-p(HPMAm-Bz) micelles was evaluated in C57BL/6 mice infected with $2x10^7$ *L. infantum* stationary promastigotes. Loaded PMs (20 mg of 1n/kg) were administered intravenously every other day for a total of 6 injections, starting 18 days post infection. Untreated mice and animals inoculated with empty PMs were used as a control. As depicted in Fig. 5, no differences in the parasite load of treated and control animals could be detected. In other words, despite the higher accumulation of PMs-entrapped 1n in the liver and the spleen relatively to free drug (Fig. 4), no leishmanicidal effect was observed.

Our study revealed that a 20 mg/kg dose of 1n entrapped in mPEG-*b*-p(HPMAm-Bz) micelles did not induce side effects, contrary to the 10 mg/kg of free drug that caused severe toxic effects. This decrease in toxicity aligns with findings from previous studies where anticancer drugs were loaded into these PMs [24, 25]. Mice were not treated with the free drug because of its high toxicity at the 20 mg/kg dose.

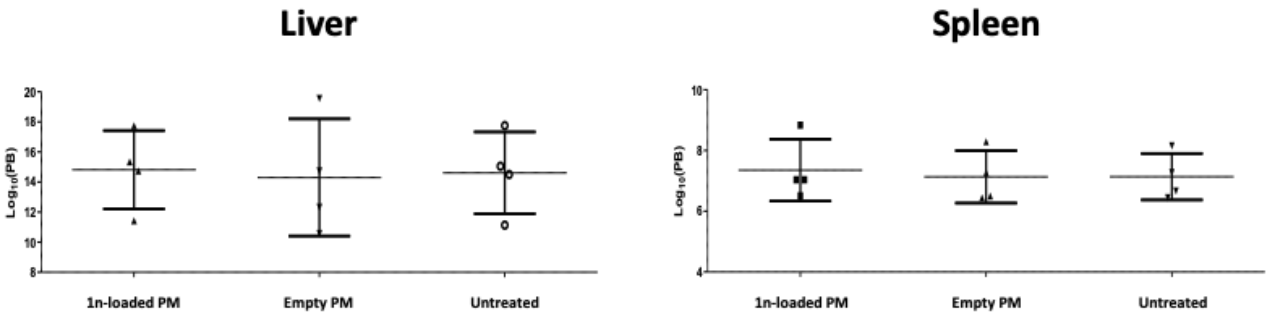

Fig. 5 – *In vivo* therapeutic activity of 1n-loaded PMs against *L. infantum*. C57BL/6 mice were infected with $2x10^7$ *L. infantum* stationary promastigotes and treated every other day for a total of 6 injections, 18 days post infection.

In contrast to our findings, previous studies have shown that certain quinoline derivative compounds, loaded onto PMs formulated with Poloxamer P407, displayed *in vivo* efficacy against leishmaniasis [45, 46]. It is possible that, differences in the route of administration (subcutaneous vs IV, in our case) and the number of inoculated parasites used ($1x10^7$ vs $2x10^7$) resulted in a significantly lower parasite burden – approximately 3-fold lower in the liver and 1.5-fold lower in the spleen – in the Poloxamer P407 study. This suggests that the dosage of the PMs-drug used in our study may have been insufficient to elicit a therapeutic response. Furthermore, the fast elimination of 1n administered in micellar observed in the first hour following IV administration, may have led to inadequate drug

accumulation in target cells, explaining the lack of any leishmanicidal activity. The Poloxamer P407 studies did not report on the pharmaceutical characteristics of the micellar formulations, making it difficult to compare their pharmacokinetics and tissue distribution with those of the PMs reported here.

Overall, this study demonstrate that mPEG-*b*-p(HPMAm-Bz) PMs are excellent solubilizers for quinolin-4(1*H*)-imine derivatives. However, the poor retention of the drug molecules within the micelles makes them less attractive for targeting purposes. Although tissue concentrations in the target tissues were higher, a much stronger retention capacity of the PMs could have resulted in higher drug levels in the infected tissues, potentially leading to stronger antileishmanial activity as the therapeutic outcome. Future studies aiming at optimizing the current PMs formulation should identify the reasons behind the inferior retention properties of these PMs compared to encapsulated PTX.

5. Conclusion

The encapsulation of quinolin-4(1*H*)-imines into mPEG-*b*-p(HPMAm-Bz) micelles significantly improved their apparent solubility and reduced their toxicity against mammalian cells *in vitro*. Despite the absence of a detectable activity *in vivo*, the increased accumulation of these micelles in target organs suggests potential benefits against *Leishmania* infections. Importantly, our study revealed that a 20 mg/kg dose of the drug encapsulated into PMs did not induce side effects, in contrast to the free drug, indicating that higher doses can be safely administered. Future work should focus on optimization of the retention properties of PMs for quinolin-4(1*H*)-imines and conducting dose-response studies (vs free drug) in the *in vivo* infection model used. If successful, further approaches may include combination therapies or new dose regimens to achieve better therapeutic outcomes.

6. References

1. World Health, O. *Fact sheets: Leishmaniasis*. 2019 on April 2023]; Available from: https://www.who.int/news-room/fact-sheets/detail/leishmaniasis.

2. Real, F. and R.A. Mortara, *The diverse and dynamic nature of Leishmania parasitophorous vacuoles studied by multidimensional imaging.* PLoS Negl Trop Dis, 2012. **6**(2): p. e1518.

3. Bruschi, F. and L. Gradoni, *The leishmaniases : old neglected tropical diseases*. 2018, New York, NY: Springer Berlin Heidelberg. pages cm.

4. Ponte-Sucre, A., et al., *Drug resistance and treatment failure in leishmaniasis: A 21st century challenge.* PLoS Negl Trop Dis, 2017. **11**(12): p. e0006052.

5. Pradhan, S., et al., *Treatment options for leishmaniasis.* Clin Exp Dermatol, 2022. **47**(3): p. 516-521.

6. Carvalho, L., et al., *Tafenoquine, an antiplasmodial 8-aminoquinoline, targets leishmania respiratory complex III and induces apoptosis.* Antimicrob Agents Chemother, 2010. **54**(12): p. 5344-51.

7. Carvalho, L., et al., *The 8-aminoquinoline analogue sitamaquine causes oxidative stress in Leishmania donovani promastigotes by targeting succinate dehydrogenase.* Antimicrob Agents Chemother, 2011. **55**(9): p. 4204-10.

8. Gomes-Alves, A.G., et al., *Biological Evaluation and Mechanistic Studies of Quinolin-(1H)-Imines as a New Chemotype against Leishmaniasis.* Antimicrob Agents Chemother, 2021. **65**(7): p. e0151320.

9. Ressurreicao, A.S., et al., *Structural optimization of quinolon-4(1H)-imines as dual-stage antimalarials: toward increased potency and metabolic stability.* J Med Chem, 2013. **56**(19): p. 7679-90.

10. Rodrigues, T., et al., *Quinolin-4(1H)-imines are potent antiplasmodial drugs targeting the liver stage of malaria.* J Med Chem, 2013. **56**(11): p. 4811-5.

11. Gelderblom, H., et al., *Cremophor EL: the drawbacks and advantages of vehicle selection for drug formulation.* Eur J Cancer, 2001. **37**(13): p. 1590-8.

12. Adams, J.D., et al., *Taxol: a history of pharmaceutical development and current pharmaceutical concerns.* J Natl Cancer Inst Monogr, 1993(15): p. 141-7.

13. van Zuylen, L., J. Verweij, and A. Sparreboom, *Role of formulation vehicles in taxane pharmacology.* Invest New Drugs, 2001. **19**(2): p. 125-41.

14. Saleem, K., et al., *Applications of Nanomaterials in Leishmaniasis: A Focus on Recent Advances and Challenges.* Nanomaterials (Basel), 2019. **9**(12).

15. Jamshaid, H., F.U. Din, and G.M. Khan, *Nanotechnology based solutions for anti-leishmanial impediments: a detailed insight.* J Nanobiotechnology, 2021. **19**(1): p. 106.

16. Mitchell, M.J., et al., *Engineering precision nanoparticles for drug delivery.* Nat Rev Drug Discov, 2021. **20**(2): p. 101-124.

17. Vargason, A.M., A.C. Anselmo, and S. Mitragotri, *The evolution of commercial drug delivery technologies.* Nat Biomed Eng, 2021. **5**(9): p. 951-967.

18. Yusuf, A., et al., *Nanoparticles as Drug Delivery Systems: A Review of the Implication of Nanoparticles' Physicochemical Properties on Responses in Biological Systems.* Polymers (Basel), 2023. **15**(7).

19. Kim, T.Y., et al., *Phase I and pharmacokinetic study of Genexol-PM, a cremophor-free, polymeric micelle-formulated paclitaxel, in patients with advanced malignancies.* Clin Cancer Res, 2004. **10**(11): p. 3708-16.

20. Lee, K.S., et al., *Multicenter phase II trial of Genexol-PM, a Cremophor-free, polymeric micelle formulation of paclitaxel, in patients with metastatic breast cancer.* Breast Cancer Res Treat, 2008. **108**(2): p. 241-50.

21. Hwang, D., J.D. Ramsey, and A.V. Kabanov, *Polymeric micelles for the delivery of poorly soluble drugs: From nanoformulation to clinical approval.* Adv Drug Deliv Rev, 2020. **156**: p. 80-118.

22. Fujiwara, Y., et al., *A multi-national, randomised, open-label, parallel, phase III non-inferiority study comparing NK105 and paclitaxel in metastatic or recurrent breast cancer patients.* Br J Cancer, 2019. **120**(5): p. 475-480.

23. Lee, S.W., et al., *Development of docetaxel-loaded intravenous formulation, Nanoxel-PM using polymer-based delivery system.* J Control Release, 2011. **155**(2): p. 262-71.

24. Shi, Y., et al., *Complete Regression of Xenograft Tumors upon Targeted Delivery of Paclitaxel via Pi-Pi Stacking Stabilized Polymeric Micelles.* ACS Nano, 2015. **9**(4): p. 3740-52.

25. Varela-Moreira, A., et al., *Polymeric micelles loaded with carfilzomib increase tolerability in a humanized bone marrow-like scaffold mouse model.* Int J Pharm X, 2020. **2**: p. 100049.

26. Gomes-Alves, A.G., et al., *Development of an automated image analysis protocol for quantification of intracellular forms of Leishmania spp.* PLoS One, 2018. **13**(8): p. e0201747.

27. Sereno, D. and J.L. Lemesre, *Axenically cultured amastigote forms as an in vitro model for investigation of antileishmanial agents.* Antimicrob Agents Chemother, 1997. **41**(5): p. 972-6.

28. Vale-Costa, S., et al., *Iron overload favors the elimination of Leishmania infantum from mouse tissues through interaction with reactive oxygen and nitrogen species.* PLoS Negl Trop Dis, 2013. **7**(2): p. e2061.

29. Castro, H., et al., *Complementary antioxidant defense by cytoplasmic and mitochondrial peroxiredoxins in Leishmania infantum.* Free Radic Biol Med, 2002. **33**(11): p. 1552-62.

30. Buffet, P.A., et al., *Culture microtitration: a sensitive method for quantifying Leishmania infantum in tissues of infected mice.* Antimicrob Agents Chemother, 1995. **39**(9): p. 2167-8.

31. Direção Geral de Alimentação e Veterinária, M.d.A., do Mar, do Ambiente e do Ordenamento do Território, *Decree-Law no.113/2013 implementing EU Directive no. 2010/63 on animal protection for scientific purposes. Diário da República no. 151/2013, Série de 2013-8-7 p 4709–4739*. 2013. p. 4709–4739.

32. Council, E.P.a., *Directive 2010/63/EU of the European Parliament and of the Council of 22 September 2010 on the protection of animals used for scientific purposes. Off J Eur Union L 276:33.* 2010.

33. Bennion, B.J., et al., *Predicting a Drug's Membrane Permeability: A Computational Model Validated With in Vitro Permeability Assay Data.* J Phys Chem B, 2017. **121**(20): p. 5228-5237.

34. Varela-Moreira, A., et al., *Utilizing in vitro drug release assays to predict in vivo drug retention in micelles.* Int J Pharm, 2022. **618**: p. 121638.

35. Bagheri, M., et al., *Effect of Formulation and Processing Parameters on the Size of mPEG- b-p(HPMA-Bz) Polymeric Micelles.* Langmuir, 2018. **34**(50): p. 15495-15506.

36. Alaarg, A., et al., *A systematic comparison of clinically viable nanomedicines targeting HMG-CoA reductase in inflammatory atherosclerosis.* J Control Release, 2017. **262**: p. 47-57.

37. Rennick, J.J., A.P.R. Johnston, and R.G. Parton, *Key principles and methods for studying the endocytosis of biological and nanoparticle therapeutics.* Nat Nanotechnol, 2021. **16**(3): p. 266-276.

38. Carneiro, M.B. and N.C. Peters, *The Paradox of a Phagosomal Lifestyle: How Innate Host Cell-Leishmania amazonensis Interactions Lead to a Progressive Chronic Disease.* Front Immunol, 2021. **12**: p. 728848.

39. Lievin-Le Moal, V. and P.M. Loiseau, *Leishmania hijacking of the macrophage intracellular compartments.* FEBS J, 2016. **283**(4): p. 598-607.

40. Bagheri, M., et al., *In Vitro and In Vivo Studies on HPMA-Based Polymeric Micelles Loaded with Curcumin.* Mol Pharm, 2021. **18**(3): p. 1247-1263.

41. Sheybanifard, M., et al., *Systematic evaluation of design features enables efficient selection of Pi electron-stabilized polymeric micelles.* Int J Pharm, 2020. **584**: p. 119409.

42. Wang, Y., et al., *Magnetic beads for the evaluation of drug release from biotinylated polymeric micelles in biological media.* J Control Release, 2022. **349**: p. 954-962.

43. Cabral, H., et al., *Block Copolymer Micelles in Nanomedicine Applications.* Chem Rev, 2018. **118**(14): p. 6844-6892.

44. Blanco, E., H. Shen, and M. Ferrari, *Principles of nanoparticle design for overcoming biological barriers to drug delivery.* Nat Biotechnol, 2015. **33**(9): p. 941-51.

45. Tavares, G.S.V., et al., *A clioquinol-containing Pluronic((R)) F127 polymeric micelle system is effective in the treatment of visceral leishmaniasis in a murine model.* Parasite, 2020. **27**: p. 29.

46. Ribeiro Antinarelli, L.M., et al., *Parasitological and immunological evaluation of a quinoline derivative salt incorporated into a polymeric micelle formulation against Leishmania infantum infection.* Parasitol Res, 2022. **121**(7): p. 2129-2140.

Currently available chemotherapies against leishmaniases exhibit important limitations such as prolonged treatment regimens with inadequate outcomes, severe adverse side effects, prohibitive prices, and the emergence of resistant parasite strains [1, 2]. Unfortunately, there is a general lack of interest from pharmaceutical companies in developing new anti-*Leishmania* drugs since these diseases affect mainly low-income populations from developing countries. This translates in the perception that the high investment needed to fulfil this objective will not be compensated by the profit that such drugs would generate. Academia and non-profit organizations continue, therefore, to play an important role in advancing this area of research. In line with this, the aim of this thesis was to discover new molecules with antileishmanial activity and formulate them in innovative drug delivery systems.

Many laboratories around the globe work in drug discovery and development, a process that beneficially makes use of automated high-throughput screening (HTS) assays to analyze compound libraries to identify possible hits and drug candidates [3]. Successful translation of hits identified from *in vitro* screens to animal models is dependent on conducting screens using the parasite stage and host cells that closely resemble *in vivo* physiological condition [4]. The life cycle of the *Leishmania* is complex as it involves both invertebrate and vertebrate hosts and two distinct developmental stages, promastigotes and amastigotes, respectively. During blood feeding of an infected sandfly, *Leishmania* promastigotes are regurgitated and injected into the skin of the host, where they are phagocytosed by macrophages and neutrophils. Within these cells, promastigotes transform into amastigotes, obligatory intracellular forms that constitute the disease-causing stage of *Leishmania* [5]. This entails the necessity to screen new compounds against amastigotes. However, automated HTS assays in leishmaniases were often performed with extracellular promastigotes or axenic amastigotes, which are easier to work with but do not fully mimic physiological conditions. This can lead to both false positive and negative results [6-9]. Additionally, macrophage-like cell lines, such the human leukemia monocytic cell line, THP-1, are frequently used in drug assays due to their ease of manipulation and unlimited source of material. However, this raises some concerns including the risk of cross-contamination with other cell lines or mycoplasma, as well as genotypic or phenotypic changes that can derive from repeated *in vitro* passages, potentially leading in inaccurate results [10, 11]. A viable alternative is the use of primary cell cultures, such as bone marrow-derived macrophages (BMDM) that, regardless their limited lifespan, exhibit physiological features akin of macrophages *in vivo*. In **Chapter II**, we developed a high-content screening (HCS) assay in a 96-well plate, using BMDM infected with *L. infantum* or *L. amazonensis* to assess drug sensitivity of intracellular amastigotes [12]. This protocol can be adapted for use with

culture plates containing a higher number of wells when appropriate automated equipment is available. Visualization of intracellular parasites was simplified using only DAPI staining, eliminating the need for genetically modified parasites expressing reporter genes (eg. GFP or DsRed2) or the use of an indirect fluorescent antibody test (IFAT). The detection of macrophages was also based on DAPI staining, with the signal distinguished from that of parasites due to their size. Using images acquired with IN Cell Analyzer 2000, the high content analysis (HCA) procedure developed, allows for the determination of the number of macrophages and intracellular amastigotes by two automated image analysis software programs: IN Cell Investigator Developer Toolbox and CellProfiler. The former has been, and continues to be, extremely used in our lab where it is utilized not only for discovering new drug molecules with anti-*Leishmania* effects, but also for other purposes, such as assessing the impact of specific proteins on the ability of parasites to infect and persist in macrophages [13]. The protocol version with the second, a free open-source software, was developed to enable other laboratories without access to HCS-microscopes to perform *Leishmania* drug development or any other study that requires analysis of infected macrophages, in a faster and more standardized way. CellProfiler is a useful image processing program, but variations in fluorescence microscopes may affect image parameters like resolution, contrast, and background noise, which may impact overall image quality and, consequently, downstream image analysis. This will lead to the need of adjustments on threshold parameters across different labs prior to large-scale application, which can be relatively time-consuming. In recent years, the advancement of machine learning has introduced new methodologies for image analysis, including the detection of protozoan pathogens [14, 15]. Machine learning has the potential to provide more robust, scalable and automated solutions that are not as dependent as conventional methods on microscope images variability. For example, FiCRoN, a deep learning-based algorithm, was designed to estimate the number of intracellular *Leishmania* parasites and of both infected and uninfected cells [15]. The data obtained with FiCRoN showed higher correlation with the manual method when compared to the CellProfiler workflow, especially in the number of amastigotes in highly infected cells. The ability of deep learning algorithms to maintain consistency across different levels of infection without the need for laborious parameters adjustments highlights their potential as efficient and reproducible tools for large-scale image analysis in the *Leishmania* field.

In our effort to identify new chemical entities with leishmanicidal activity, we screened in **Chapter III** in-house libraries previously reported as potent dual-stage antimalarials, against *L. infantum* promastigotes and axenic amastigotes [16-19]. We showed that several compounds belonging to a

family of quinolin-4(1*H*)-imines were highly effective against *L. infantum*. Curiously, *L. infantum* intramacrophagic amastigotes were significantly more susceptible than the axenic counterparts. This finding may be attributed to the compound's immunomodulatory properties, the formation of a derivative – resulting from drug metabolism in macrophages – with higher efficiency against intramacrophagic amastigotes, or to metabolic differences between the two parasite forms. Regardless the explanation, these results further support the recommendation that drug testing should be carried out on intramacrophagic amastigotes [8, 9].

Obtaining a universal treatment for the different types of leishmaniasis, albeit desirable, is challenging, one of the reasons being the variation in drug susceptibility among *Leishmania* species, which is in part attributed to biochemical and molecular differences [20]. Notwithstanding, we report in **Chapter III** that four of the quinolin-4(1*H*)-imines with the highest SI against *L. infantum*, showed also strong activity against *L. major* and *L. amazonensis*. This chemotype holds therefore therapeutic potential for multiple species of *Leishmania*. Although the mechanism of action of quinolin-4(1*H*)-imines is not fully understood yet, their effect in *Leishmania* parasites likely involves, at least partially, inhibition of mitochondrial respiration through interaction at the Q_o binding pocket of the cytochrome bc_1 complex [21]. Interestingly, DNDI-6174, a drug currently being prepared to start clinical trials, acts by interfering with the *Leishmania* cytochrome bc_1 complex [22]. DNDI-6174 progression to Phase I depends on the results of preclinical studies in both mice and hamster models for VL, where it has demonstrated good efficacy. These findings suggest that targeting mitochondrial respiration is a promising strategy against *Leishmania*. Drugs affecting this pathway are already used in the clinics to treat or prevent other infectious diseases. As an example, bedaquiline, a member of the diarylquinoline class of drugs, inhibits the ATP synthase enzyme and is used to treat rifampicin-resistant and multidrug-resistant tuberculosis [23]. Another example is atovaquone, a member of naphthoquinones class, that inhibits the mitochondrial electron transport chain at the bc_1 complex in *Plasmodium* parasites and is primarily used in combination with proguanil to prevent malaria in travelers [24].

The poor aqueous solubility of the identified quinolin-4(1*H*)-imines presents a significant challenge for their development as effective drugs. To solubilize hydrophobic compounds, frequently excipients are pharmaceutically employed. However, the amount of excipient needed to solubilize a certain drug is frequently associated with toxicity, thereby limiting the drug dosage that can be administered in clinical settings and reducing patient compliance with the treatment [25]. One example of a commonly used excipient is Cremophor EL (CrEL) which, combined with dehydrated ethanol, solubilizes paclitaxel (PTX),

a well-known anti-cancer drug, resulting in the so-called Taxol® formulation. However, concerns were raised about CrEL side effects and its negative impact on the biodistribution of PTX [26, 27].

To circumvent the need for rather toxic solubilizing agents such as CrEL, nanocarriers, like polymeric micelles (PMs) are being explored as drug solubilizers [28]. Polymeric micelles are formed in aqueous media by the self-assembly of amphiphilic block copolymers into a core-shell structure consisting of two distinct regions: a hydrophobic core and a hydrophilic shell. The former accommodates poorly water-soluble drugs, while the latter, usually poly(ethylene glycol) (PEG), prolongs blood circulation of encapsulated drugs, assuming stable retention, enabling them to reach the target organ [29-31]. Also, PMs which do not stable retain the loaded drug in their core have clinical potential. A well-known example is Genexol® PM, a CrEL-free PM formulation of PTX, allows for an increased drug dosage without additional toxicity [32]. Also, Genexol® PM showed an overall response rate superior to that of Taxol® in patients with metastatic breast cancer [33]. Apart from Genexol®, several other PMs formulations have advanced to clinical trials [34]. NK105, another PTX-loaded polymeric micelle formulation, is undergoing a phase III trial targeting metastatic or recurrent breast cancer. Despite its failure to enhance PTX efficacy, NK105 successfully improved the drug pharmacokinetics and safety profiles [35]. Nanoxel® M, a docetaxel-loaded polymeric micelle formulation used in the treatment of various types of cancers, was developed to overcome the need for Tween 80, an excipient used in conventional docetaxel (Taxotere) known for its associated side effects [36]. As a result, Nanoxel® M showed better drug safety profile than Taxotere in a phase I trial [34].

In **Chapter IV** we evaluated the potential of mPEG-*b*-p(HPMAm-Bz) micelles as nanocarriers for delivery of the quinolin-4(1*H*)-imines previously shown to display *Leishmania* therapeutic potential. The rationale for selecting these PMs was based on their promising results with PTX and their proven ability to establish π–π stacking interactions through non-covalent bonding between the aromatic rings of mPEG-*b*-p(HPMAm-Bz) micelles and drugs, such as quinolin-4(1*H*)-imines [37]. These π–π stacking interactions enhance the solubility of poorly water-soluble drugs and improve the stability of PMs, which is crucial for maintaining their integrity during circulation and delivering the drug to the infection site. Stable PMs may also protect the drug from interacting with healthy cells until it reaches the target site, enabling a reduced drug dosage and consequently minimizing toxicity effects [30, 31]. In fact, in **Chapter IV**, we demonstrate that the encapsulated quinolin-4(1*H*)-imines exhibited lower toxicity compared to their free counterparts, both *in vitro* against mammalian cells and *in vivo* in a mice model. *In vitro* studies showed that, despite not apparently co-localizing with intracellular amastigotes, PMs

were internalized by macrophages and the encapsulated drugs had higher selectivity indexes compared to the free drug. In addition to enhancing drug solubility, these nanoparticles also 'slightly' increased the circulation time of the selected quinolin-4(1*H*)-imine allowing the compound to accumulate in liver, spleen and bone marrow - organs widely known for their role during *Leishmania* infection. Unfortunately, and unexpectedly, the *in vivo* stability of these formulations was lower when compared to PTX-loaded mPEG-*b*-p(HPMAm-Bz) micelles [37]. Indeed, we observed that only approximately 10% of the injected encapsulated drug and 35% of the PMs remained in circulation one hour post-injection. This rapid clearance and/or a low dose of drug used may explain the lack of therapeutic efficacy of our formulation observed in a *L. infantum*-infected C57BL/6 mice model. Rapid drug clearance aligns with the unexpectedly fast clearance of the PMs, but it could also be ascribed to the observed poor retention of the drug in the micelles after intravenous administration. Importantly, further observations revealed no acute toxicity. This will allow in future studies to increase the amount of injected polymer and of loaded drug. Alternatively, covalent conjugation of the drug to the core of the micelles via a degradable linker may improve stability and enable targeted delivery as observed for the clinically evaluated polymeric micellar formulation of the anticancer drug docetaxel [38].

The study reported in **Chapter IV** confirms the presence of the nanocarrier in the liver, spleen and, to a lesser extent in the bone marrow of animals, suggesting that the investigated micellar formulation holds promise for the delivery of antileishmanial drugs, other than the quinolin-4(1*H*)-imines. A specific type of cells found in the BM, known as long-term hematopoietic stem cells (LT-HSC), was recently identified as a protective cellular niche for persisting parasites and a source for the relapse of leishmaniasis [39]. These cells were observed to be more tolerant to antileishmanial drugs, probably due to their high parasite burden. Therefore, the efficacy of antileishmanial drugs depends largely on the capacity of the compounds to reach the bone marrow and effectively target intracellular parasites. The use of nanoformulations may enhance drug delivery to the bone marrow and reduce the risk of disease relapse. Unfortunately, the amount of encapsulated drug (1n) in the bone marrow was suboptimal, highlighting the need to optimize the formulation used. Increasing the stability of PMs to extend their circulation time, as referred before, could significantly improve drug delivery to the BM. Additionally, the diameter of the drug loaded micelles, above 100 nm, may have impaired their accumulation in the BM. It is known that nanocarriers with diameters below 100 nm can accumulate more efficiently in this organ [40, 41]. Controlling PMs size can be achieved by optimizing the polymer

molecular weight, adjusting the hydrophilic-to-hydrophobic ratios, and refining the processing methods, such as using fast mixing with water to obtain smaller micelles [42].

Various nanocarriers have been tested to enhance the performance of anti-leishmanial drugs. However, the lack of standardized protocols makes it challenging to compare results across different studies, including our own. Discrepancies exist in multiple aspects, from animal models (species, strains, gender, or age) to the species of *Leishmania* used, the parasite stage (promastigotes vs amastigotes), the number of parasites inoculated, the route of infection and the tissues analyzed for treatment effects [43]. Establishing standardized methodologies are therefore recommended to facilitate comparisons of results obtained by different research groups [43]. Regarding the animal model, the mouse is the most frequently used. However, hamsters should be prioritized in VL research, as they more closely mimic the features of active human disease [44]. Another important consideration is the need to consistently include parasite quantification in the bone marrow, one of the main organs where *Leishmania* parasites reside. Currently, such analysis is seldom performed.

The guidelines for developing new antileishmanial drugs are very stringent, including requirements such as oral administration, which is generally preferred by patients [45, 46]. Pharmaceutical development of compounds for IV administration often necessitates hospital care and a cold chain. However, IV delivery offers important advantages, including high bioavailability, a rapid pharmacodynamic effect, and the flexibility to adjust dosing rates.

The research conducted in this thesis aimed to advance drug development for leishmaniases. We established a HCS assay that facilitates *in vitro* testing and enabled identification of a family of compounds, the quinolin-4(1*H*)-imines, with promising efficacy against several *Leishmania* species. The HCS protocol was also adapted to the free open-source CellProfiler, offering a valuable tool for research groups with limited resources to search for new compounds with antileishmanial activity.

In the final part of the thesis, we developed a nanocarrier system, based on micelles formed from block copolymers of methoxy poly(ethylene glycol)-*b*-poly(N-2-benzoyloxypropyl methacrylamide) [mPEG-*b*-p(HPMA-Bz]). This polymer was selected due to its ability to establish π-π stacking interactions with selected compounds, promoting micelle self-assembly and enabling drug entrapment in the micelle core, thus maintaining nanocarrier stability.

Furthermore, we successfully used PMs to encapsulate quinolin-4(1*H*)-imines, though further optimization is necessary. While the therapeutic outcome was not ideal yet, we demonstrated an effective system for solubilizing poorly water-soluble drugs that holds potential for future applications for leishmaniasis treatment.

References

1. Field, M.C., et al., *Anti-trypanosomatid drug discovery: an ongoing challenge and a continuing need.* Nat Rev Microbiol, 2017. **15**(4): p. 217-231.

2. Pradhan, S., et al., *Treatment options for leishmaniasis.* Clin Exp Dermatol, 2022. **47**(3): p. 516-521.

3. DNDi. *High-throughput screening: testing millions of molecules to find drugs for neglected diseases*. On January 2025]; Available from: https://stories.dndi.org/drug-discovery-explained-high-throughput-screening/.

4. Lamotte, S., et al., *Discovery of novel hit compounds with broad activity against visceral and cutaneous Leishmania species by comparative phenotypic screening.* Sci Rep, 2019. **9**(1): p. 438.

5. Kaye, P. and P. Scott, *Leishmaniasis: complexity at the host-pathogen interface.* Nat Rev Microbiol, 2011. **9**(8): p. 604-15.

6. Siqueira-Neto, J.L., et al., *Antileishmanial high-throughput drug screening reveals drug candidates with new scaffolds.* PLoS Negl Trop Dis, 2010. **4**(5): p. e675.

7. Shimony, O. and C.L. Jaffe, *Rapid fluorescent assay for screening drugs on Leishmania amastigotes.* J Microbiol Methods, 2008. **75**(2): p. 196-200.

8. De Rycker, M., et al., *Comparison of a high-throughput high-content intracellular Leishmania donovani assay with an axenic amastigote assay.* Antimicrob Agents Chemother, 2013. **57**(7): p. 2913-22.

9. Vermeersch, M., et al., *In vitro susceptibilities of Leishmania donovani promastigote and amastigote stages to antileishmanial reference drugs: practical relevance of stage-specific differences.* Antimicrob Agents Chemother, 2009. **53**(9): p. 3855-9.

10. Capes-Davis, A., et al., *Check your cultures! A list of cross-contaminated or misidentified cell lines.* Int J Cancer, 2010. **127**(1): p. 1-8.

11. Kaur, G. and J.M. Dufour, *Cell lines: Valuable tools or useless artifacts.* Spermatogenesis, 2012. **2**(1): p. 1-5.

12. Gomes-Alves, A.G., et al., *Development of an automated image analysis protocol for quantification of intracellular forms of Leishmania spp.* PLoS One, 2018. **13**(8): p. e0201747.

13. Castro, H., et al., *The cytosolic hyperoxidation-sensitive and -robust Leishmania peroxiredoxins cPRX1 and cPRX2 are both dispensable for parasite infectivity.* Redox Biol, 2024. **71**: p. 103122.

14. Hu, R.S., A.E. Hesham, and Q. Zou, *Machine Learning and Its Applications for Protozoal Pathogens and Protozoal Infectious Diseases.* Front Cell Infect Microbiol, 2022. **12**: p. 882995.

15. Juez-Castillo, G., et al., *FiCRoN, a deep learning-based algorithm for the automatic determination of intracellular parasite burden from fluorescence microscopy images.* Med Image Anal, 2024. **91**: p. 103036.

16. Ressurreicao, A.S., et al., *Structural optimization of quinolon-4(1H)-imines as dual-stage antimalarials: toward increased potency and metabolic stability.* J Med Chem, 2013. **56**(19): p. 7679-90.

17. Rodrigues, T., et al., *Quinolin-4(1H)-imines are potent antiplasmodial drugs targeting the liver stage of malaria.* J Med Chem, 2013. **56**(11): p. 4811-5.

18. Rodrigues, T., et al., *Flavones as isosteres of 4(1H)-quinolones: discovery of ligand efficient and dual stage antimalarial lead compounds.* Eur J Med Chem, 2013. **69**: p. 872-80.

19. Rodrigues, T., et al., *Design, synthesis and structure-activity relationships of (1H-pyridin-4-ylidene)amines as potential antimalarials.* Bioorg Med Chem Lett, 2009. **19**(13): p. 3476-80.

20. Wijnant, G.-J., et al., *Tackling Drug Resistance and Other Causes of Treatment Failure in Leishmaniasis.* Frontiers in Tropical Diseases, 2022. **3**.

21. Gomes-Alves, A.G., et al., *Biological Evaluation and Mechanistic Studies of Quinolin-(1H)-Imines as a New Chemotype against Leishmaniasis.* Antimicrob Agents Chemother, 2021. **65**(7): p. e0151320.

22. Braillard, S., et al., *DNDI-6174 is a preclinical candidate for visceral leishmaniasis that targets the cytochrome bc(1).* Sci Transl Med, 2023. **15**(726): p. eadh9902.

23. Mbuagbaw, L., et al., *Outcomes of Bedaquiline Treatment in Patients with Multidrug-Resistant Tuberculosis.* Emerg Infect Dis, 2019. **25**(5): p. 936-943.

24. CDC. *Medicines for the Prevention of Malaria While Traveling Atovaquone-Proguanil (Malarone™)*. 2017 On December 2024]; Available from: https://www.cdc.gov/malaria/resources/pdf/fsp/drugs_2017/atovaquoneproguanil_2017.pdf.

25. van Zuylen, L., J. Verweij, and A. Sparreboom, *Role of formulation vehicles in taxane pharmacology.* Invest New Drugs, 2001. **19**(2): p. 125-41.

26. Adams, J.D., et al., *Taxol: a history of pharmaceutical development and current pharmaceutical concerns.* J Natl Cancer Inst Monogr, 1993(15): p. 141-7.

27. Gelderblom, H., et al., *Cremophor EL: the drawbacks and advantages of vehicle selection for drug formulation.* Eur J Cancer, 2001. **37**(13): p. 1590-8.

28. Rodriguez-Aller, M.G., D.; Veuthey, J.; and Gurny, R., *Strategies for formulating and delivering poorly water-soluble drugs.* Journal of Drug Delivery Science and Technology, 2015. **30**(2015): p. 342-351.

29. Varela-Moreira, A., et al., *Clinical application of polymeric micelles for the treatment of cancer.* Materials Chemistry Frontiers, 2017. **1**(8): p. 1485-1501.

30. Cabral, H., et al., *Block Copolymer Micelles in Nanomedicine Applications.* Chem Rev, 2018. **118**(14): p. 6844-6892.

31. Beach, M.A., et al., *Polymeric Nanoparticles for Drug Delivery.* Chemical Reviews, 2024. **124**(9): p. 5505-5616.

32. Kim, T.Y., et al., *Phase I and pharmacokinetic study of Genexol-PM, a cremophor-free, polymeric micelle-formulated paclitaxel, in patients with advanced malignancies.* Clin Cancer Res, 2004. **10**(11): p. 3708-16.

33. Lee, K.S., et al., *Multicenter phase II trial of Genexol-PM, a Cremophor-free, polymeric micelle formulation of paclitaxel, in patients with metastatic breast cancer.* Breast Cancer Res Treat, 2008. **108**(2): p. 241-50.

34. Hwang, D., J.D. Ramsey, and A.V. Kabanov, *Polymeric micelles for the delivery of poorly soluble drugs: From nanoformulation to clinical approval.* Adv Drug Deliv Rev, 2020. **156**: p. 80-118.

35. Fujiwara, Y., et al., *A multi-national, randomised, open-label, parallel, phase III non-inferiority study comparing NK105 and paclitaxel in metastatic or recurrent breast cancer patients.* Br J Cancer, 2019. **120**(5): p. 475-480.

36. Lee, S.W., et al., *Development of docetaxel-loaded intravenous formulation, Nanoxel-PM using polymer-based delivery system.* J Control Release, 2011. **155**(2): p. 262-71.

37. Shi, Y., et al., *Complete Regression of Xenograft Tumors upon Targeted Delivery of Paclitaxel via Pi-Pi Stacking Stabilized Polymeric Micelles.* ACS Nano, 2015. **9**(4): p. 3740-52.

38. Rijcken, C.J.F., et al., *Design, development and clinical translation of CriPec®-based core-crosslinked polymeric micelles.* Advanced Drug Delivery Reviews, 2022. **191**: p. 114613.

39. Dirkx, L., et al., *Long-term hematopoietic stem cells as a parasite niche during treatment failure in visceral leishmaniasis.* Commun Biol, 2022. **5**(1): p. 626.

40. Jiang, Y., W. Lin, and L. Zhu, *Targeted Drug Delivery for the Treatment of Blood Cancers.* Molecules, 2022. **27**(4).

41. de la Puente, P. and A.K. Azab, *Nanoparticle delivery systems, general approaches, and their implementation in multiple myeloma.* Eur J Haematol, 2017. **98**(6): p. 529-541.

42. Bagheri, M., et al., *Effect of Formulation and Processing Parameters on the Size of mPEG- b-p(HPMA-Bz) Polymeric Micelles.* Langmuir, 2018. **34**(50): p. 15495-15506.

43. van der Ende, J. and H. Schallig, *Leishmania Animal Models Used in Drug Discovery: A Systematic Review.* Animals (Basel), 2023. **13**(10).

44. Saini, S. and A.K. Rai, *Hamster, a close model for visceral leishmaniasis: Opportunities and challenges.* Parasite Immunol, 2020. **42**(10): p. e12768.

45. DNDi. *Target product profile for primary visceral leishmaniasis*. On March 2025]; Available from: https://dndi.org/diseases/visceral-leishmaniasis/target-product-profile/.

46. DNDi. *Target product profile for cutaneous leishmaniasis*. On March 2025]; Available from: https://dndi.org/diseases/cutaneous-leishmaniasis/target-product-profile/.